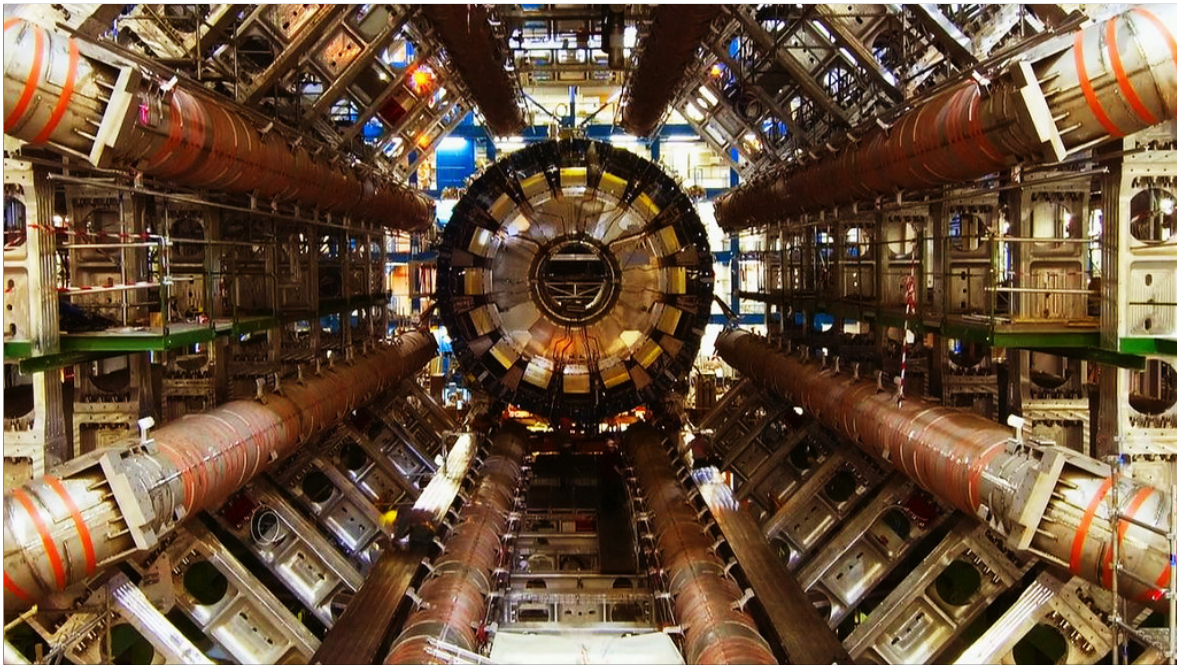**Universiteit Utrecht**

Nik hef

Faculteit Bètawetenschappen

Simulating QGP-like effects in pp collisions

BACHELOR THESIS

Pim te Rietmole

Physics and Astronomy

Supervisors:

Prof. Panos CHRISTAKOGLOU
GRASP

June 10, 2020

Abstract

Our goal is to set the first step towards a microscopic model of Quark Gluon Plasma (QGP). QGP is a state of matter where quarks and gluons, which are normally bound inside hadrons, attain a quasi-freedom. Quarks and gluons are the fundamental constituents of Quantum Chromo-dynamics (QCD).

Our approach to this goal is to use simulations to try to recreate QGP-like effects observed experimentally in pp collisions. Specifically, we try to test whether we can qualitatively reproduce the multiplicity dependence found experimentally in the baryon over meson transverse momentum spectra. We hypothesize that we can do this by introducing color reconnection (CR) in a model called Pythia. The Pythia model uses simulations to describe the final state products from particle collisions.

We used Pythia 8.2 [1] with the Monash tune [2]. We varied three parameters; CR (on or off), the type of QCD used (hard or soft), and the center-of-mass energy (7 TeV or 13 TeV). For each combination of these parameters we simulated roughly $2 * 10^9$ events. We then focused on the transverse momentum spectra for various particle types and their ratios (p/π, Λ/K_s^0, and Λ_c/D^0).

In our results, we found that CR introduced a multiplicity dependence in the baryon over meson ratio transverse momentum spectra for light flavors. The effect qualitatively agreed with the effects observed experimentally in pp collisions. We were unable to reach a similar conclusion for charm flavor due to a lack of statistics.

We conclude that CR is a highly promising candidate for capturing QGP-like effects in simulations of pp collisions.

Contents

1 Introduction

In 2005, physicists at the Relativistic Heavy Ion Collider (RHIC) first saw experimental evidence of the long-theorized existence of the quark gluon plasma [3], QGP for short. This extremely hot and dense form of matter, whose behavior seems to resemble that of a liquid, is characterized by the deconfinement of quarks and gluons. Quarks and gluons are normally bound strongly together by the strong force, confining them inside hadrons. Under the extreme circumstances of QGP however, they attain quasi-freedom.

The study of QGP can provide numerous valuable insights. It might allow for a deeper understanding of the mechanisms of flavor and quark confinement. Moreover, it could provide a window into the state of matter in the early universe, just after the Big Bang [4, Sec 1.1].

At the Large Hadron Collider (LHC), the QGP is primarily being studied by colliding lead (Pb) ions. These ions are quite heavy, and a collision between two of them will likely result in a highly energetic event with large multiplicity. From lattice QCD we know that an environment with such high energy density and temperature is perfect for the creation of QGP.

A lot of research has gone into trying to describe the behavior of the QGP in Pb-Pb collisions. There are numerous methods for studying the properties of the QGP. Some involve probing the QGP with jets of particles produced in the collision. Another method is to compare the statistical properties of the produced particles, such as the momentum distribution, to a control-case in which no QGP is produced. Historically, pp collisions have played the role of such a control case. Lead ions and protons are much alike, in the sense that one can think of lead as being a large collection of protons. The difference between the two lies in the fact that proton-proton collisions have a much smaller scale than Pb-Pb. Because of this, the assumption was originally made that the QGP would not be formed in pp collisions.

As a result of all these experiments, we have gained an excellent description of the macroscopic qualities of the QGP. Most notably, it has been found that the macroscopic behavior of QGP can be described by using hydro-dynamical models [5]. Such models describes the collective flow of the particles.

What we lack, however, is a microscopic description of the QGP. While we can recognize the presence of the QGP by looking at the collective behavior of particles, we don't know how this emergent behavior follows from that of individual particles.

One of the largest problems with describing QGP from the basis of individual particles, is the sheer size of the system. Pb-Pb collisions can produce many thousands of particles. Even with supercomputers, simulating all of these particles interacting with one another on such a scale, and repeating that simulation numerous times, is highly infeasible. In addition, making calculations from first principles is notoriously difficult in this regime. Ideally, we would like to have an example of QGP occurring in a much smaller system, that is easier to simulate.

A recent shift of paradigm within the field of particle physics might be the key to enabling such an approach. Over the past few years, several studies have pointed out that some effects indicative of the presence of QGP can also be observed in proton-proton collisions [6]. It is currently challenging to confirm that these effects are indeed caused by the presence of QGP. Nevertheless, this research certainly challenges the previously widely held conviction that pp collisions are incapable of producing QGP.

The details of what constitutes these 'QGP-like' effects will be discussed in section 2. For now, we will suffice with an abbreviated explanation.

In a droplet of QGP, there is an extremely large pressure gradient. This gradient causes the particles in the droplet to be propelled outwards explosively. This expansion has the effect of a common velocity boost on all particles. Such a boost can be seen back in the transverse momentum spectra of the final state particles. Transverse momentum spectra can be thought of as the probability-density distribution for a particle to be created with a specific transverse momentum.

Because of various effects, different final-state particles are affected by this boost in differing degrees. Specifically, baryons (hadrons that consist of three quarks) are affected differently compared to mesons

(hadrons that consist of a quark and an anti-quark) of the same flavor. Furthermore, it turns out that the size of the boost due to the expansion of the QGP depends on the multiplicity of the event.

In the end, one way to identify the presence of the common velocity boost is by looking at the multiplicity dependence of the ratio of the transverse momentum spectra of baryons and mesons with the same flavor.

Such a multiplicity dependence of the baryon over meson ratio transverse momentum spectra has been observed experimentally in pp collisions. This is the QGP-like effect mentioned earlier. Though it seems indicative of some sort of common velocity boost being applied to the particles, we can not definitively conclude that this boost is caused by QGP.

These QGP-like effects experimentally observed in pp collisions provide us with a new opportunity. Unlike Pb-Pb collisions, pp collisions have a relatively small scale. If we can identify the set of parameters that allows us to capture QGP-like effects in a simulation of pp collisions, that could form the first step towards creating a microscopical model of QGP.

In this paper we will use pre-existing models of pp collisions as our basis. The details of the software and parameters that we use is described in section 3.

In addition to a fairly standard setup for simulating pp collisions, we look towards one parameter in particular to provide us with the QGP-like effects observed experimentally. This parameter is the one that turns on color reconnection, abbreviated CR.

Details on what CR is and how it works can be found in section 3. There as well, we explain the effects we expect it to have.

One effect we expect to observe by turning on CR is an increase in the average transverse momentum of final state particles. We furthermore expect that this increase will be more significant for higher multiplicities.

This expectation of a multiplicity-dependent increase in transverse momenta is the main reason we want to study the effects of CR. Our hope is that this effect can play the role of the multiplicity-dependent common velocity boost due to the expansion of the medium of QGP. That would mean that CR might replicate the QGP-like effects observed experimentally in pp collisions.

In summary, we would like to find which set of simulation parameters allows us to replicate the QGP-like effects in experimental data for pp collisions. Specifically, we would like to know whether the addition of CR to a standard pp simulation can be used to qualitatively reproduce the curves found experimentally for the transverse momentum spectra of the baryon over meson ratios for particles of various flavors.

Our hypothesis is that CR will introduce a multiplicity-dependent boost to the transverse momenta of final state particles. We furthermore expect that this boost will affect the baryon over meson ratio transverse momentum spectra in a way that qualitatively agrees with the multiplicity-dependent shift in the baryon over meson ratio transverse momentum spectra observed experimentally in pp collisions.

In section 2, we will elaborate on the experimental background of our research. Next, in section 3 we will go into the details of the way we conduct our simulations and the way we analyze the simulation data. Following that, the results of these simulations will be discussed in section 4. We state our conlusions in section 5.1. Finally, in section 5.2, we reflect on our research, and discuss future possibilities.

2 Experimental background

At the LHC, particles are collided with one another at near-light velocities to study the behavior of matter under extreme conditions. One of the types of particles used is lead ions. Collisions between two lead ions are denoted as Pb-Pb, A-A, or lead-lead collisions.

The particles that emerge from such collisions are reconstructed and identified using the data from the numerous detectors surrounding the collision point. The information accumulated in this way over the course of many events can then be used to extract statistical knowledge about the relations between observables.

One of the aspects of the event data that one can consider is the transverse momentum spectrum of specific species of particles. This spectrum can be interpreted as a sort of probability density distribution for the momentum of a particle of a specific species created from the collision. These spectra can then be studied to draw various conclusions about the physics at play in that type of event. It is important to note we are using the transverse momentum rather than the complete momentum. This is on purpose, and standard practice. Momentum along the incident axis might be a 'leftover' from the momentum of the colliding particles. We can be certain however that any transverse momentum is due to the collision itself. By omitting the part of the momentum along the incident axis, we focus ourselves on the quantity relevant to describing the physics of the collision.

Examples of transverse momentum spectra can be seen in figure 1. Each plot shows the transverse momentum spectrum of a specific particle species, as measured from collision events between a proton and a lead ion, denoted p-Pb. These events took place at a center of mass energy of 5.02 TeV. The differently colored lines in each plot indicate the different multiplicities of the events. The word 'multiplicity' in this context refers to the number of particles produced in a given event. The red line at the top corresponds to the highest multiplicities, while the blue one at the bottom corresponds to the lowest multiplicities. These lines have been re-scaled with the factors mentioned in the bottom right of the figure so as to make them not overlap.

As a side-note, the definition of multiplicity used in figure 1 is different from the definition of multiplicity used in our research. Our multiplicity is defined as the number of particles created at central rapidity, i.e. in the region of momentum space that corresponds to particles that have most of their momentum orthogonal to the incident axis. Figure 1 on the other hand, defines multiplicity using V0M classes. These are linked to the amplitude of signals from the V0 solid state detectors in the forward rapidity regions. The forward rapidity region is the part of momentum space that corresponds to particles that have most of their momentum along the incident axis. Though these two definitions of multiplicity are to an extent analogous, they are not the same. This means that while we might expect qualitative agreement between our results and the ones shown in figure 1, we do not expect quantitative agreement.

The physically relevant thing to consider in figure 1 is the overall shape of the curves rather than their precise values. The p_T spectra appear to most resemble a Boltzmann distribution. They peak at low p_T, and have a long tail. Such a shape of the distribution is exactly what one would expect to follow from thermodynamics.

Due to the different scales of the x-axes of these plots, it is not easy to directly compare the transverse momentum spectra between different particle species. From the theory side however, we have a rough idea of what to expect. If the particles are indeed Boltzmann-distributed, then the shape of the distribution will be qualitatively the same for each species. However, the location of the peak scales with the mass of the particle. Particles from a more massive particle species will reach their peak at a higher value of p_T compared to less massive particles.

Another useful comparison to make using these spectra is the difference between proton-proton (pp) and lead-lead collisions. Since lead ions consist of a large number of protons and neutrons, one can think of lead-lead collisions as being similar to the combination of a large number of proton-proton collisions. Suppose we were to assume these separate collisions don't affect one another. In that case we would expect to see the same transverse momentum spectra in Pb-Pb as observed in pp. In other words, we can expect the transverse momentum spectra for both types of collisions to look quite similar to a first order of approximation. Differences between the two are likely caused by additional effects related to the larger number of particles.

Figure 2 shows experimental data for the transverse momentum spectra of three particle species, π, K and p respectively. The filled dots represent data from Pb-Pb collisions, and the empty dots represent data from pp collisions. As noted in the figure, the normalization is arbitrary. The important part is the overall shape of the spectra.

Immediately it is clear that there is a distinct difference between the spectra for lead-lead and proton-proton collisions. In lead-lead, there are comparatively fewer particles at very low momenta. Overall, in lead-lead collisions the spectra are harder; the average transverse momentum of the particles is higher in Pb-Pb than in pp collisions. Both of these effects seem to be more extreme the heavier the particle is. Protons are more affected than the lighter kaons, and kaons less than the even lighter pions. These differences have long since been understood, and are well-explained. They can be related to the production of a quark gluon plasma, and to the concept of radial flow.

Quark gluon plasma is known to be created only created under very extreme circumstances. It requires a very large density and very high temperature. One example of a situation in which QGP is thought to have been created is in the very early universe, just after the Big Bang. Another example is a Pb-Pb collision at the LHC.

The extreme heat and particle density present in a droplet of QGP give rise to a extremely high pressure gradient. Due to this gradient, the medium formed by the QGP rapidly expands, and drags the particles it contains along with it. This results in a boost to the velocity of these particles. The collective flow of the particles in the QGP medium can be described quantitatively using radial flow. Radial flow is an azimuthal average of the flow velocity, which can in turn be defined based on the four-momenta of the particles in the medium. Details of this description can be found in Heinz [8].

On theoretical grounds, we know that the boost due to the expansion of the medium is a common velocity boost. This is not to say that each particle's velocity will be boosted equally; the magnitude of the added velocity might still depend on the position of the particle within the droplet. The word 'common' here reflects the fact that particles on the same hyper-surface will receive the same boost to their velocity. Importantly, the velocity boost explicitly does not depend on the particle's mass. This means that heavier particles will receive a comparatively larger boost to their momentum.

This boost is what causes the differences in shape between the transverse momentum spectra in Pb-Pb versus pp collisions. The creation of an explosively expanding QGP in Pb-Pb collisions causes a common velocity boost to the product particles. Particles at low p_T will be lifted to higher p_T. This explains both the lower abundance of particles at low transverse momentum as well as the higher abundance of particles at large transverse momentum. Overall the result is a hardening of the spectra.

The fact that the difference between Pb-Pb and pp collisions seems to be larger for heavier particle species is also explained. The boost received is a common velocity boost. This means that heavier particles will receive a comparatively larger boost to their momentum. The differences in the transverse momentum spectra will therefore also be more pronounced.

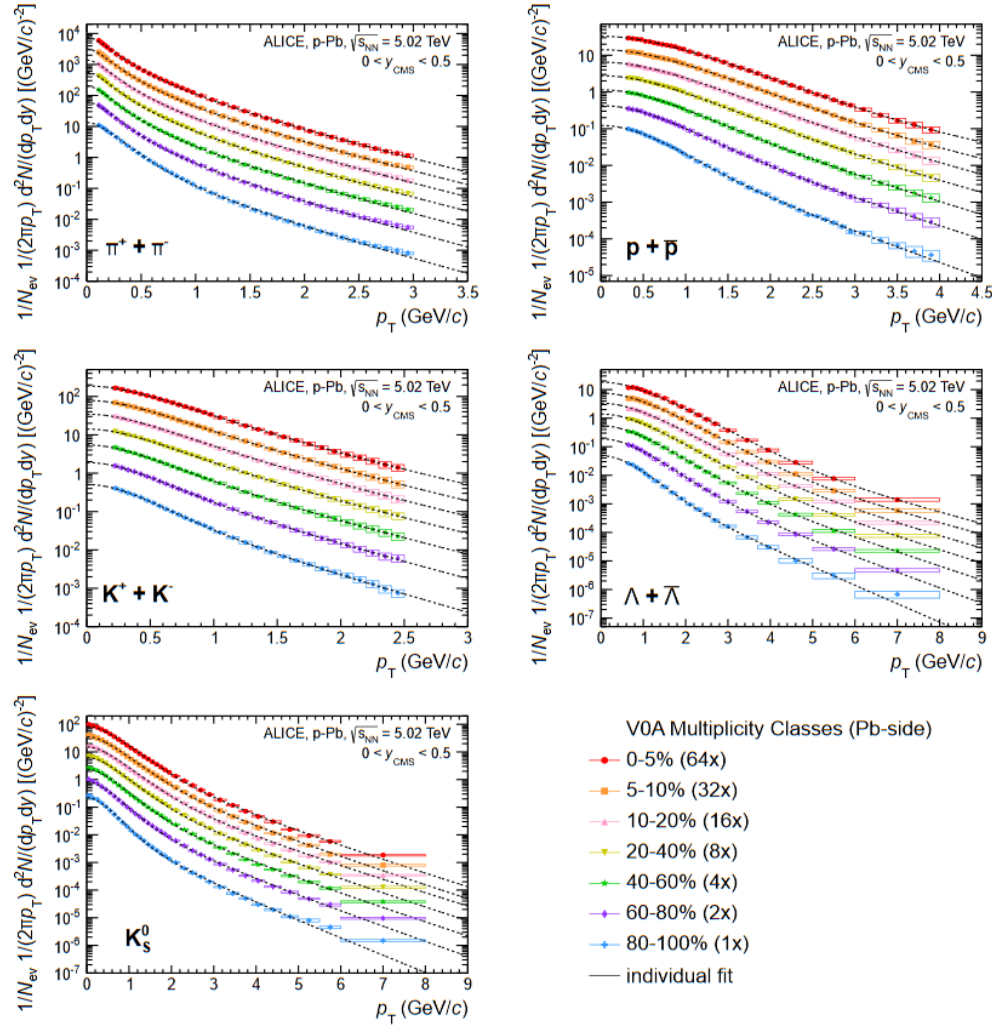## 1: Transverse momentum spectra of various particle species in p-Pb, split into different multiplicities

Figure 1: This figure consists of five plots, each for one particle species. From left to right, top to bottom they are π, p, K, Λ and K_s^0. Each plot shows experimental data for the transverse momentum spectra for different multiplicity ranges in p-Pb collisions. Each multiplicity range is given a different color. The red data-points correspond to the highest multiplicity, while the blue data-points correspond to the lowest multiplicity. The data from each multiplicity class is multiplied by a factor as listed in the lower right of the figure. This is done so as to not have the data for different multiplicities overlap. The spectra appear to closely resemble Boltzmann-distributions. Source: [7].

2: Transverse momentum spectra for π, K and p, compared for Pb-Pb vs. pp
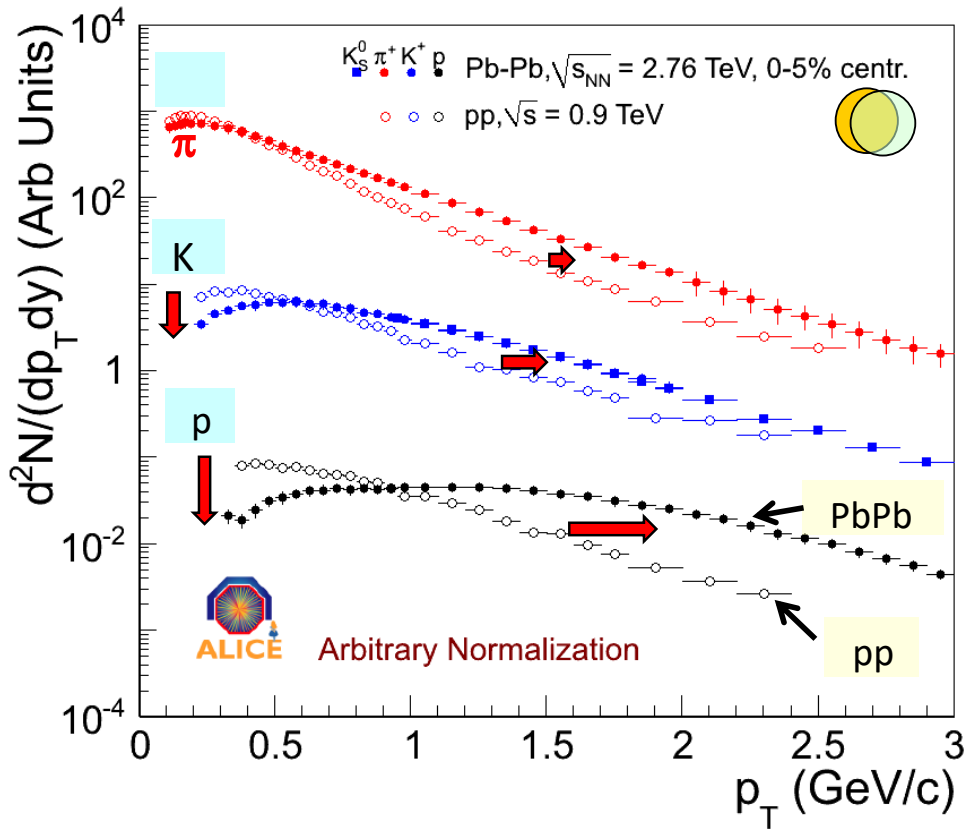
Figure 2: This figure shows experimental data for the transverse momentum spectra of π, K and p. For each particle species, there are two sets of data-points; the filled ones show data from Pb-Pb collisions with a high centrality between 0% and 5%, while the empty ones show data from pp collisions. All these spectra have been arbitrarily normalized. As indicated by the red arrows, significant differences are visible between the data from pp collisions and those from Pb-Pb collisions. In Pb-Pb collisions there are fewer particles in the very low p_T range, and overall the spectra are harder. Source: [9] and [10]

Instead of looking at the transverse momentum spectrum of single particles, we can also consider the ratio of their spectra. This will turn out to be useful in terms of observing the effects of QGP.

An example of these ratio spectra can be found in figure 3. The left-hand side plot shows experimental data from pp collisions, while the right shows data from p-Pb collisions. In each plot, three ratios are displayed. These are the ratios p/π, Λ/K_s^0 and Λ_c/D^0 respectively.

These ratios are not chosen randomly. Each is the ratio of a baryon over a meson of corresponding flavor. A baryon is a particle consisting of three quarks, while a meson is a particle consisting of a quark and an anti-quark. Protons and pions contain the light variety of quarks, called up and down. Λ_c baryons and D^0 mesons both contain the charm quark, which is far more massive. It will shortly become clear why these ratios are chosen specifically.

It can be seen in figure 3 that the ratios show a distinct peak roughly around 2 GeV to 4 GeV p_T. The presence of these peaks can be explained by remembering that the single-particle transverse momentum spectra are approximately shaped like a Boltzmann-distribution. The baryons, containing an extra quark, are more massive than their same-flavor meson counterparts. Therefore, the peak of the Boltzmann-distribution for the baryon lies to the right of the peak for the meson. The ratio of the two is very small around the p_T where the peak for the meson lies. However, around the p_T where the peak for the baryon lies, the ratio becomes very large. This results in the steep rise for the ratio at low p_T. Once the transverse momentum spectra for both particles have passed their peak, they gradually decline. Their ratio goes back to a lower value, and then reaches a plateau. This can all be clearly observed in the figure.

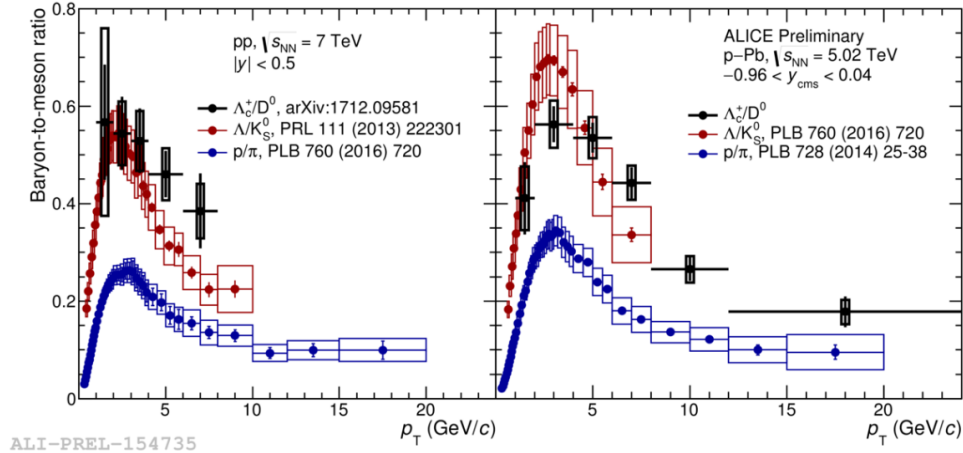## 3: Experimental baryon over meson ratio spectra

Figure 3: This figure shows experimental measurements of the p_T spectra of the yield ratios of baryons over mesons of corresponding flavors. It contains p/π as well as Λ/K_s^0 and Λ_c/D^0. The ratios p/π and Λ/K_s^0 for show a steep rise, followed by a peak around 2 to 4 GeV p_T, after which they gradually decline again. For Λ_c/D^0 there is not enough statistical data to conclude whether the spectra behave the same as for the lighter flavors. Source: Figure taken from [11], with data from [12], [13], [14] and [15].

A peculiar feature of the baryon over meson ratio in Pb-Pb collisions is its dependence on event multiplicity. This feature is clearly illustrated in the right halves of figures 4 and 5.

The right half of figure 4 shows experimental data for the transverse momentum spectra of the p/π ratio in Pb-Pb collisions. The red data-points represent a high event multiplicity, while the purple ones represent low event multiplicity. It can be clearly seen that the spectra look different for the different multiplicities. The peak for high multiplicity is higher, and occurs later than its low multiplicity counterpart. Figure 5 shows the same data for the Λ/K_s^0 ratio. The same effect can be observed here. The high multiplicity peak is higher and later than the one for low multiplicity.

This phenomenon can be explained using the concept of coalescence. Coalescence is the process of the combination of quasi-free quarks and anti-quarks to bind together in the form of baryons or mesons. This process occurs at the outer edge of the QGP droplet in Pb-Pb collisions. It is part of the freeze-out process, in which the final state hadrons from the collision are created.

Before the quarks coalesce, they are inside the QGP medium. There, they receive a common velocity boost due to the expansion of th medium of the QGP. The additional momentum from this boost is carried along with them until they coalesce into hadrons. These hadrons end up being the recipients of the extra momentum provided by the boost.

However, not all particles are affected the same way by this mechanism. Baryons, containing three quarks, are effectively boosted three times through this effect, while mesons on the other hand are only boosted twice. This causes a hardening of the spectra of baryons compared to that of mesons. This comparative hardening of the baryon spectrum causes a shift in the peak of the spectrum of the ratio of same-flavored baryons over mesons.

The magnitude of this shift depends on the size of the common velocity boost, and therefore on the pressure-gradient inside the QGP. It turns out that multiplicity is the relevant quantity to describe this. At higher event multiplicities, particle density is higher. This higher density results in more QGP being formed, with a larger pressure gradient. Therefore a higher multiplicity results in a larger common velocity boost, and we see this effect back in the shape of the baryon over meson ratio spectrum.

What this means is that we can view the multiplicity dependent shift of the baryon over meson ratio spectrum as another indication of the presence of QGP in the event. However, now we notice something
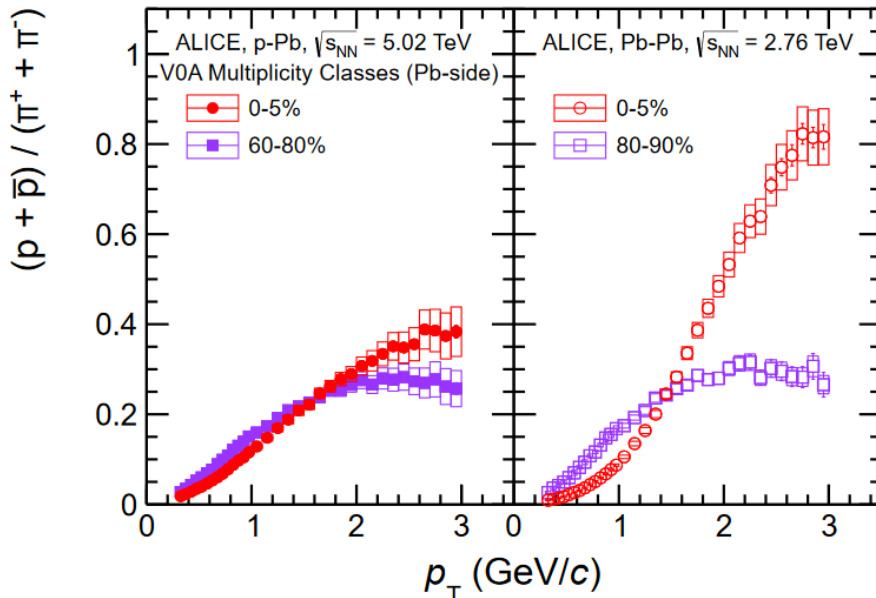
4: p/π ratio spectra in p-Pb and Pb-Pb, comparing high and low multiplicity

Figure 4: This figure shows experimental data for p/π transverse momentum spectra. The left plot shows data from p-Pb collisions at 5.02 TeV, while the right plot shows data from Pb-Pb collisions at 2.76 TeV. The red data-points in each plot correspond to a high event multiplicity, while the purple data-points correspond to a low event multiplicity. In both plots there is a clear dependence of the p/π ratio on the multiplicity. The peak of the p/π ratio shifts to the right and is higher for higher multiplicities. This shift is more pronounced in the right-hand plot compared to the left-hand plot. That is to say, the multiplicity dependent shift seems to be larger in Pb-Pb collisions compared to p-Pb collisions. Source: [7].

very peculiar. Similar multiplicity-dependent shift in the baryon over meson ratio spectra can actually be observed for p-Pb, and even pp collisions.

In the left half of figure 4, we see experimental data for the p/π spectrum in p-Pb collisions. The red data-points again show data for high multiplicity, while the purple data-points show data for low multiplicities. Similar to Pb-Pb collisions, we see that ratio spectrum depends on the multiplicity. At high multiplicity, the peak is higher and to the right compared the peak for low multiplicity. The effect is similar to that found in Pb-Pb collisions, except it seems to be slightly less pronounced. The left half of figure 5 shows the same multiplicity dependence for the Λ/K_s^0 ratio in p-Pb collisions. Here as well, the peak for high multiplicity lies to the right and above the peak for low multiplicity.

Figure 6 considers experimental data regarding the p/π and Λ/K_s^0 ratio spectra for pp collisions. The left plot shows the p/π ratio spectra, with the red data-points representing high multiplicity and the purple data-points representing low multiplicity. Though the effect is far less pronounced than in Pb-Pb, we see here as well that the ratio shows a dependence on multiplicity. For low multiplicity the peak lies at about 2 GeV p_T, and has a value of the ratio of approximately 0.2. For high multiplicity we see that the ratio peaks slightly after 2 GeV p_T. Additionally, the value of the peak is close to 0.3.

In the right plot in figure 6 we see the Λ/K_s^0 ratio spectrum. Like in the left plot, the red data-points represent high multiplicity while the purple data-points represent low multiplicity. Again, we see that the ratio spectrum is multiplicity dependent in the same manner. For low multiplicity, the peak lies slightly before 2 GeV p_T, at a value of approximately 0.4. For high multiplicity however, the ratio peaks between 2 and 3 GeV p_T, and its value goes up to approximately 0.6.
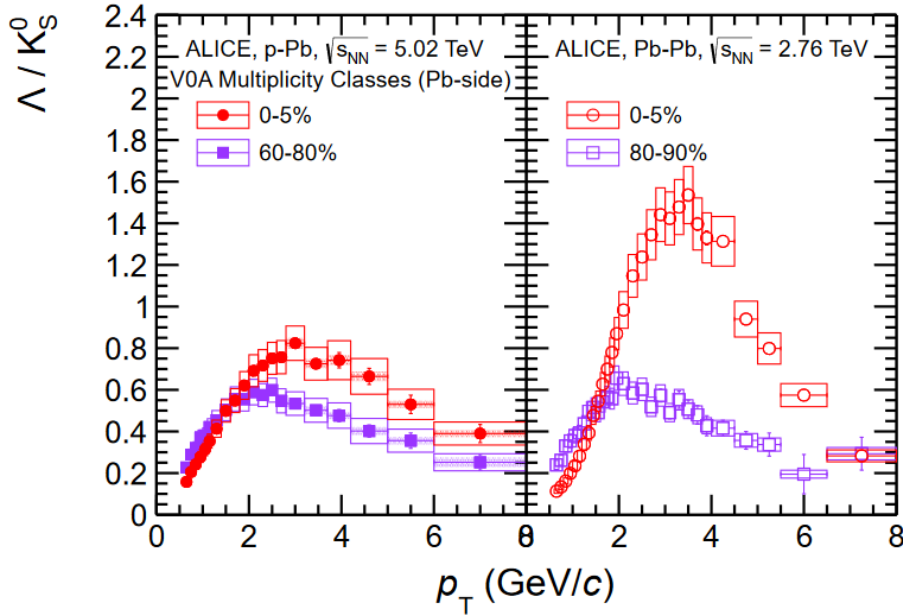
5: Λ/K_s^0 ratio spectra in p-Pb and Pb-Pb, comparing high and low multiplicity

Figure 5: This figure shows experimental data for Λ/K_s^0 transverse momentum spectra. The left plot shows data from p-Pb collisions at 5.02 TeV, while the right plot shows data from Pb-Pb collisions at 2.76 TeV. The red data-points in each plot correspond to a high event multiplicity, while the purple data-points correspond to a low event multiplicity. In both plots there is a clear dependence of the Λ/K_s^0 ratio on the multiplicity. The peak of the Λ/K_s^0 ratio shifts to the right and is higher for higher multiplicities. This shift is more pronounced in the right-hand plot compared to the left-hand plot. That is to say, the multiplicity dependent shift seems to be larger in Pb-Pb collisions compared to p-Pb collisions. Source: [7].

It is clear from this data that the baryon over meson ratio transverse momentum spectra in pp collisions show a multiplicity dependence that highly resembles the dependence found in Pb-Pb collisions. The latter dependence, for Pb-Pb collisions, has since been explained by the presence of QGP. This raises the question whether a similar explanation can be made for pp collisions. There are strong indications that a similar multiplicity-dependent common velocity boost might also be affecting particles in pp collisions. This might be caused by miniscule QGP droplets, but it might also be related to something completely different altogether. Whichever the case may be, the quest is now on for a model that can accurately describe and explain these effects in pp collisions.

6: p/π and Λ/K_s^0 ratio spectra in pp, comparing low and high multiplicity
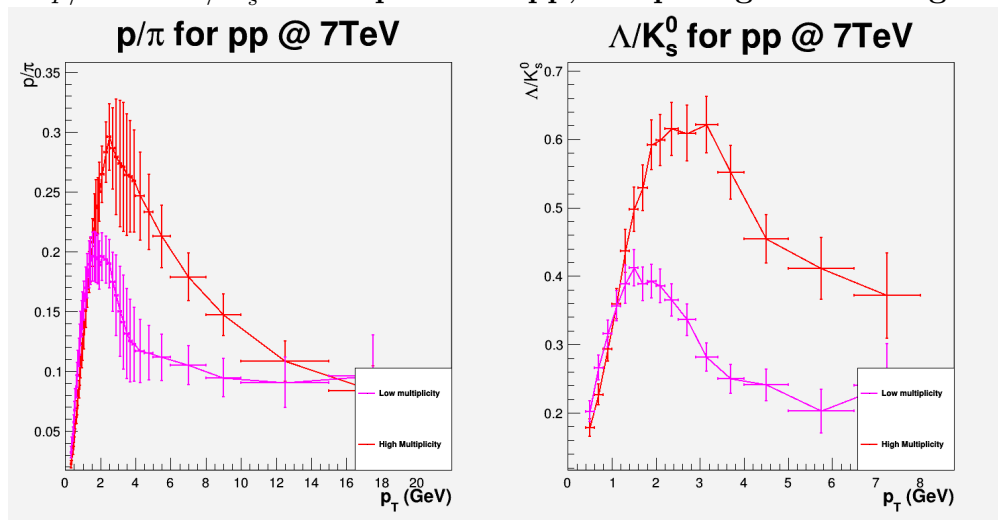
Figure 6: This figure shows experimental data for p/π and Λ/K_s^0 transverse momentum spectra in pp collisions at a center-of-mass energy of 7 TeV. The left plot shows the p/π spectrum, while the right plot shows the Λ/K_s^0 spectrum. The color of the data-points each plot represents the multiplicity range of the data. The red data-points represent high multiplicity, while the purple data-points represent low multiplicity. For both p/π and Λ/K_s^0 we observe that the red data-points lie above and to the right of the purple data-points. Source: [6].

3 Data analysis method

For our simulation we use Pythia 8.2. As described by its developers; "The Pythia program is a standard tool for the generation of events in high-energy collisions, comprising a coherent set of physics models for the evolution from a few-body hard process to a complex multiparticle final state."[1]

We configure our Pythia parameters according to the Monash Tune [2]. Additionally, there are three parameters that are varied.

The first varied parameter is color reconnection, CR. In order to understand the concept of color reconnection, it is first important to understand the Lund String model.

The Lund string model is a theoretical model that provides a simplified version of quantum chromo-dynamics, the theory underlying the strong interaction. In this model, the complex superimposed potentials caused by color charges are replaced by strings between oppositely charged particles. At large enough range, the potential between two oppositely color-charged particles increases roughly linearly. This means that we can think of this potential as a string stretching between two of the particles. The string represents the gluon field. It is like a piece of rubber, pulling the two particles together. The further the two get apart, the more potential energy is stored in the string.

If the potential energy between color-charged particles goes past a certain threshhold, something peculiar happens. The strong-force between color-charged particles is exceptionally strong. The energy needed to separate two oppositely charged particles beyond a certain range is so great that it is sufficient to spontaneously create new particles. If the system can lower the total energy by creating a new pair of oppositely charged particles in between the original pair, it will do so. In terms of the Lund string model, one can think of this as the string snapping in the middle. Afterwards we are left with two strings, the ends of which again correspond to our color-charged particles.

One very important condition for the Lund string model to be a good approximation, is that the string configuration is chosen correctly. Each color-charged particle must be connected with a string to exactly one oppositely charged particle. If we were to connect two particle all the way on opposite sides of the system with a string, the model would not work well. While in the model the large distance between the two particles will cause the string to split, in reality the two charges are shielded from one another by the charges that lie between them.

To gain as accurate a description as possible, the string configuration is chosen such that it minimizes the total string length. One can also think of this as the choice that minimizes the potential energy.

During a simulation however, the position of particles in space will change. They will move, be accelerated, and accelerate others. Because of this, a string configuration that initially minimizes the string length will likely no longer minimize the string length after enough time has passed. This can possibly affect the accuracy of the Lund string model.

This is where color reconnection comes in. To put it simply, turning on CR means that string configurations will be recalculated mid-simulation. Each time the recalculation takes place, the configuration with the shortest total string length will be chosen, taking into account the position of all particles at that time.

One of the expected effects of CR is that it will increase the average transverse momentum of the final state particles. This can be intuitively understood by considering the following. When recalculating the string configuration mid-simulation, the total string length will always either stay the same, or decrease. Particle production is linked to the breaking of strings that grow past a certain length. Therefore, we can expect CR to lead to reduced particle production. However, the energy in the same frame of reference must be preserved. If this energy is not manifested in the length of the strings, nor in the creation of particles, it must be in the form of kinetic energy. Thus, we expect that turning on CR will overall have the effect of increasing the transverse momentum of particles.

This boost will likely also be dependent on multiplicity. The more particles there are, the more significant the effects of changing the string configuration will be.

CR is of interest to our research because it might be possible to relate the microscopic effect of increased average momentum to the common velocity boost due to the expansion of the medium in QGP. In this sense, CR is a candidate for helping describe the system of QGP from a microscopical level.

We expect that turning on CR will increase the average transverse momentum of particles produced.

It will likely act similarly to a common velocity boost. Furthermore, this effect will probably be multiplicity-dependent, as color reconnection will change the string configuration more if it has a larger number of particles to work with. Therefore we think that the effect of turning on CR will be more pronounced for high multiplicity events.

The second varied parameter is the QCD type. It has two possible settings; hard QCD and soft QCD. The choice of the type of QCD determines what sort of processes can occur in the simulation. Lists of the precise processes included in each can be found in Sjostrand [16]. The words soft and hard refer to the momentum of the particles involved. Hard QCD processes involve the ones between partons that take place with a large momentum transfer. A distinction between these two types is often made, primarily because perturbative QCD can only accurately describe events with sufficient momentum. For softer events usually phenomenological models have to be used.

We surmise that using hard QCD will result in the production of more heavy-flavor particles compared to soft QCD. The reason is that heavy-flavor particles require a lot of energy to be produced, which is typically only possible in hard interactions. This enhancement of the production of charm quarks in particular is our main motivation for testing the effects of hard QCD. We think this setting will allow us to have more statistics for charm particles. Furthermore we suspect it might impact the shape of transverse momentum spectra of the baryon over meson ratio for charm particles. However, we do not expect a significant effect on the baryon over meson ratio for lighter flavors.

The third varied parameter is the center-of-mass energy of the collision. Our experimental data is comprised of events at two different center-of-mass energies, 7 TeV and 13 TeV. By simulating at both of these energies, our simulation data most approximately resembles the experimental data. We will hopefully also be able to tell if the effectiveness of the simulation depends on the energy of the event.

Our expectations for the effects of varying the center-of-mass energy are based on the paper Vislavicius [17]. This paper studies the effect of varying the center-of-mass energy on p/π and K/π ratio transverse momentum spectra in pp collisions. They did this both for experimental data and data from simulations using Pythia 8 and the Monash Tune, similar to our research.

In this paper it was concluded that in the experiment, a higher center-of-mass energy caused the p/π ratio transverse momentum spectrum to shift to slightly higher p_T. However in the simulations, no dependence of the ratio transverse momentum spectra on the center-of-mass energy was found.

Because of the results from the simulations by Vislavicius [17], we do not expect to find a dependence on the center-of-mass energy in our simulations either. This is despite the fact that there is in fact an energy dependence in experimental results from that same paper.

If we observe an energy dependence in our simulations regardless, it will likely only be for simulations with CR, since CR forms the main difference between our simulations and those in the paper Vislavicius [17].

Roughly $2 * 10^9$ events are simulated for each of the eight possible combinations of these parameters. The generated events are split into groups on basis of their multiplicity; 'low' (1-8), 'medium' (9-24), 'high' (25-46), and 'inclusive' (0-200). Multiplicity refers to the number of particles produced in the central rapidity region of that event.

There is also a significant fraction of events with a multiplicity of zero. This is because of single-diffractive or double-diffractive events, in which one or both protons stay intact and fly on past the collision point. In such events, particles are only produced in the forward and backward rapidity region, if they are produced at all. Our definition of the event multiplicity only takes into account particles produced in the central rapidity region. That is to say, we omit particles that have a momentum that mainly lies along the incident axis.

Because we are mainly interested in the physics of collisions where neither proton stays intact, we do not include events with a multiplicity of zero in the low multiplicity range. They are, however, included in the inclusive range.

Note that the inclusive multiplicity range extends up to a multiplicity of 200, beyond the range of the 'high' multiplicity region. This means that one cannot reconstruct the inclusive data simply by combining the data for other multiplicity ranges. The ranges were chosen in this way to be in accordance with the traditional ranges used in studies of heavy flavor. This was done under the assumption that the number of

events in the multiplicity range from 47 to 200 would be negligible. This assumption turns out to be false.

Figures 7, 8, 9 and 10 show the multiplicity distributions for the pp collisions simulations. Figure 7 contains the data for simulations with color reconnection and hard QCD, figure 8 contains the data for simulations with no color reconnection and hard QCD, figure 9 contains the data for simulations with color reconnection and soft QCD, and figure 10 contains the data for simulations with no color reconnection and soft QCD.

Each figure contains five differently colored regions to indicate the multiplicity ranges. The blue, purple, and red color represent low, medium, and high multiplicity respectively. The green color represents events with a multiplicity of zero. The yellow color represents events with a multiplicity between 47 and 200, above high multiplicity. The legends of these figures indicates for each of these ranges the percentage of total events that they constitute. These percentages have been rounded to integers.

Especially in figure 10 it is clear that by defining high multiplicity as only going up to a multiplicity of 46, we are omitting a large number of events. In figure 10 the number of events with a multiplicity between 47 and 200 is almost equal to half the number of events in the high multiplicity range of 25 to 46. In principle we do not expect the omission of these extra data to have a qualitative effect on our final results. However, in retrospect it might have been more optimal to define the high multiplicity range to also include these events.

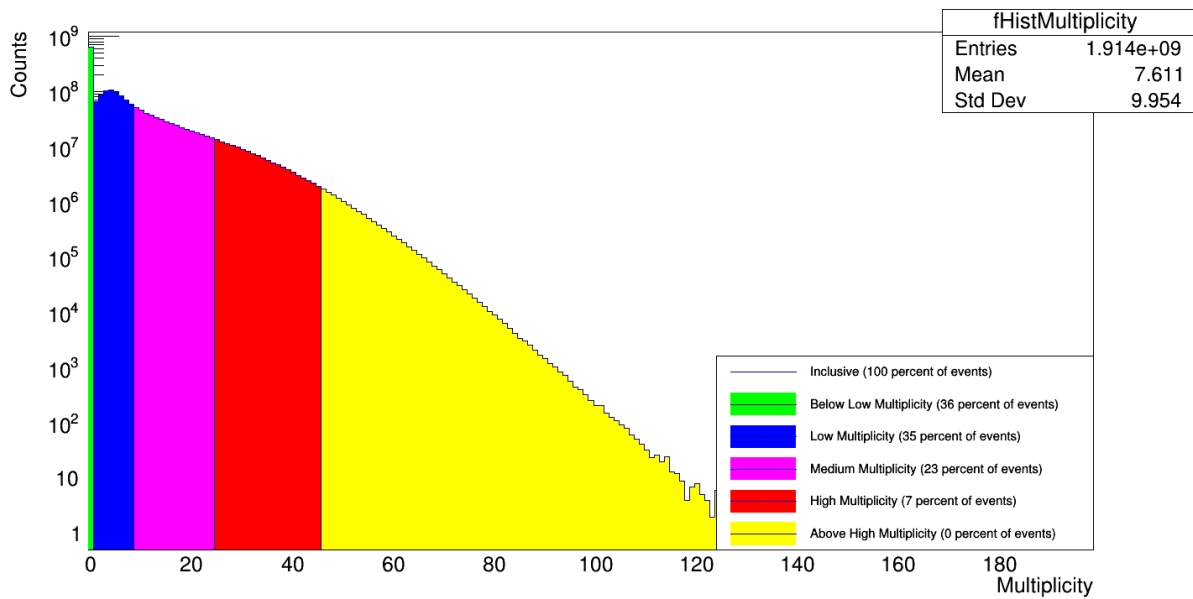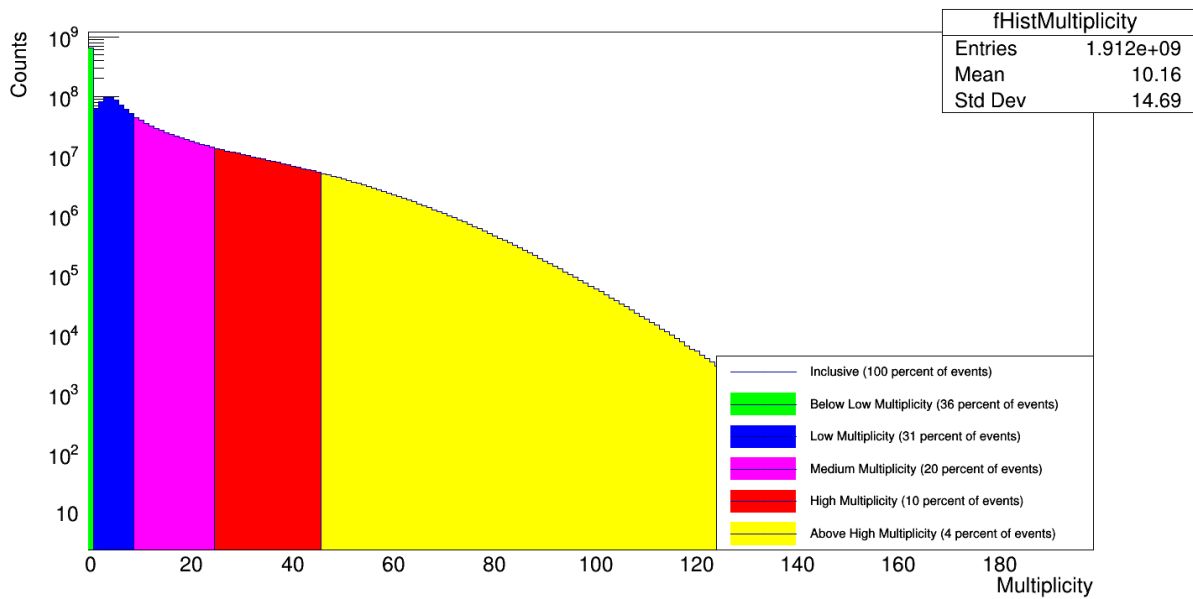## 7: Multiplicity distribution pp simulations @ 7TeV with CR for hard QCD
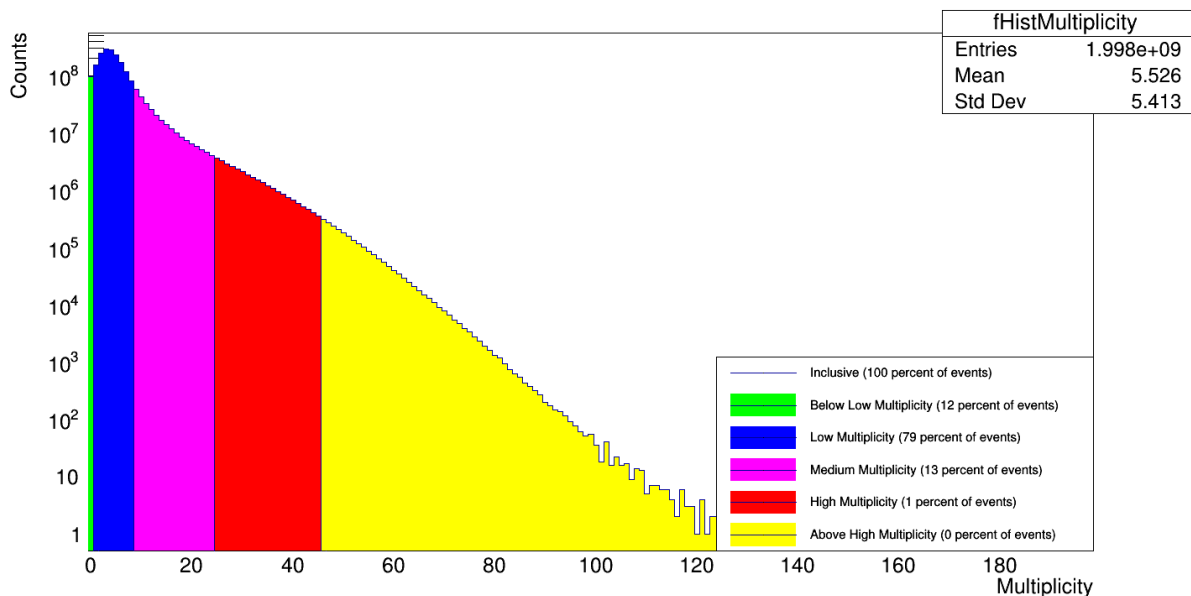
Figure 7: This figure shows the multiplicity distribution of the $2 * 10^9$ pp collision events that were simulated with CR for hard QCD. The y-axis is logarithmic. Five regions under the distribution have been colored to indicate different multiplicity ranges. The blue, purple, and red color represent low, medium, and high multiplicity respectively. The green color represents events with a multiplicity of zero. The yellow color represents events with a multiplicity between 47 and 200, above high multiplicity. The legend of this figure indicates for each of these ranges the percentage of total events that they constitute. These percentages have been rounded to integers.

The yields from different multiplicity ranges are normalized by dividing by the total number of events in that multiplicity range. This number is calculated by taking the integral over the various regions in the relevant multiplicity distribution.

The resulting data is used to look at the transverse momentum spectra of baryons and mesons of corresponding flavor, as well as the transverse momentum spectrum of their ratio. The pairs of baryons and mesons considered here are, respectively: protons (p) and pions (π), lambda (Λ) and k-zero short (K_s^0), and lambda-c (Λ_c) and d-zero (D^0).

8: Multiplicity distribution pp simulations @ 7TeV without CR for hard QCD
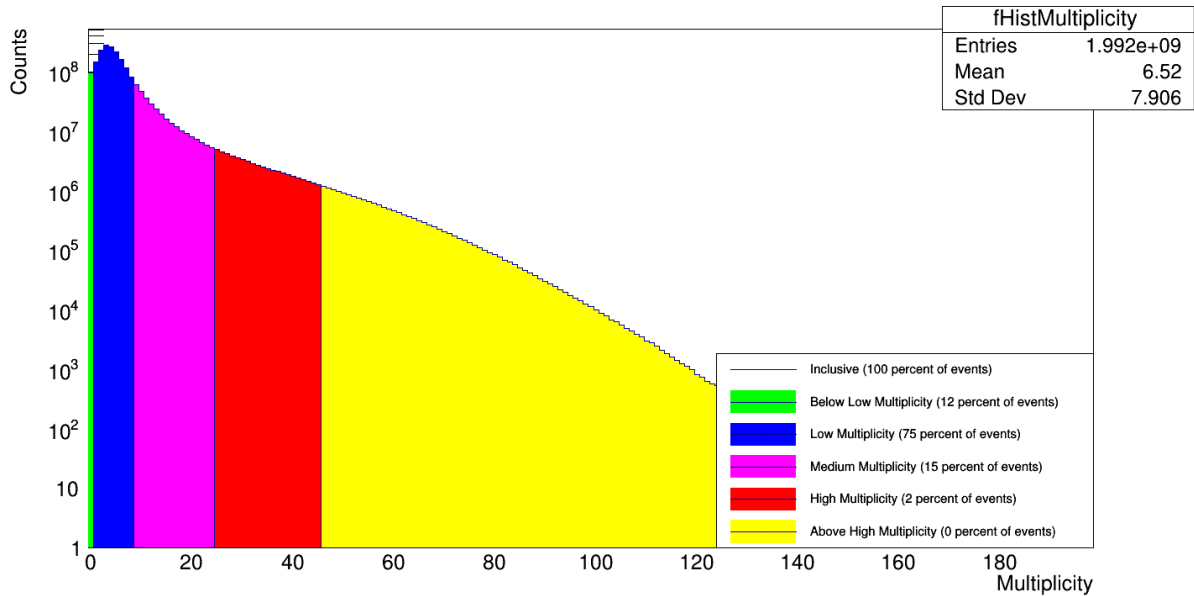
Figure 8: This figure shows the multiplicity distribution of the $2 * 10^9$ pp collision events that were simulated without CR for hard QCD. The y-axis is logarithmic. Five regions under the distribution have been colored to indicate different multiplicity ranges. The blue, purple, and red color represent low, medium, and high multiplicity respectively. The green color represents events with a multiplicity of zero. The yellow color represents events with a multiplicity between 47 and 200, above high multiplicity. The legend of this figure indicates for each of these ranges the percentage of total events that they constitute. These percentages have been rounded to integers.

There is one last thing to note. Because the production of heavy-flavor particles is relatively rare, we do not have sufficient statistics to treat the charm-flavor particles in the same way we do the lighter flavors. For this reason, the transverse momentum spectra of D^0 and Λ_c have been re-binned by a factor four. This should help reduce the statistical uncertainties to a manageable level, and make the figures more easy to interpret.

9: Multiplicity distribution pp simulations @ 7TeV with CR for soft QCD

Figure 9: This figure shows the multiplicity distribution of the $2 * 10^9$ pp collision events that were simulated with CR for soft QCD. The y-axis is logarithmic. Five regions under the distribution have been colored to indicate different multiplicity ranges. The blue, purple, and red color represent low, medium, and high multiplicity respectively. The green color represents events with a multiplicity of zero. The yellow color represents events with a multiplicity between 47 and 200, above high multiplicity. The legend of this figure indicates for each of these ranges the percentage of total events that they constitute. These percentages have been rounded to integers.

10: Multiplicity distribution pp simulations @ 7TeV without CR for soft QCD

Figure 10: This figure shows the multiplicity distribution of the $2*10^9$ pp collision events that were simulated without CR for soft QCD. The y-axis is logarithmic. Five regions under the distribution have been colored to indicate different multiplicity ranges. The blue, purple, and red color represent low, medium, and high multiplicity respectively. The green color represents events with a multiplicity of zero. The yellow color represents events with a multiplicity between 47 and 200, above high multiplicity. The legend of this figure indicates for each of these ranges the percentage of total events that they constitute. These percentages have been rounded to integers.

4   Results

The histograms containing the results from our simulations can be found in Appendices B and C. Copies of the figures found to be most important or representative have also been inserted below.

In this section we will first discuss the single-particle transverse momentum spectra for several flavors of particles. Then we will move on to the baryon over meson ratio transverse momentum spectra for particles of corresponding flavor. We first determine the dependence of these baryon over meson ratio transverse momentum spectra on CR. Finally, we also consider their dependence on the center-of-mass energy.

4.1   Single particle transverse momentum spectra

First of all, let us consider figures 11 and 12. These figures present the transverse momentum spectra normalized to the number of events in pp collisions at 7 TeV, for p and Λ particles respectively. Each figure contains four plots, each of which corresponds to one of the Pythia tunes. The top-left plot shows data for simulations with color reconnection and hard QCD, the top right for simulations without color reconnection and with hard QCD, the bottom left for simulations with color reconnection and with soft QCD, and the bottom right for simulations without color reconnection and with soft QCD. In each plot there are four differently colored types of data-points. As indicated by the legend, each color respresents a specific multiplicity range. The green data-points represent the inclusive multiplicity range, the blue data-points represent the low multiplicity range, the purple data-points represent the medium multiplicity range, and the red data-points represent the high multiplicity range.

By showing the data in this manner, there are several observations we can make. First of all, these figures allow us see the qualitative behavior of the transverse momentum spectra of specific particle species produced in our simulations. Secondly, by showing the different multiplicities in a single plot, we can more easily compare them against each other. This helps in identifying the multiplicity-dependence of the transverse momentum spectra in the simulation.

The shapes of the transverse momentum spectra in figures 11 and 12 appear to closely resemble a Boltzmann distribution, with many particles at low p_T, gradually decreasing towards higher p_T. In figure 11 the spectra show a peak around 1 GeV/c. Similarly in figure 12 there is also a peak at approximately the same value of p_T. Boltzmann distributions also have a peak, the location of which is dependent of the particle mass.

The fact that the transverse momentum spectra look like Boltzmann distributions is in line with what was observed in the experimental data (See figure 1 in section 2). In this respect, the simulations seem to be doing a good job reproducing the experimental results.

When comparing the transverse momentum spectra in figures 11 and 12 based on their multiplicity, we see a common trend for each of the different tunes. The red data-points, representing the high multiplicity range, consistently lie above and right of the purple data-points that represent the medium multiplicity range. Similarly, the purple data-points, representing the medium multiplicity range, lie above and to the right of the blue data-points, representing the low multiplicity range. Though the extent to which this difference is present seems to differ per tune, the difference is clearly observable in each of the plots. These observations suggest that increasing the multiplicity has the effect of hardening the transverse momentum spectra of the particles.

This hardening of the spectra for higher multiplicity corresponds to experimental observations in pp collisions. This can be seen in figure 13 (Copied here from section 2). This figure has five plots that show the transverse momentum spectra for π, p, K, Λ, and K_s^0 particles respectively. Each plot contains seven differently colored sets of data-points, each respresenting a different multiplicity range. The red data-points correspond to the highest multiplicity and the blue data-points correspond to the lowest multiplicity.

It can be seen in each plot that, when moving towards higher p_T, the decrease of the red data-points is less steep than that of the blue data-points. This difference in the shape of these curves suggests that the average transverse momentum of a given particle is higher at high multiplicity. In other words, the transverse momentum spectra become harder as the multiplicity increases.

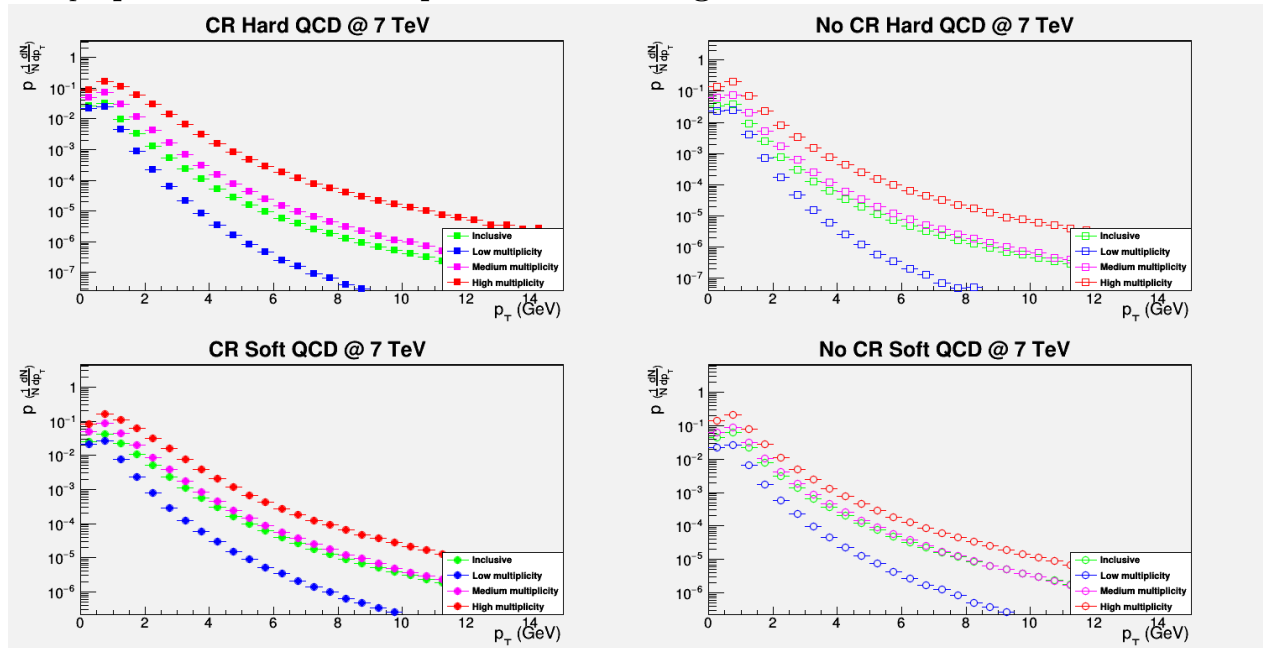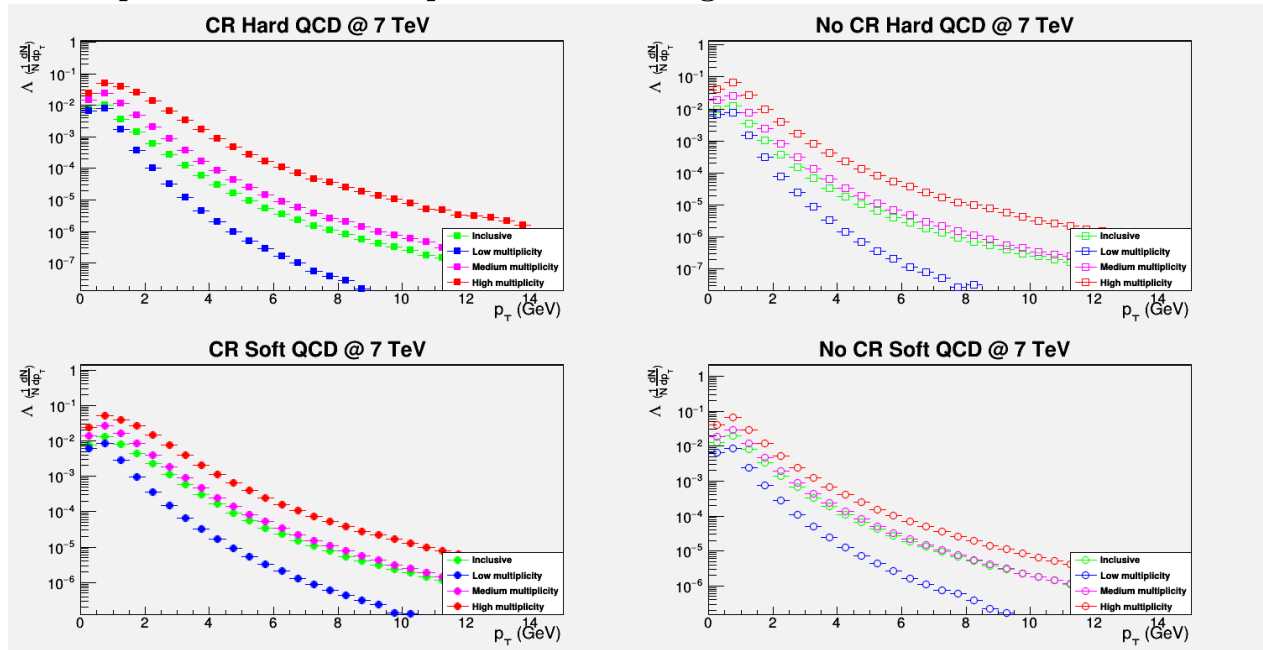Our simulations are in agreement with experimental results on this point.

11: p spectrum with multiplicities shown together

Figure 11: This figure shows the transverse momentum spectra of protons using data from pp collision simulations at 7 TeV. It contains four plots. Each plot shows data for one specific Pythia tune. The top left plot shows data for simulations with CR and with hard QCD, the top right plot for simulations without CR and with hard QCD, the bottom left plot for simulations with CR and with soft QCD, and the bottom right plot for simulations without CR and with soft QCD. Each plot contains four differently colored sets of data-points. These each represent the data for different multiplicity ranges. The green data-points represent the inclusive range, the blue data-points represent the low multiplicity range, the purple data-points represent the medium multiplicity range, and the red data-points represent the high multiplicity range.

12: Λ spectrum with multiplicities shown together

Figure 12: This figure shows the transverse momentum spectra of Λ baryons using data from pp collision simulations at 7 TeV. It contains four plots. Each plot shows data for one specific Pythia tune. The top left plot shows data for simulations with CR and with hard QCD, the top right plot for simulations without CR and with hard QCD, the bottom left plot for simulations with CR and with soft QCD, and the bottom right plot for simulations without CR and with soft QCD. Each plot contains four differently colored sets of data-points. These each represent the data for different multiplicity ranges. The green data-points represent the inclusive range, the blue data-points represent the low multiplicity range, the purple data-points represent the medium multiplicity range, and the red data-points represent the high multiplicity range.

13: Transverse momentum spectra of various particle species in p-Pb, split into different multiplicities
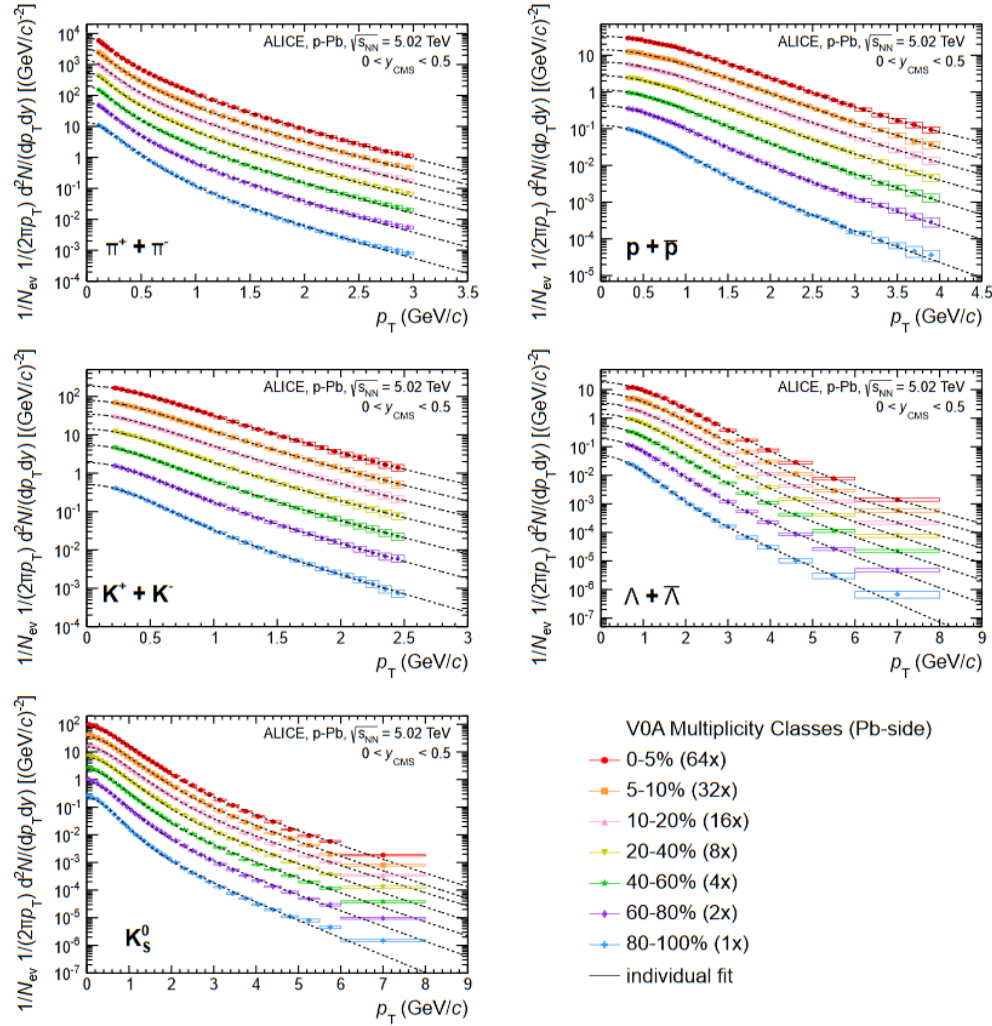
Figure 13: This figure consists of five plots, each for one particle species. From left to right, top to bottom they are π, p, K, Λ and K_s^0. Each plot shows experimental data for the transverse momentum spectra for different multiplicity ranges in p-Pb collisions. Each multiplicity range is given a different color. The red data-points correspond to the highest multiplicity, while the blue data-points correspond to the lowest multiplicity. The data from each multiplicity class is multiplied by a factor as listed in the lower right of the figure. This is done so as to not have the data for different multiplicities overlap. The spectra appear to closely resemble Boltzmann-distributions. Source: [7].

Next, please refer to figure 14. This figure shows the transverse momentum spectra of protons normalized to the number of events in pp collisions at 7 TeV. Each plot in the figure corresponds to a specific multiplicity range. The plot in the top-left, containing the green data-points, represents the inclusive multiplicity range. The plot in the top-right, containing the blue data-points, represents the low multiplicity range. The plot in the bottom-left, containing the purple data-points, represents the medium multiplicity range. The plot in the bottom-right, containing the red data-points, represents the high multiplicity range. Each plot contains data-points for four different Pythia tunes. As indicated by the legend, these can be distinguished by their markers. Data-points for simulations with color reconnection are represented by filled markers, while data-points for simulations without color reconnection are indicated by empty markers. Similarly, data-points for simulations with hard QCD are represented by square markers, while data-points for simulations with soft QCD are represented by circular markers.

This figure contains the same data as figure 11. However, by organizing the data in this manner, we can more easily compare the effects of the CR and QCD-type tune-parameters on the transverse momentum spectra.

Looking at figure 14, we see that the data-points for the tunes with soft QCD seem to consistently lie above those for the tunes with hard QCD. This is more apparent at larger values of p_T. From the figures in section B.1 we see that this difference between soft QCD and hard QCD is shared by all particle species.

This observation seems to suggest that soft QCD has a tendency to produce events with a larger number of particles compared to hard QCD. This observation is in line with what can be seen in figures 7, 8, 9, and 10 in section 3.

We are unable to explain why soft QCD would produce more particles than hard QCD. According to Sjostranda et al. [1], the cross sections of events in both soft QCD and hard QCD have been adjusted so as to produce a faithful reproduction of experimental results. The fact that the overall particle-yield between the two differs in this manner is puzzling.

Perhaps this difference is an indication that something is wrong with our normalization if the transverse momentum spectra. However, we have not been able to identify any such mistake.

At high multiplicity we see that the filled data-points representing the simulations with CR show a harder spectrum than those representing the simulations without CR. At low p_T the data-points for simulations with CR lie below the data-points for simulations without CR, while at higher p_T they lie above the data-points for simulations without CR. At medium multiplicity this effect is far less pronounced. At low multiplicity the effect is hardly visible at all. In this regard also, figure 14 can be considered representative of the transverse momentum spectra of other particle species from the simulations. Please refer to B.1 for the figures containing the data for other particle species.

This difference between the tunes seems to indicate that CR plays the role of a 'boost', increasing the average transverse momentum of particles produced. This boost appears to be multiplicity-dependent.
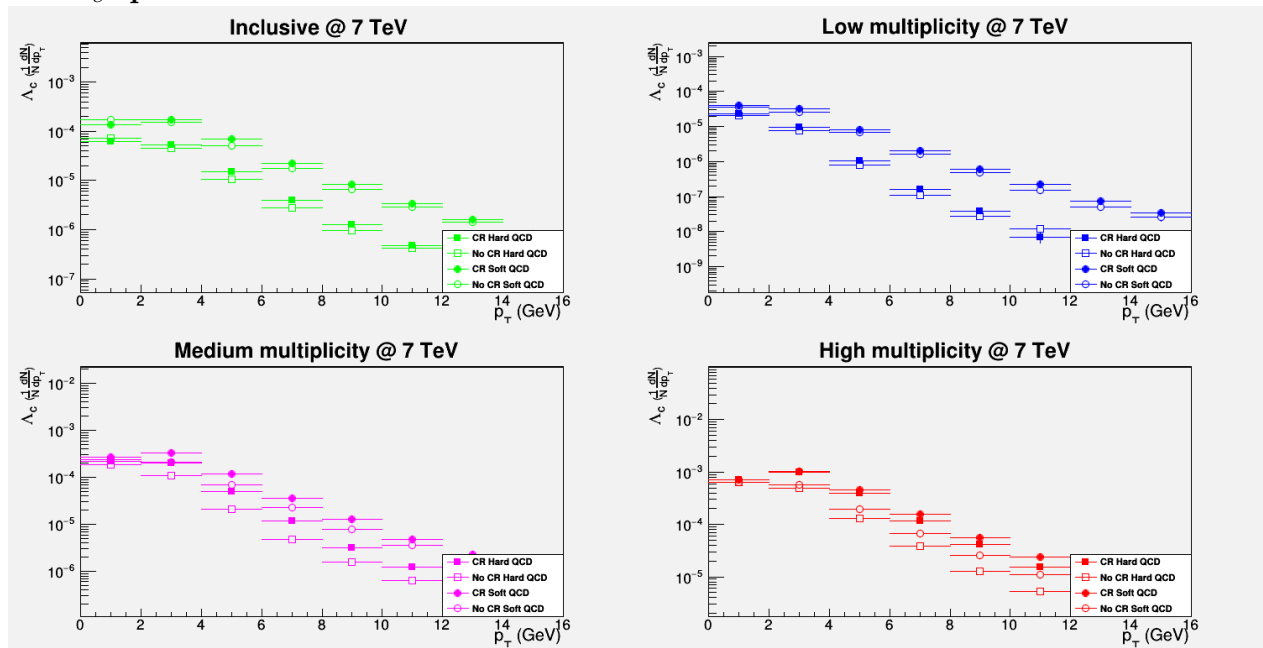
14: p spectrum with tunes shown together

Figure 14: This figure shows the transverse momentum spectra of protons using data from pp collision simulations at 7 TeV. It contains four plots. Each plot shows data for one specific multiplicity range. The top left plot shows data for the inclusive range, the top right plot for the low multiplicity range, the bottom left plot for the medium multiplicity range, and the bottom right plot for the high multiplicity range. Each plot contains four sets of data-points. These each represent the data for simulations using different Pythia tunes. The data-points with filled markers represent simulations with CR, while the data-points with empty markers represent simulations without CR. The data-points with square markers represent simulations using hard QCD, while the data-points with circular markers represent simulations using soft QCD.

The last single-particle transverse momentum spectra we consider are those for charm-flavored particles. See figure 15. This figure contains the transverse momentum spectra for Λ_c baryons. Each plot again shows the data for a specific multiplicity range. Each plot again contains four sets of data-points, each representing one specific tune. These tunes are listed in the legends.

By looking at this figure we can determine whether the conclusions we drew about the lighter-flavor transverse momentum spectra also hold true for the heavier charm-flavor particles. We only explicitly discuss the transverse momentum spectra for Λ_c here. However, the transverse momentum spectra for D^0 particles are very similar, and can be found in the appendix.

First of all we see that these spectra as well resemble a Boltzmann-like distribution. The peaks of these spectra are not as clearly identifiable because of the broader bins used here. The fact that the particles are distributed in this way is in line with expectations based on experimental data.

Another effect observed for the lighter flavor spectra that is also present here, is the fact the data-points for soft QCD lie above the data-points for hard QCD. We are again unable to explain why this would be the case. We conclude that, contrary to our expectations, turning on hard QCD does not seem to enhance the production of strange-flavor particles.

Lastly, we see here as well that at high multiplicity, in the bottom right plot, the data-points spectra with CR seem to be harder than the spectra without CR. This corresponds with our observations for lighter flavors.
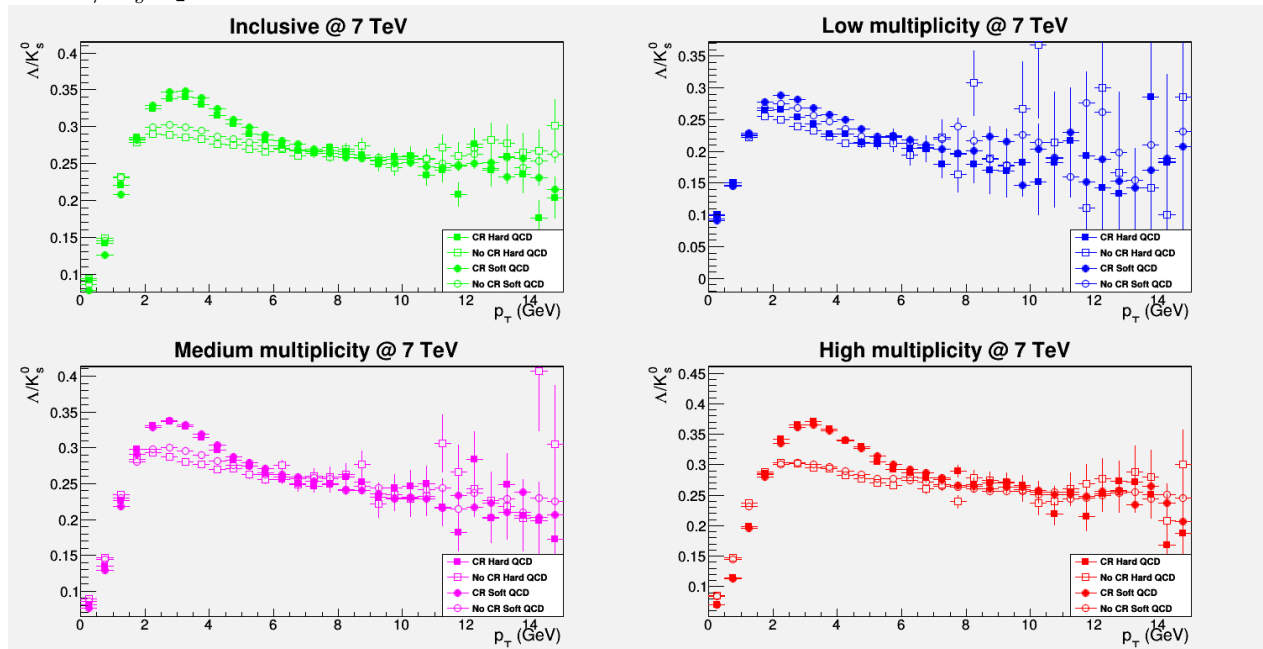
15: Λ_c spectrum

Figure 15: This figure shows the transverse momentum spectra of Λ_c baryons using data from pp collision simulations at 7 TeV. It contains four plots. Each plot shows data for one specific multiplicity range. The top left plot shows data for the inclusive range, the top right plot for the low multiplicity range, the bottom left plot for the medium multiplicity range, and the bottom right plot for the high multiplicity range. Each plot contains four sets of data-points. These each represent the data for simulations using different Pythia tunes. The data-points with filled markers represent simulations with CR, while the data-points with empty markers represent simulations without CR. The data-points with square markers represent simulations using hard QCD, while the data-points with circular markers represent simulations using soft QCD.

4.2 Baryon over meson ratio transverse momentum spectra

4.2.1 CR and multiplicity dependent effects

Next, we will consider the figures showing transverse momentum spectra of the yield ratio of baryons over mesons of corresponding flavor. In this section our focus is especially on the multiplicity dependence of this ratio. In experimental results for pp collisions (See figure 3) there is a distinct peak around 2 to 4 GeV p_T. Furthermore, the position of the peak is dependent on multiplicity, shifting to higher p_T for high multiplicity ranges. This behaviour is similar to the effect seen in lead-lead collisions. In such collisions, the shift of the peak of the baryon over meson ratio is caused by the common velocity boost due to the expansion of the medium formed by QGP.

The main question we want to answer is whether we can use CR to reproduce the multiplicity-dependent shift of the peak in the experimental data from pp collisions. This would be an indication that CR could play a role in describing QGP-like effects from a microscopic perspective.

Please refer to figure 16. This figure shows the transverse momentum spectra of the Λ/K_s^0 ratio using data from pp collision simulations at 7 TeV. It contains four plots. Each plot shows data for one specific multiplicity range. The top left plot shows data for the inclusive range, the top right plot for the low multiplicity range, the bottom left plot for the medium multiplicity range, and the bottom right plot for the high multiplicity range. Each plot contains four sets of data-points. These each represent the data for simulations using different Pythia tunes. The data-points with filled markers represent simulations with CR, while the data-points with empty markers represent simulations without CR. The data-points with square markers represent simulations using hard QCD, while the data-points with circular markers represent simulations using soft QCD.

From this plot we want to conclude whether the overall shape of the Λ/K_s^0 ratio agrees with experimental data. Furthermore, this representation of the data allows us to easily see any multiplicity-dependent effects of turning on CR.

Firstly, the overall shape of the transverse momentum spectrum of the ratio does indeed resemble the result from experimental data. Comparing with figure 3 we see that in both cases the ratio spectra are close to zero for very low p_T. Then there is a peak around 3 GeV/c. At higher p_T the spectra gradually decline until they reach a plateau.

Next, we check whether there is any multiplicity dependence in these ratio spectra. Looking at the right two plots in figure 16, it is clear that there is indeed a multiplicity dependent effect of CR. The bottom right plot shows that at high multiplicity, the peak in the ratio spectra for simulations with CR lies above and to the right of the peak for simulations without CR. However, the top-right plot shows that for low multiplicity the peaks lie a lot closer together.

This can be interpreted as an indication that CR here plays the role of a multiplicity-dependent common velocity boost. Because of coalescence, this boost affects the transverse momentum of the Λ baryons more than it affects the transverse momentum of the K_s^0 mesons. At high multiplicities, the boost is sufficiently large that this effect can be seen back in the shape of the baryon over meson transverse momentum spectra.

These observations similarly hold true for the p/π ratio transverse momentum spectra, as can be seen in the appendix. It seems that for these light-flavor particles, turning on CR indeed has an effect qualitatively resembling a multiplicity-dependent common velocity boost. This is exactly what we hoped to show.

The question is now whether we can observe something similar in the case of strange flavor particles. The relevant data are shown in figure 17 below.
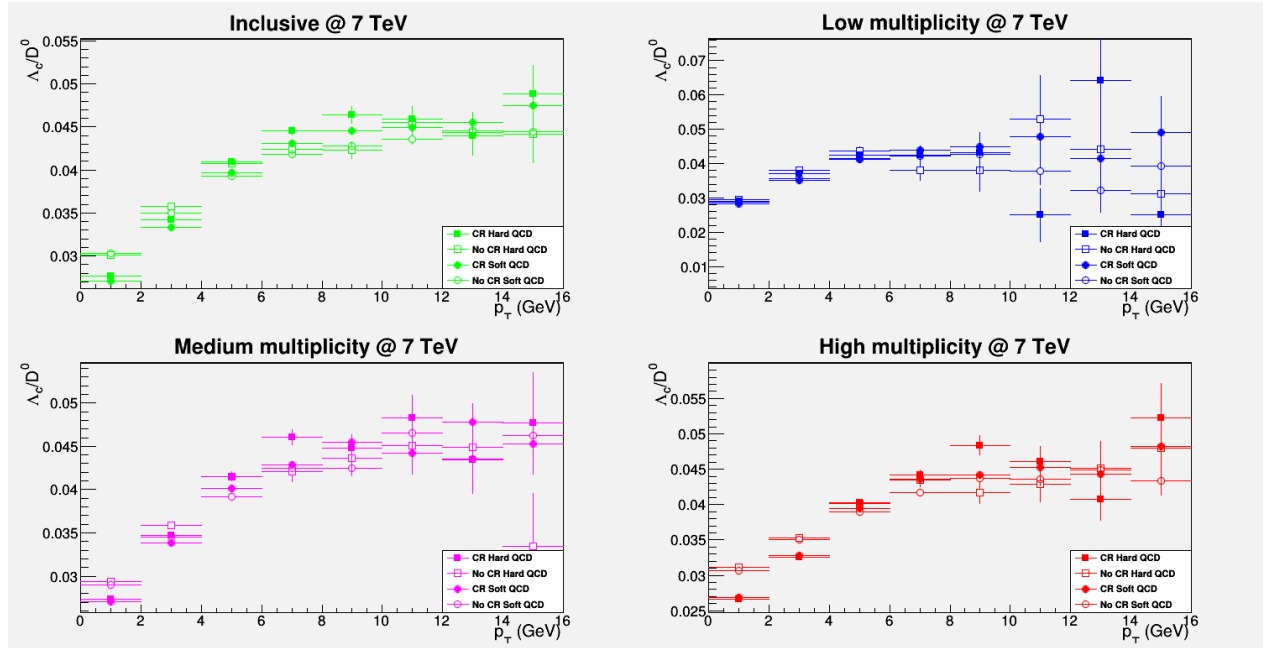
Figure 17 shows the transverse momentum spectra of the Λ_c/D^0 ratio using data from pp collision simulations at 7 TeV. It contains four plots. Each plot shows data for one specific multiplicity range, in the same way as figure 16. These plots each contain four sets of data-points, each corresponding to a different Pythia tune. These are also marked in the same way as in figure 16.

This figure will help us answer two questions. First of all, it will help us determine whether the Λ_c/D^0 ratio transverse momentum spectra are qualitatively the same as those found experimentally. Secondly, we will try to determine whether CR introduces a multiplicity-dependent common velocity boost for this flavor as well.

Looking at figure 17, we see that for all multiplicities and all tunes, the data-points have a value of
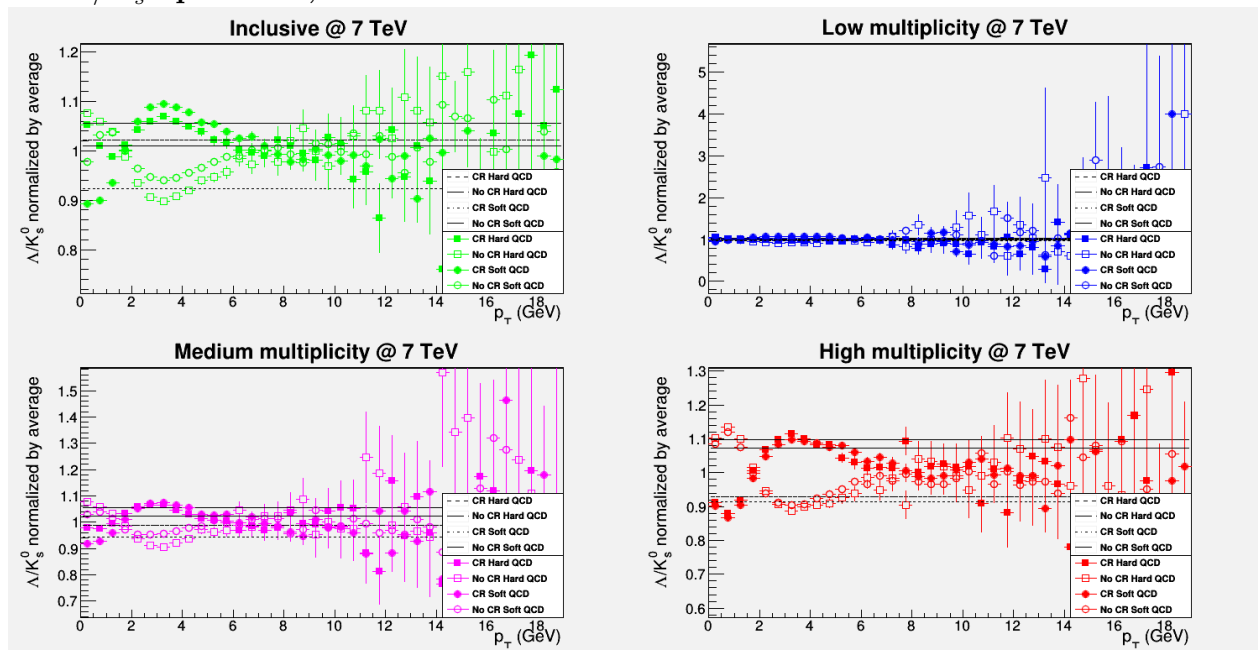
16: Λ/K_s^0 spectrum

Figure 16: This figure shows the transverse momentum spectra of the Λ/K_s^0 ratio using data from pp collision simulations at 7 TeV. It contains four plots. Each plot shows data for one specific multiplicity range. The top left plot shows data for the inclusive range, the top right plot for the low multiplicity range, the bottom left plot for the medium multiplicity range, and the bottom right plot for the high multiplicity range. Each plot contains four sets of data-points. These each represent the data for simulations using different Pythia tunes. The data-points with filled markers represent simulations with CR, while the data-points with empty markers represent simulations without CR. The data-points with square markers represent simulations using hard QCD, while the data-points with circular markers represent simulations using soft QCD.

approximately 0.03 at low p_T. After that, the value increases slowly, until it reaches approximately 0.045 somewhere around 6 to 8 p_T. At higher p_T the value stays about the same.

This is different from what we saw for the experimental behavior of the Λ_c/D^0 ratio transverse momentum spectra in pp collisions. The experimental behavior was shown in figure 3. There we saw a decrease for higher p_T, instead of an increase.

However, in figure 3 the uncertainties in the data are extremely large. Therefore it is difficult to definitively conclude whether the Λ_c/D^0 ratio transverse momentum spectra from our simulations conflict with experimental data.

Next, we want to know whether we can observe any multiplicity-dependent effects of turning on CR. In figure 16 we did this for the Λ/K_s^0 ratio by comparing the upper right and lower right plots, showing data for low and high multiplicity respectively. We now repeat this comparison in the same manner for figure 17.

Looking at the plots, it is a lot harder here to observe any effects due to turning on CR. Most of the filled data-points, representing data from simulations with CR turned on, lie very close to the empty data-points, representing data from simulations with CR turned off. The differences between the two seem to mostly fall within the range of the uncertainty in the data-points.

The one exception to this can be seen in the lower right plot of figure 17. For low p_T, we see that the data-points for the Λ_c/D^0 ratio transverse momentum spectra for simulations with CR lie significantly below those for simulations without CR. This is the same effect as can be seen in the lower right plot of figure 16.

This effect could be explained with a multiplicity-dependent common velocity boost. If the particles receive a boost, relatively fewer of them will have such a low transverse momentum. The baryons, whose transverse momentum is boosted more than that of the mesons, will become comparatively more unlikely

to be found at low p_T. This would then result in a lowering of the baryon over meson ratio transverse momentum spectrum at low p_T, as observed here.

Nevertheless, we can not simply conclude the presence of a common velocity boost from merely the first two data-points of figure 17. This would be reading into the data too much. Though there seems to be some minor indication of the effects of a common velocity boost, we can not draw a definitive conclusion from this representation of the data.

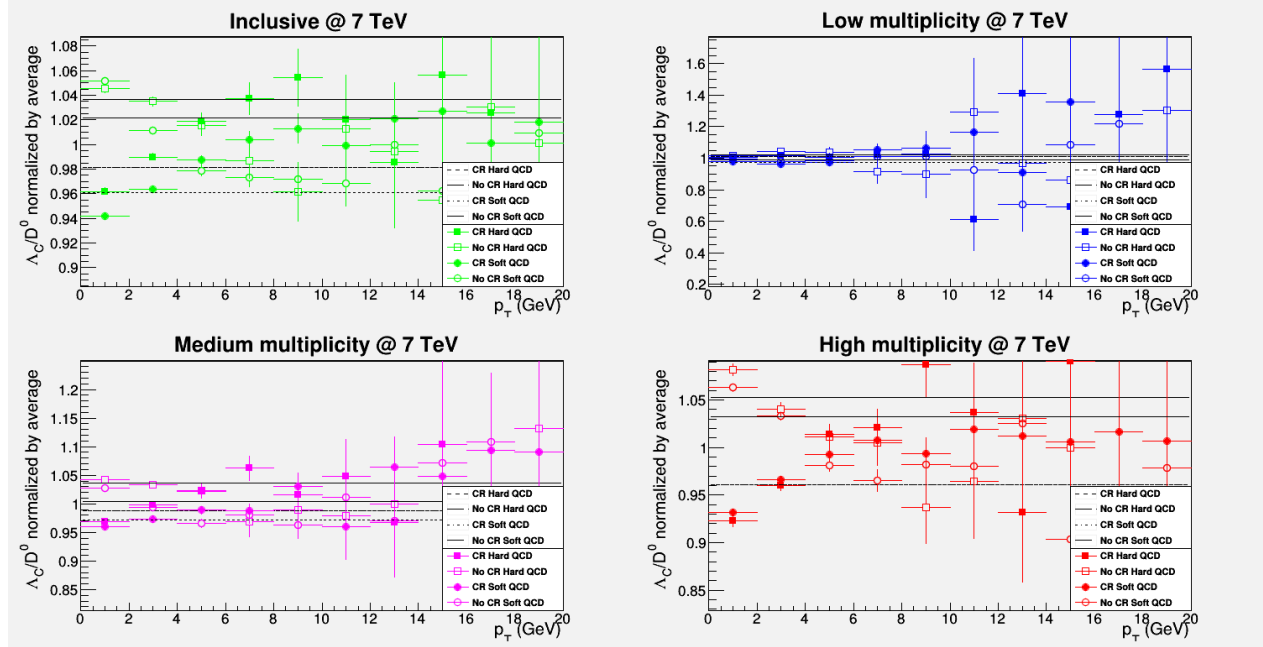## 17: Λ_c/D^0 spectrum

Figure 17: This figure shows the transverse momentum spectra of the Λ_c/D^0 ratio using data from pp collision simulations at 7 TeV. It contains four plots. Each plot shows data for one specific multiplicity range. The top left plot shows data for the inclusive range, the top right plot for the low multiplicity range, the bottom left plot for the medium multiplicity range, and the bottom right plot for the high multiplicity range. Each plot contains four sets of data-points. These each represent the data for simulations using different Pythia tunes. The data-points with filled markers represent simulations with CR, while the data-points with empty markers represent simulations without CR. The data-points with square markers represent simulations using hard QCD, while the data-points with circular markers represent simulations using soft QCD.

However, it might still be possible to make any effects of CR more easily visible by using a different representation of the data. Let us consider the same baryon over meson ratio transverse momentum spectrum plots as before. This time however, we normalize the spectra differently. We take the average p_T spectrum of the the four Pythia tunes present in each figure, then divide each spectrum by that average. This should make relative differences between the tunes more readily apparent.

We have already concluded that CR introduces a multiplicity-dependent boost for lighter flavor baryons and mesons. For this, we used figure 16. We will now use this earlier conclusion to our advantage. By first looking what this new representation of the data does to figure 16, we will gain an expectation of what the multiplicity-dependent boost due to CR looks like in this new representation. Then we will prepare this to the new representation of the data in figure 17, to conclude whether we see similar effects due to CR there.

The new representation of the data for the Λ/K_s^0 ratio transverse momentum spectra can be seen in figure 18. Similarly to figure 16, this figure contains four plots, each corresponding to a different multiplicity range. Each plot again contains four sets of data-points, were each set represents data for a specific Pythia tune. These tunes are marked in the same manner as before. In addition, a constant fit has been made to each set of data-points. The fit-lines, and which data-set they belong to, can be seen in the legend of the

figure.

From this figure we hope to gain an expectation of what the CR-induced multiplicity dependence of the baryon over meson ratio transverse momentum spectra looks like in this new representation. This will help us interpret the newly represented data for the Λ_c/D^0 ratio transverse momentum spectra.

Looking at figure 18, we again compare the upper-right and lower-right plot. In the upper-right plot we see that, for low multiplicity, all data-points seem to lie close to the constant line through 1. This suggests that at low multiplicity, there is little to no dependence of the Λ/K_s^0 ratio transverse momentum spectra on CR or QCD type. In the lower-right plot however, there does seem to be a dependence on CR. Specifically, we see that at low p_T, the filled data-points representing the data from simulations with CR, lie below the empty data-points representing the data from simulations without CR. Around 2 GeV p_T the two cross. Then from 2 GeV to around 6 GeV p_T, the filled data-points lie above the empty data-points, but they grow gradually closer again. After 6 GeV p_T the empty and filled data-points roughly overlap, with any differences between the two well within the bounds of simple statistical effects.

This behavior in the new representation of the data follows directly from the CR-induced multiplicity dependence observed in figure 16. The filled data-points are first below the empty ones at p_T below 2 GeV, then the filled data-points are above the empty ones for 2 to 6 GeV, and at higher p_T the filled and empty data-points lie roughly on top of one another. This new representation of the data simply makes these differences easier to see at a glance.

18: Λ/K_s^0 spectrum, normalized

Figure 18: This figure shows the differently normalized transverse momentum spectra of the Λ/K_s^0 ratio using data from pp collision simulations at 7 TeV. This figure is derived from figure 16 by taking the average over all four data-sets in one of the plots, and dividing by it. It contains four plots. Each plot shows data for one specific multiplicity range. The top left plot shows data for the inclusive range, the top right plot for the low multiplicity range, the bottom left plot for the medium multiplicity range, and the bottom right plot for the high multiplicity range. Each plot contains four sets of data-points. These each represent the data for simulations using different Pythia tunes. The data-points with filled markers represent simulations with CR, while the data-points with empty markers represent simulations without CR. The data-points with square markers represent simulations using hard QCD, while the data-points with circular markers represent simulations using soft QCD. There are four fit-lines in each plot. Each represents a fit to one specific tune using a constant function. Which line corresponds to which tune can be seen in the legends.

Now we know what the multiplicity-dependent shift of the Λ/K_s^0 ratio transverse momentum spectra looks like in this new representation. Next, we will try to determine if we can observe a similar effect for the Λ_c/D^0 ratio.

See figure 19. In this figure, we look at the new representation of the Λ_c/D^0 ratio transverse momentum spectra. The figure consists of four plots, each showing the data for a different multiplicity range. Each plot contains four sets of data-points, each of which corresponds to a specific Pythia tune. As before, the tunes can be distinguished by their markers.

We again focus on the upper-right and lower-right plot. In the upper-right plot, which shows the data for low multiplicity, the filled data-points and the empty data-points, representing simulations with and without CR respectively, lie roughly on top of one another. The differences between the tunes seems to fall within the range where they can be explained by purely statistical effects. It appears that at low multiplicity, there is no dependence of the Λ_c/D^0 ratio transverse momentum spectra on turning on or off CR.

In the lower-right plot, which shows the data for high multiplicity, the filled data-points and the empty data-points clearly behave differently. from one another. This difference is very pronounced in the first two bins. In these bins, the filled data-points lie below the empty data-points, with a difference of many standard deviations. This is in line with the behavior observed in figure 18.

For the other bins however, the uncertainties in the data quickly become quite large. In the end, we are unable to definitively conclude whether there is a dependence of the Λ_c/D^0 ratio transverse momentum spectra on turning on or off CR.

To summarize; the p/π and Λ/K_s^0 ratio transverse momentum spectra show behavior that indicates the presence of a multiplicity-dependent common velocity boost induced by turning on CR. We are unable to draw the same conclusion for the Λ_c/D^0 ratio transverse momentum spectra, possibly because of a lack of statistics.

19: Λ_c/D^0 spectrum, normalized

Figure 19: This figure shows the differently normalized transverse momentum spectra of the Λ_c/D^0 ratio using data from pp collision simulations at 7 TeV. This figure is derived from figure 17 by taking the average over all four data-sets in one of the plots, and dividing by it. It contains four plots. Each plot shows data for one specific multiplicity range. The top left plot shows data for the inclusive range, the top right plot for the low multiplicity range, the bottom left plot for the medium multiplicity range, and the bottom right plot for the high multiplicity range. Each plot contains four sets of data-points. These each represent the data for simulations using different Pythia tunes. The data-points with filled markers represent simulations with CR, while the data-points with empty markers represent simulations without CR. The data-points with square markers represent simulations using hard QCD, while the data-points with circular markers represent simulations using soft QCD. There are four fit-lines in each plot. Each represents a fit to one specific tune using a constant function. Which line corresponds to which tune can be seen in the legends.

4.2.2   Energy-dependent effects

We will now consider the dependence of the baryon over meson ratio transverse momentum spectra on the center-of-mass energy of the simulations.

Please refer to figures 20 and 21. These figures show the baryon over meson transverse momentum spectra from pp collision simulations at low and high multiplicity respectively. Each contains twelve separate plots, arranged in three columns and four rows. The columns, from left to right, show the data for different flavors. The first shows data for p/π ratio spectra, the second for Λ/K_s^0 ratio spectra, and the third for Λ_c/D^0 ratio spectra. The rows, from top to bottom, show data for different Pythia tunes. The first shows data for simulations with CR using hard QCD, the second shows data for simulations with CR and soft QCD, the third shows data for simulations without CR using hard QCD, and the fourth shows data for simulations without CR using soft QCD. Each plot contains two differently colored sets of data-points. The blue data-points represent simulations with an energy of 7 TeV, and the red data-points represent simulations with an energy of 13 TeV.

By arranging the spectra in this manner, we can easily determine whether there is any dependence on the center-of-mass energy of the simulation. We can do this by searching for the plots where the red and blue data-points do not overlap. If we find a plot where the red and blue data-points differ significantly, we will also immediately know for which tune, flavor, and multiplicity this dependence occurs.

Looking at figures 20 and 21, we see that the red and blue data-points practically overlap for all tunes, flavors and multiplicities. At higher p_T we sometimes see a difference between the data-points for both energies. However, these differences fall within the bounds imposed by the uncertainty of the data-points. We conclude that there seems to be no center-of-mass energy dependence in the simulations.

This conclusion mirrors the one found in the paper Vislavicius [17]. In this paper, there was found to be a center-of-mass energy dependence in the p/π ratio transverse momentum spectrum. They failed however to reproduce this dependence in simulations (using Pythia 8 and the Monash tune, similarly to our setup).

To summarize, the lack of a center-of-mass energy dependence in our simulation data for the baryon over meson ratio transverse momentum spectra seems to signal a discrepancy between the simulation and the real experiment. This suggests that, in this regard, there is still room for improvement in our model of pp collisions. However, this should have no direct bearing on our goal to determine the viability of simulating QGP-like effects in pp collisions using CR.

20: Ratio spectra for all flavors, all tunes, and both energies, at low multiplicity
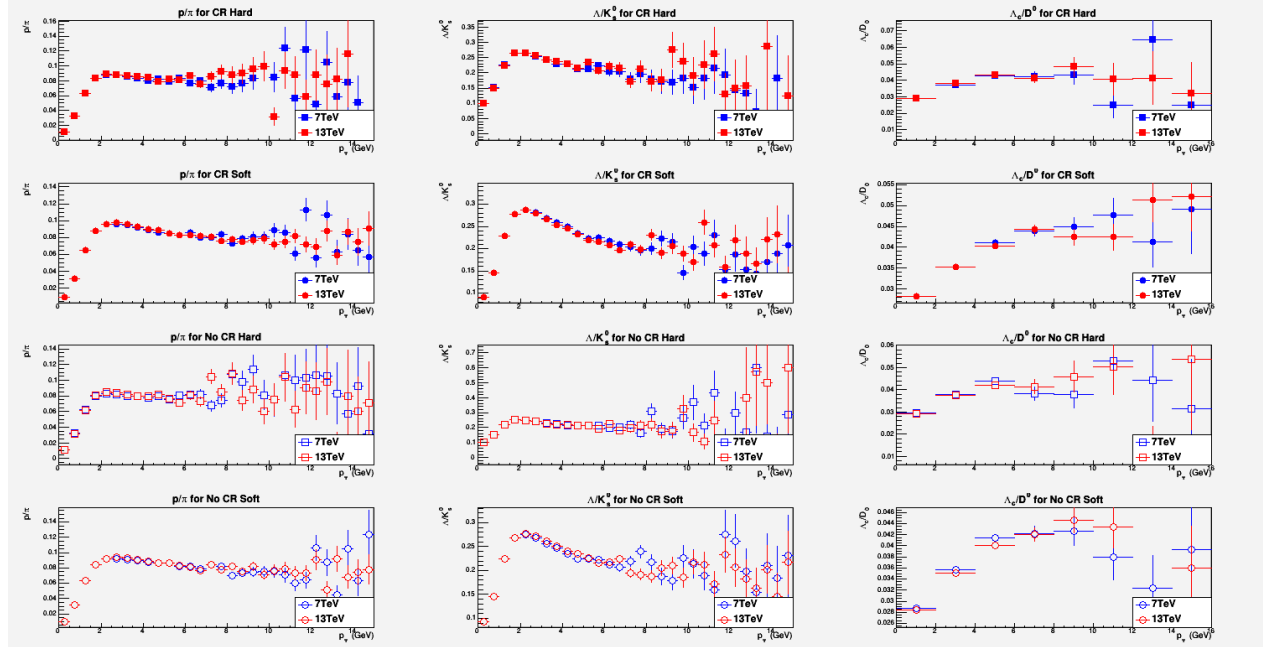
Figure 20: This figure shows the baryon over meson transverse momentum spectra from low multiplicity pp collision simulations. It contains twelve separate plots, arranged in three columns and four rows. The columns, from left to right, show the data for different flavors. The first shows data for p/π ratio spectra, the second for Λ/K_s^0 ratio spectra, and the third for Λ_c/D^0 ratio spectra. The rows, from top to bottom, show data for different Pythia tunes. The first shows data for simulations with CR using hard QCD, the second shows data for simulations with CR and soft QCD, the third shows data for simulations without CR using hard QCD, and the fourth shows data for simulations without CR using soft QCD. Each plot contains two differently colored sets of data-points. The blue data-points represent simulations with an energy of 7 TeV, and the red data-points represent simulations with an energy of 13 TeV. From this figure we can see that for all flavors and all tunes, the data-points for the two energies do not differ significantly from one another. It appears that for simulations at low multiplicity, the baryon over meson ratio spectra do not depend on the energy.

21: Ratio spectra for all flavors, all tunes, and both energies, at high multiplicity
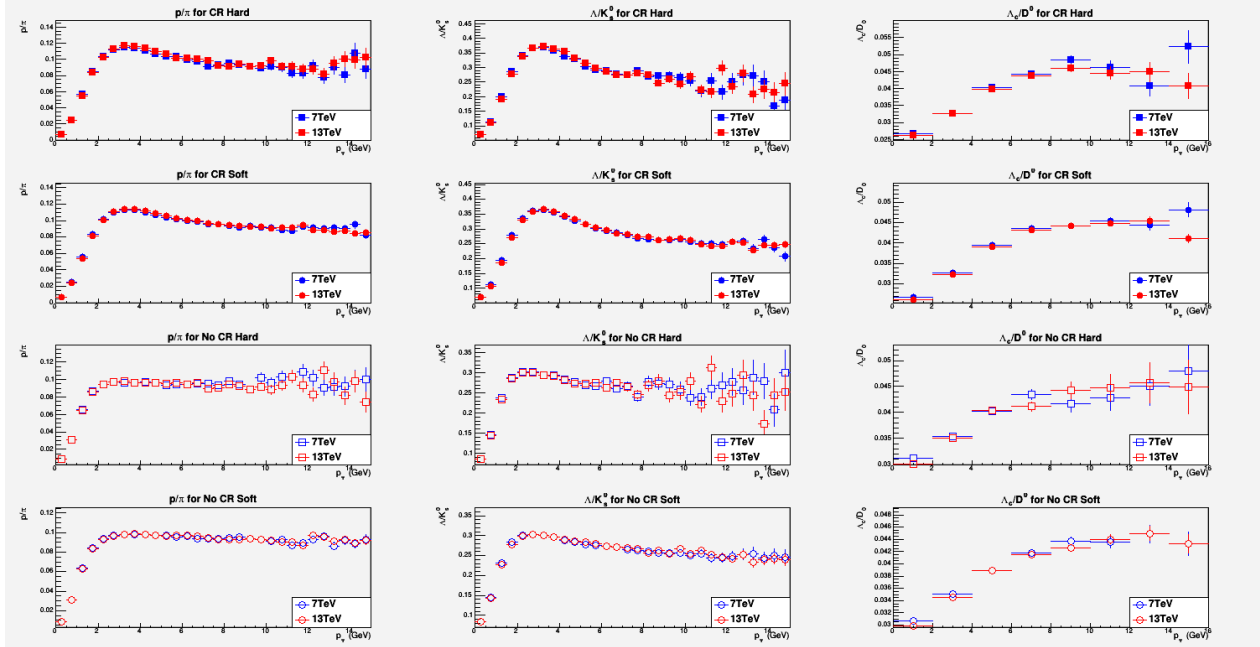
Figure 21: This figure shows the baryon over meson transverse momentum spectra from high multiplicity pp collision simulations. It contains twelve separate plots, arranged in three columns and four rows. The columns, from left to right, show the data for different flavors. The first shows data for p/π ratio spectra, the second for Λ/K_s^0 ratio spectra, and the third for Λ_c/D^0 ratio spectra. The rows, from top to bottom, show data for different Pythia tunes. The first shows data for simulations with CR using hard QCD, the second shows data for simulations with CR and soft QCD, the third shows data for simulations without CR using hard QCD, and the fourth shows data for simulations without CR using soft QCD. Each plot contains two differently colored sets of data-points. The blue data-points represent simulations with an energy of 7 TeV, and the red data-points represent simulations with an energy of 13 TeV. From this figure we can see that for all flavors and all tunes, the data-points for the two energies do not differ significantly from one another. It appears that for simulations at high multiplicity, the baryon over meson ratio spectra do not depend on the energy.

5   Conclusion and outlook

5.1   Conclusion

Using the Monash tune in Pythia 8.2, we confirm that turning on CR introduces a multiplicity-dependent effect in the tranverse momentum spectra of light-flavor particles. This effect qualitatively resembles the multiplicity-dependent shift in the baryon over meson ratio transverse momentum spectra observed experimentally in pp collisions.

We were unable to distinctly observe the same effect for charm flavor particles in the pp collision simulation, possibly because of a lack of statistics.

We found no dependence on the center-of-mass energy in the baryon over meson ratio transverse momentum spectra from our simulations.

Contrary to our expectations we did not observe an enhancement in the production of charm particles in hard QCD tunes compared to soft QCD tunes. Though there were some differences between the transverse momentum spectra for hard QCD versus soft QCD tunes, this dependence does not seem immediately relevant with regards to capturing the QGP-like effects present in experimental data from pp collisions.

We conclude that CR is a highly promising candidate for capturing QGP-like effects in simulations of pp collisions.

5.2   Outlook

There are a number of things in our research that could be improved upon.

Firstly, there is the definition of the inclusive (0-200), low (1-8), medium (9-24), and high (25-46) multiplicity ranges as discussed in section 3. Our definition of the multiplicity ranges was mainly motivated by the fact that it maintained the traditional ranges used in the discussion of charm particles. After running our simulations however, we found out that a significant number of events had such a high multiplicity that they fell above the 'high' multiplicity range. This can be clearly seen in figure 10 in particular.

We do not expect the omission of this data from our analysis to have changed our results in a qualitative manner. Nevertheless, throwing out valuable data in this manner is clearly bad practice. It seems wise to shift the upper boundary on the definition of the 'high' multiplicity range upwards. This would help to also include events with a higher multiplicity in our analysis, and thus raise the amount of statistics.

Another improvement that could be made would be to run a larger number of simulations. As it stands, we are unable to definitively conclude whether CR introduces a multiplicity dependent boost in the case of charm-flavor particles. This is possibly because we lack significant statistics, as charm-flavor particles are produced relatively rarely. If we were to run more simulations, we could perhaps solve this problem.

Another thing to mention is the fact that there were some observations about the data that we are unable to explain.

Most notably, we found that soft QCD caused an increased production of particles compared to hard QCD, for all flavors. This was discussed in section 4. We are unable to explain why using soft QCD as opposed to hard QCD would have this effect. The Pythia 8.2 manual[1] which discusses these settings in detail, does not offer an explanation.

We were also naively expecting that using hard QCD would enhance the production of charm flavor particles. This expectation was based on the supposition that hard interactions would be for more likely to have sufficient energy to produce the comparatively highly massive charm quarks. In our results we saw no such effects however. Here, as with all other particles, there seemed to be a larger number of particles being created when using soft QCD as compared to when using hard QCD.

There are a number of suggestions we would like to make for possible further research.

Firstly, it would be valuable to see whether we can also reach a quantitative agreement between simulations and experimental data. In this paper we have only concerned ourselves with qualitative observations. We have established that there is a qualitative agreement between the multiplicity dependent shift of the baryon over meson ratio transverse momentum spectra for the lighter flavored particles. The logical next

step is to see whether this agreement also holds on a quantitative level. If not, one could look into how to tune the simulations further in order to reach a quantitative agreement.

Another direction in which research could be done is on the topic of scaling up this simulation. We have confirmed that some QGP-like effects can be found back in simulations through the implementation of CR. However, this gives us no guarantee that the simulations using CR actually form a microscopical model of the system of QGP. If we could simulate a larger-scale system such as p-Pb or Pb-Pb collisions while using CR, we could test whether we can recover the macroscopic behavior of a QGP. This would then form a strong argument that CR is a correct way of modeling QGP microscopically.

It is important to note that this scaling up of the simulations might well be extremely difficult. There are certain to be problems with regards to computational power. Furthermore, simulations from first principles are notoriously difficult in the regime of Pb-Pb collisions. However, these things do not mean that such a simulation is strictly impossible. If done successfully it could provide many valuable insights.

6 Acknowledgments

A   Simulation multiplicity distributions

A.1   Multiplicity distributions @ 7TeV

A.1: Multiplicity distribution for CR and Hard QCD @ 7 TeV
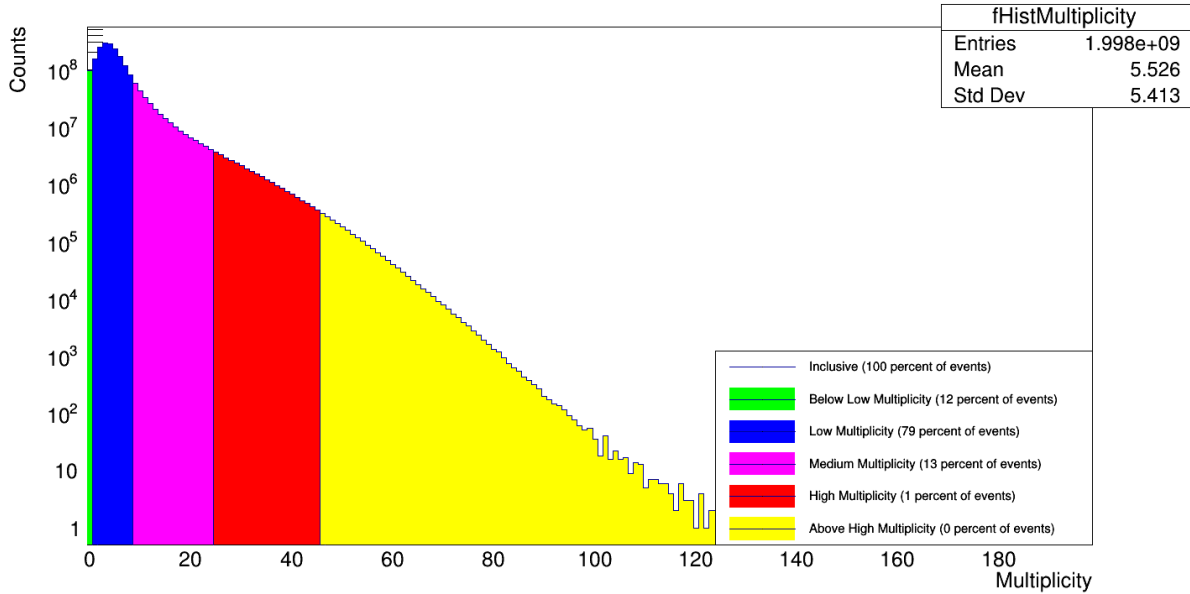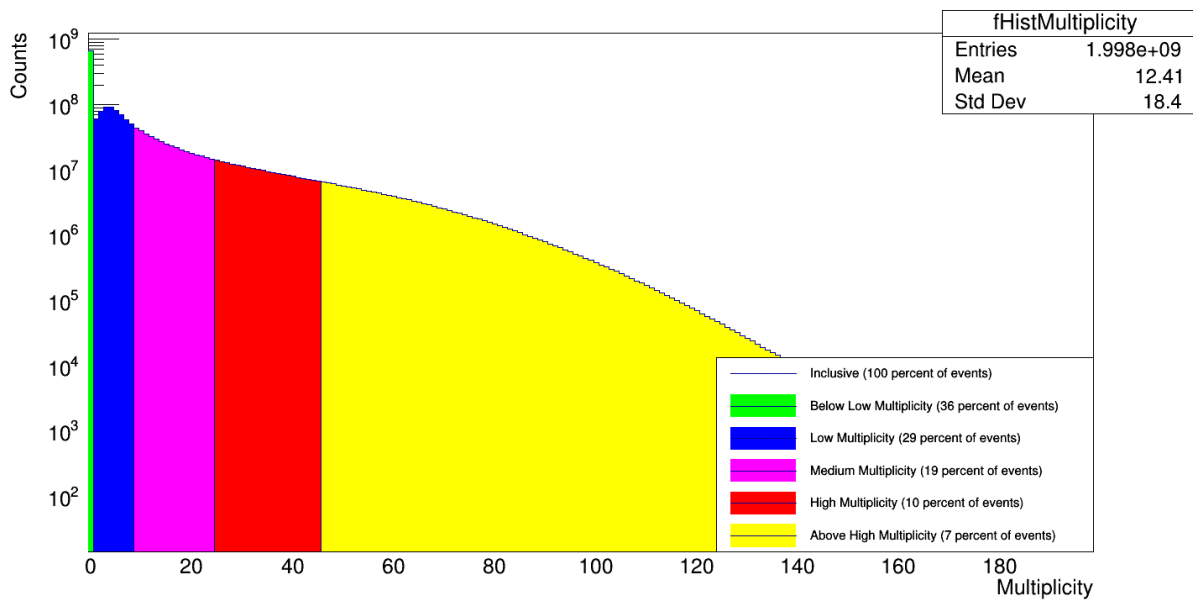

Figure A.1: This figure shows the multiplicity distribution of roughly $2 * 10^9$ pp collisions, simulated with CR, using hard QCD, at a center-of-mass energy of 7 TeV. The figure has been subdivided in five regions, each marked with a distinct color. The blue, purple, and red regions correspond to the low (1-8), medium (9-24) and high (25-46) multiplicity ranges respectively. The green region corresponds to events with a multiplicity of zero. The yellow region corresponds to events with a multiplicity that falls above our definition of the high multiplicity range.

A.2: Multiplicity distribution for No CR and Hard QCD @ 7 TeV
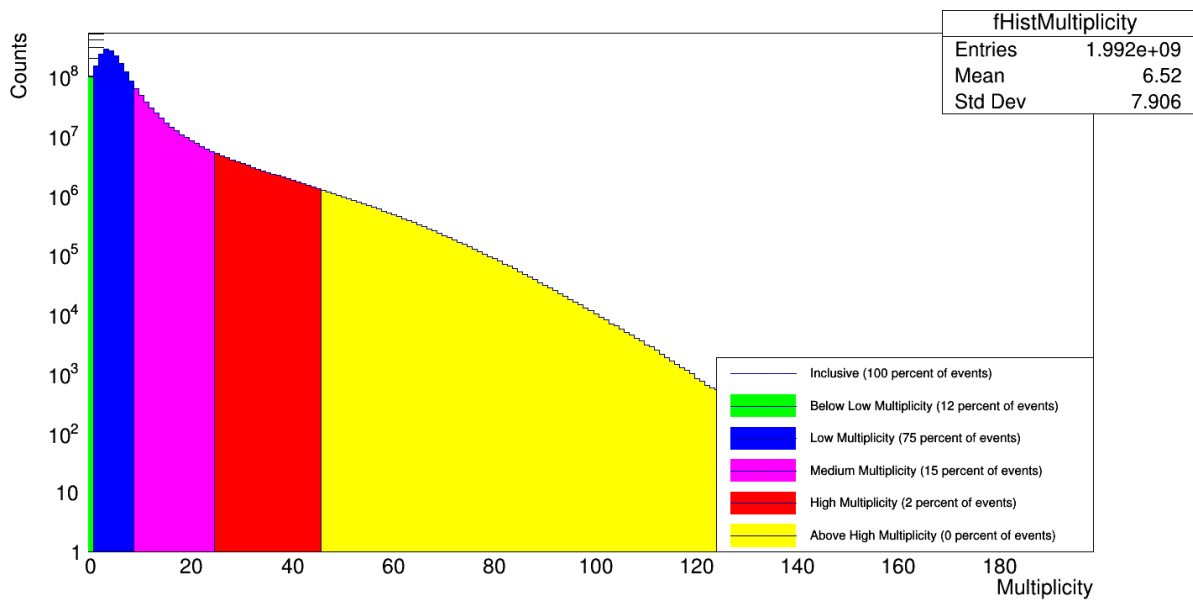
Figure A.2: This figure shows the multiplicity distribution of roughly $2*10^9$ pp collisions, simulated without CR, using hard QCD, at a center-of-mass energy of 7 TeV. The figure has been subdivided in five regions, each marked with a distinct color. The blue, purple, and red regions correspond to the low (1-8), medium (9-24) and high (25-46) multiplicity ranges respectively. The green region corresponds to events with a multiplicity of zero. The yellow region corresponds to events with a multiplicity that falls above our definition of the high multiplicity range.

A.3: Multiplicity distribution for CR and Soft QCD @ 7 TeV
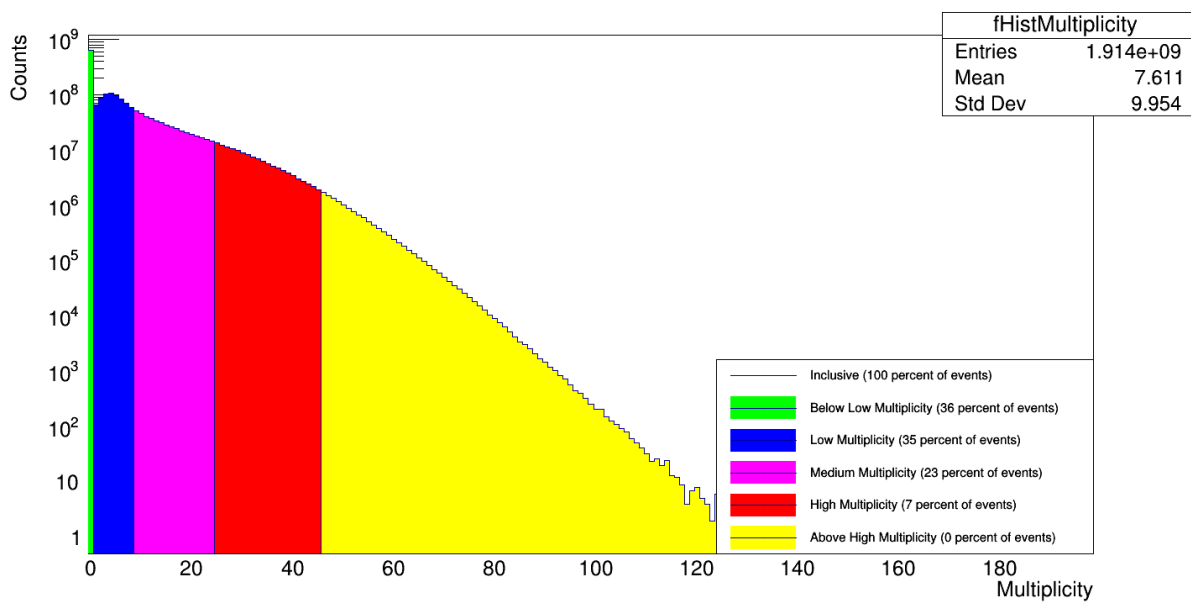
Figure A.3: This figure shows the multiplicity distribution of roughly $2 * 10^9$ pp collisions, simulated with CR, using soft QCD, at a center-of-mass energy of 7 TeV. The figure has been subdivided in five regions, each marked with a distinct color. The blue, purple, and red regions correspond to the low (1-8), medium (9-24) and high (25-46) multiplicity ranges respectively. The green region corresponds to events with a multiplicity of zero. The yellow region corresponds to events with a multiplicity that falls above our definition of the high multiplicity range.

A.4: Multiplicity distribution for No CR and Soft QCD @ 7 TeV
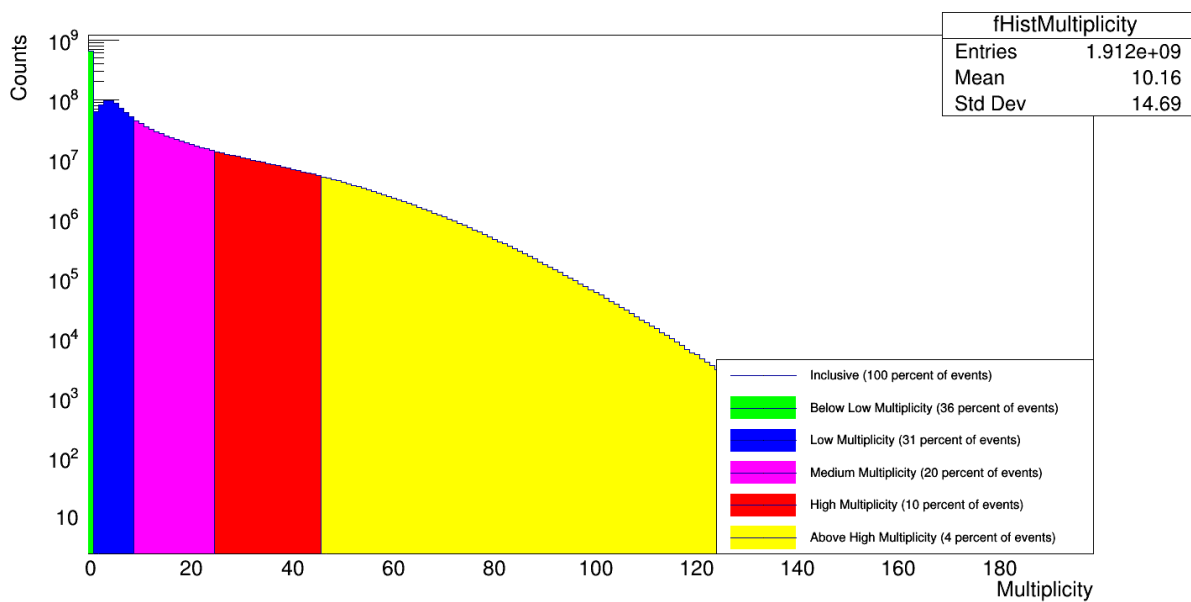
Figure A.4: This figure shows the multiplicity distribution of roughly $2 * 10^9$ pp collisions, simulated without CR, using soft QCD, at a center-of-mass energy of 7 TeV. The figure has been subdivided in five regions, each marked with a distinct color. The blue, purple, and red regions correspond to the low (1-8), medium (9-24) and high (25-46) multiplicity ranges respectively. The green region corresponds to events with a multiplicity of zero. The yellow region corresponds to events with a multiplicity that falls above our definition of the high multiplicity range.

A.2   Multiplicity distributions @ 13 TeV

A.5: Multiplicity distribution for CR and Hard QCD @ 13 TeV
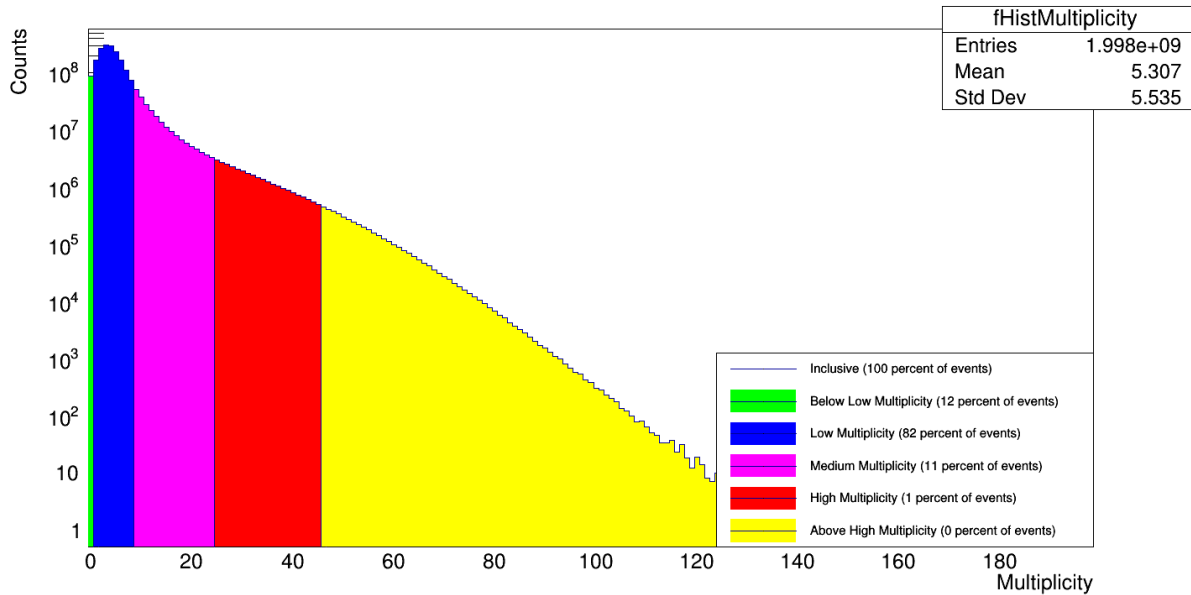
Figure A.5: This figure shows the multiplicity distribution of roughly $2*10^9$ pp collisions, simulated with CR, using hard QCD, at a center-of-mass energy of 13 TeV. The figure has been subdivided in five regions, each marked with a distinct color. The blue, purple, and red regions correspond to the low (1-8), medium (9-24) and high (25-46) multiplicity ranges respectively. The green region corresponds to events with a multiplicity of zero. The yellow region corresponds to events with a multiplicity that falls above our definition of the high multiplicity range.

A.6: Multiplicity distribution for No CR and Hard QCD @ 13 TeV
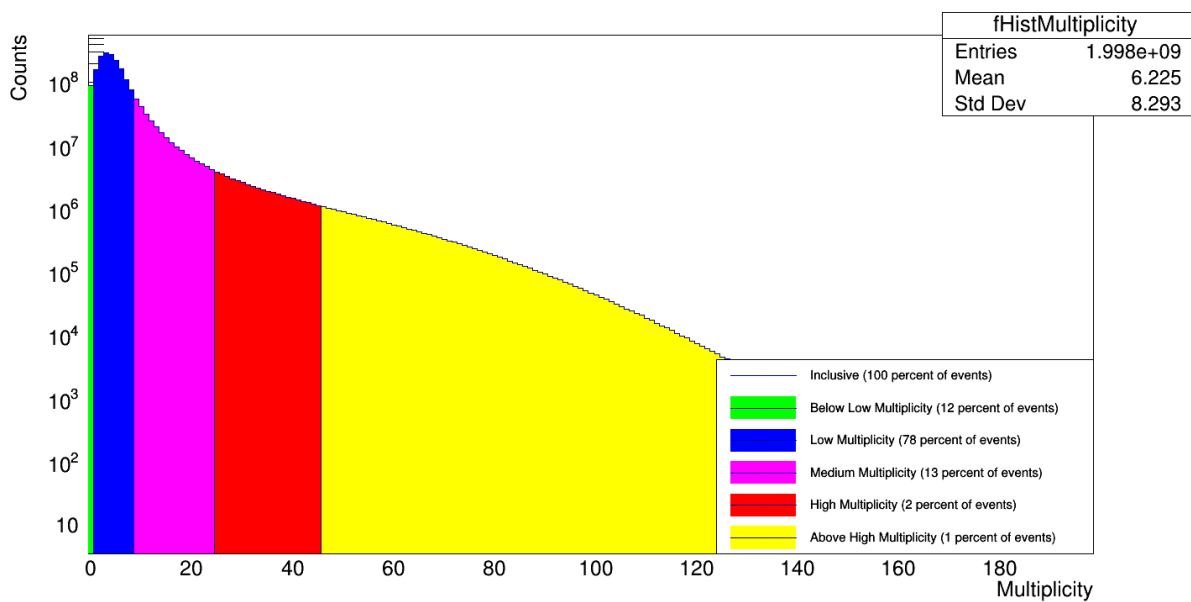
Figure A.6: This figure shows the multiplicity distribution of roughly $2 * 10^9$ pp collisions, simulated without CR, using hard QCD, at a center-of-mass energy of 13 TeV. The figure has been subdivided in five regions, each marked with a distinct color. The blue, purple, and red regions correspond to the low (1-8), medium (9-24) and high (25-46) multiplicity ranges respectively. The green region corresponds to events with a multiplicity of zero. The yellow region corresponds to events with a multiplicity that falls above our definition of the high multiplicity range.

A.7: Multiplicity distribution for CR and Soft QCD @ 13 TeV
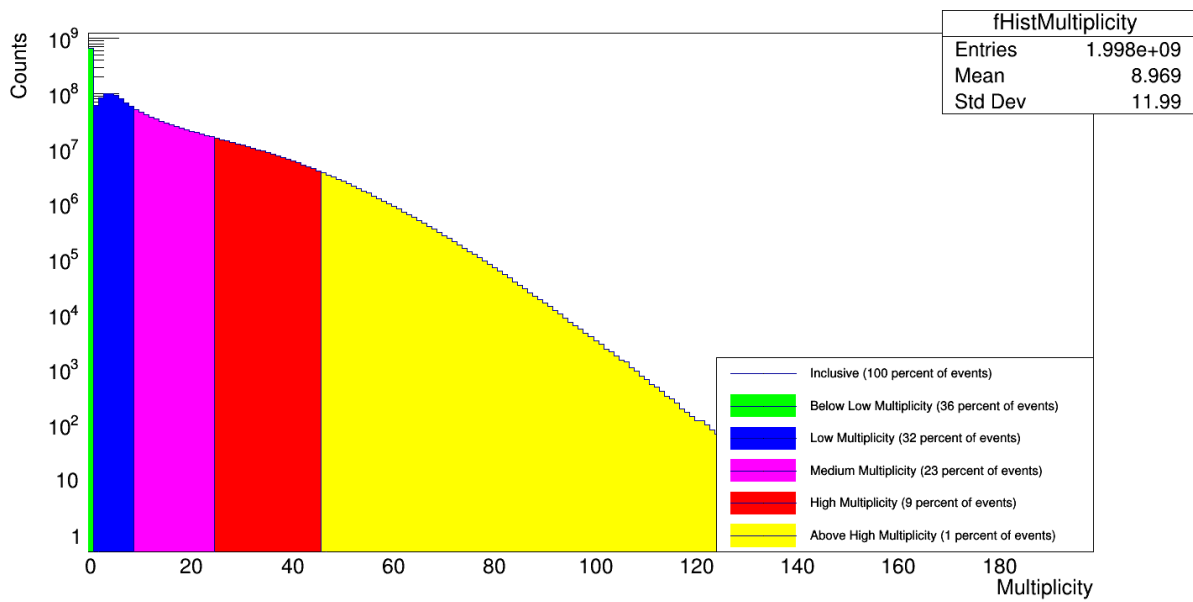
Figure A.7: This figure shows the multiplicity distribution of roughly $2*10^9$ pp collisions, simulated with CR, using soft QCD, at a center-of-mass energy of 13 TeV. The figure has been subdivided in five regions, each marked with a distinct color. The blue, purple, and red regions correspond to the low (1-8), medium (9-24) and high (25-46) multiplicity ranges respectively. The green region corresponds to events with a multiplicity of zero. The yellow region corresponds to events with a multiplicity that falls above our definition of the high multiplicity range.

A.8: Multiplicity distribution for No CR and Soft QCD @ 13 TeV

Figure A.8: This figure shows the multiplicity distribution of roughly $2 * 10^9$ pp collisions, simulated without CR, using soft QCD, at a center-of-mass energy of 13 TeV. The figure has been subdivided in five regions, each marked with a distinct color. The blue, purple, and red regions correspond to the low (1-8), medium (9-24) and high (25-46) multiplicity ranges respectively. The green region corresponds to events with a multiplicity of zero. The yellow region corresponds to events with a multiplicity that falls above our definition of the high multiplicity range.

B   Simulation transverse momentum spectra @ 7 TeV

B.1   Multiplicities shown together @ 7 TeV

B.1: p spectrum
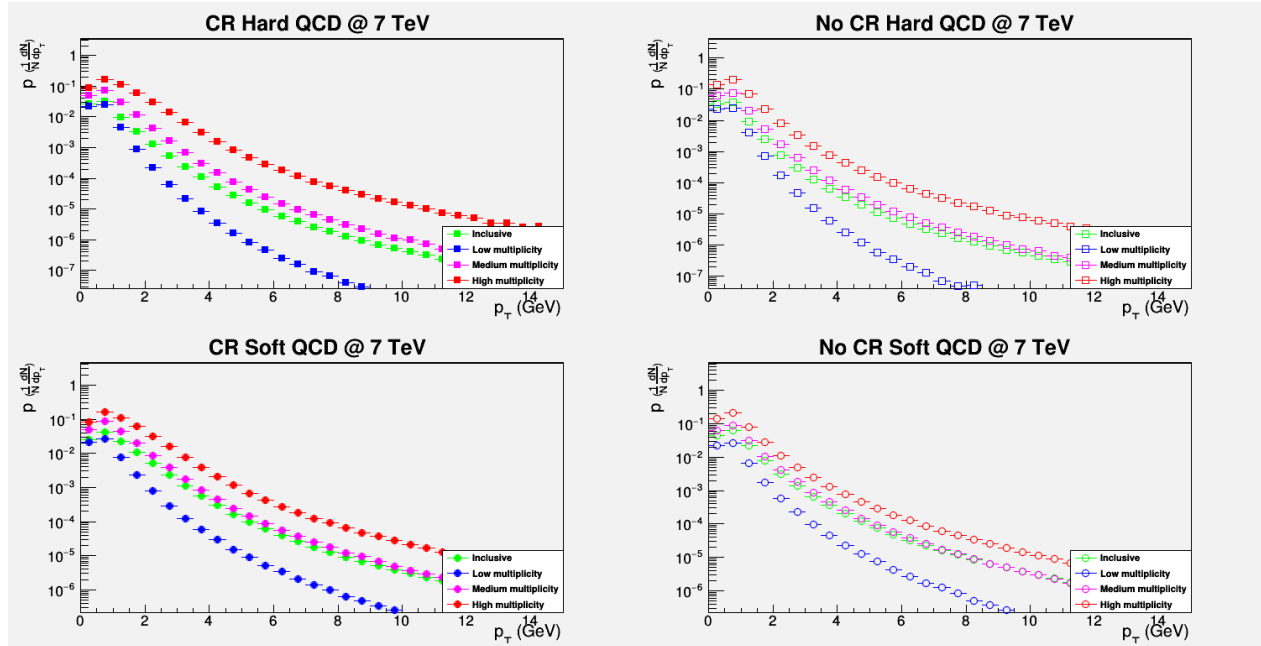
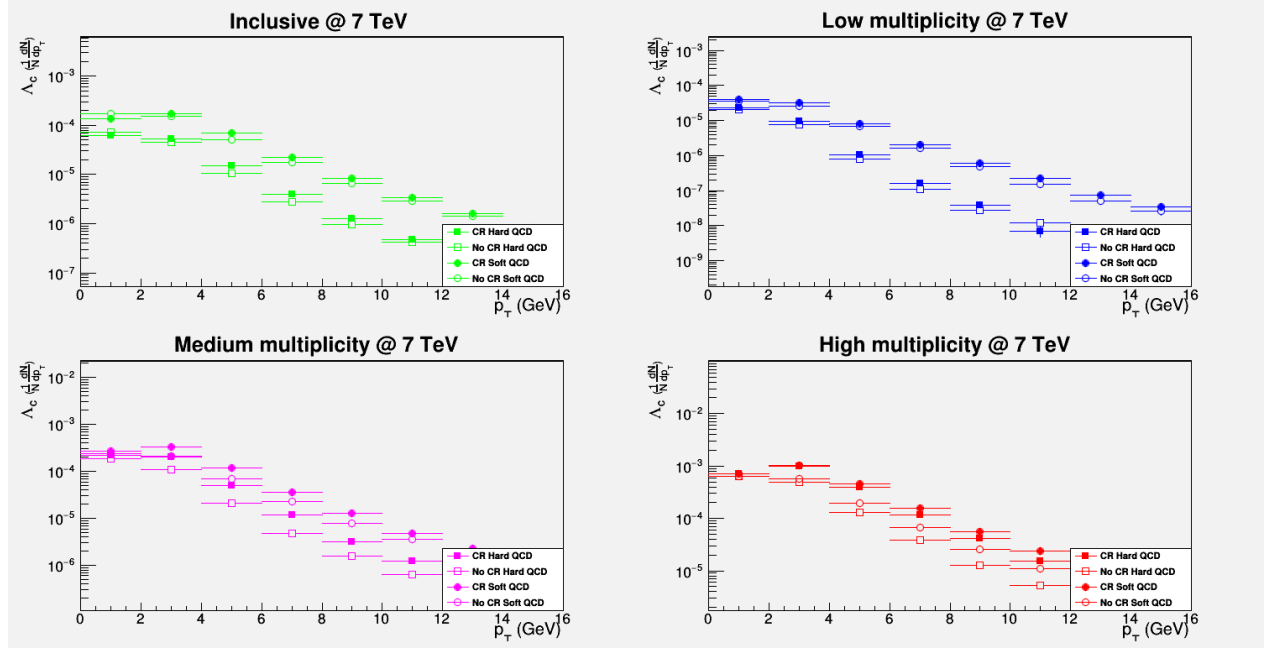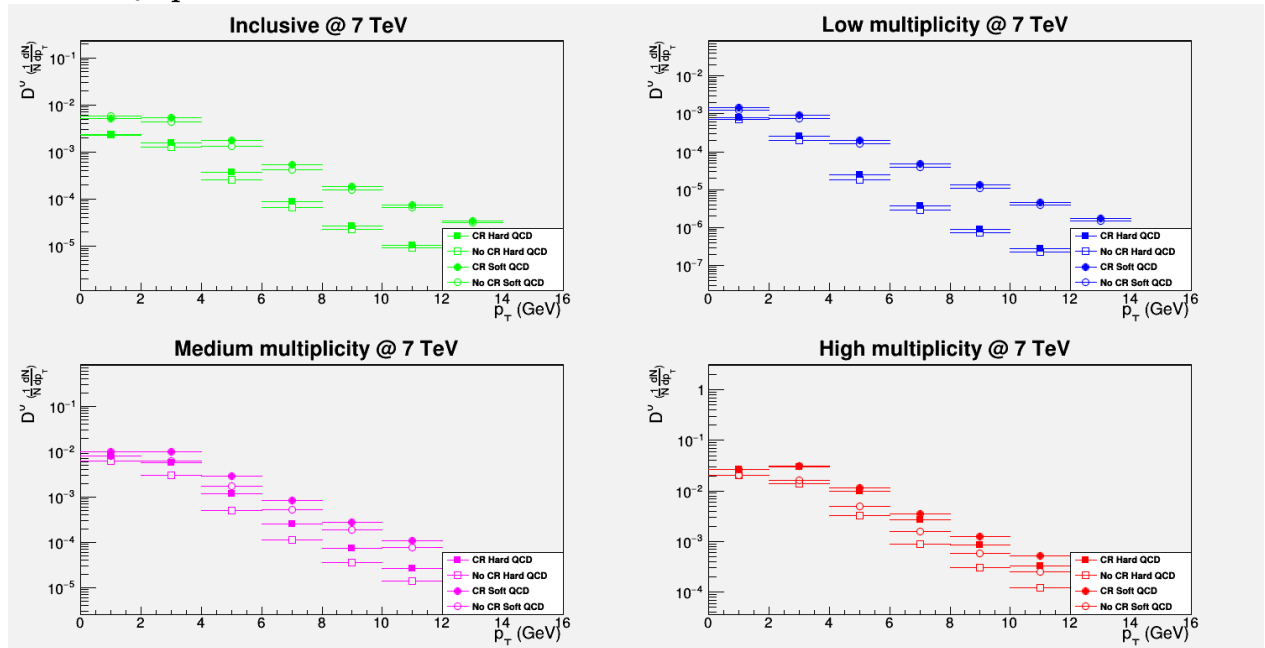Figure B.1: The p_T spectrum of the yield of p for simulations at 7 TeV, with all multiplicities shown together for each pythia tune

B.2   Pythia tunes shown together @ 7 TeV

B.2: π spectrum
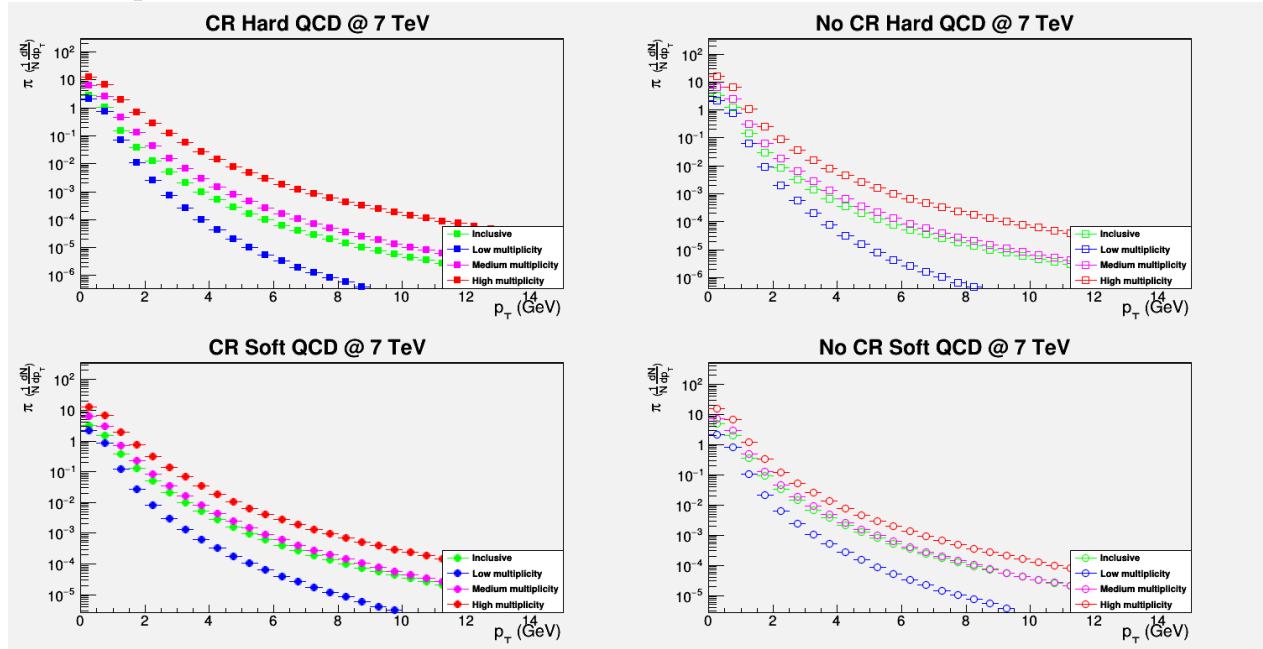
Figure B.2: The p_T spectrum of the yield of π for simulations at 7 TeV, with all multiplicities shown together for each pythia tune

C   Simulation transverse momentum spectra @ 13 TeV

C.1   Multiplicities shown together @ 13 TeV

C.2   Pythia tunes shown together @ 13 TeV

B.3: Λ spectrum
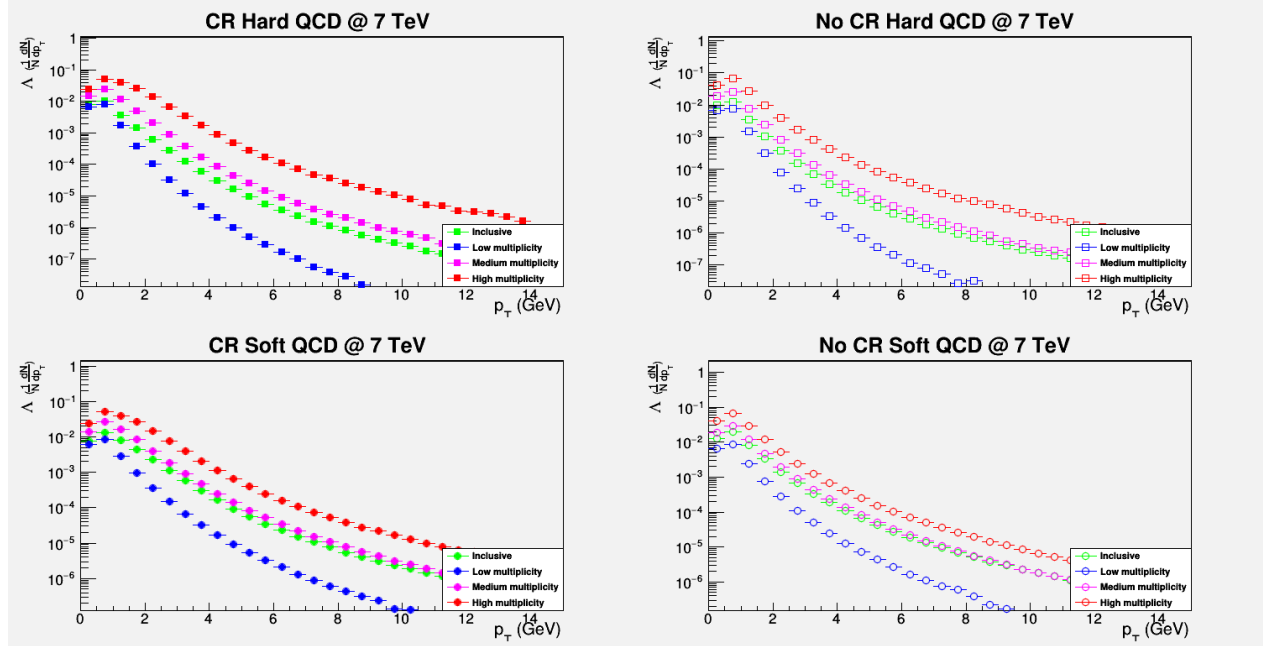
Figure B.3: The p_T spectrum of the yield of Λ for simulations at 7 TeV, with all multiplicities shown together for each pythia tune

B.4: K_0 spectrum
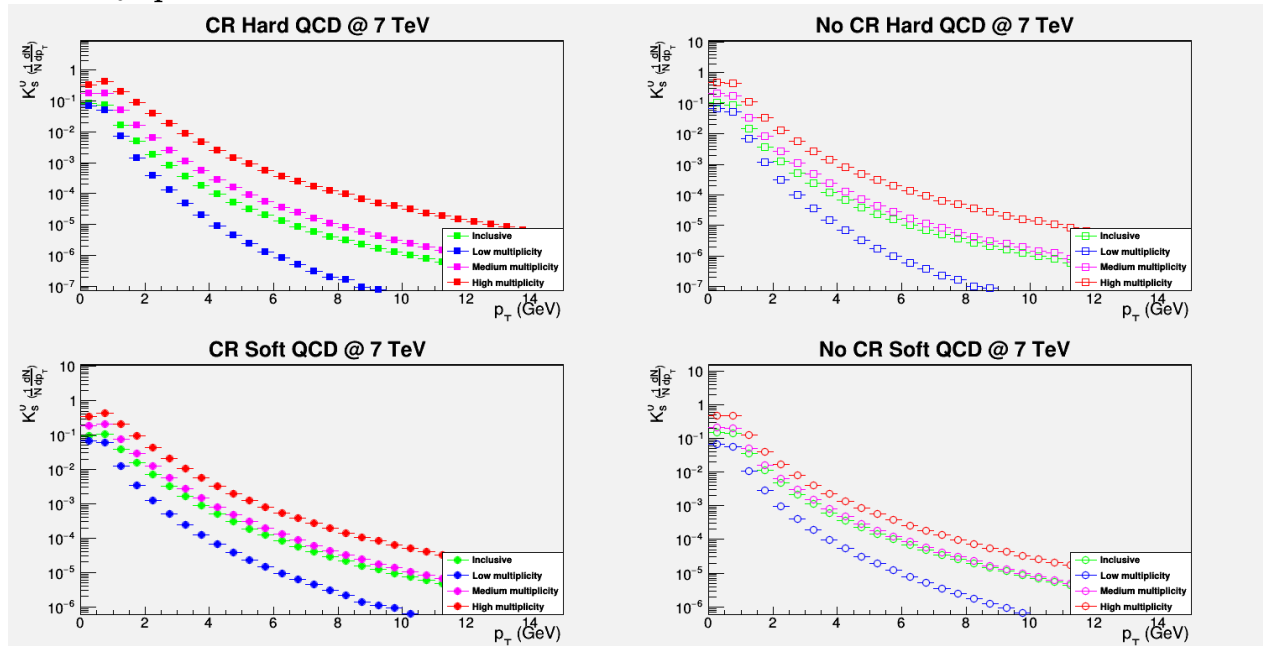
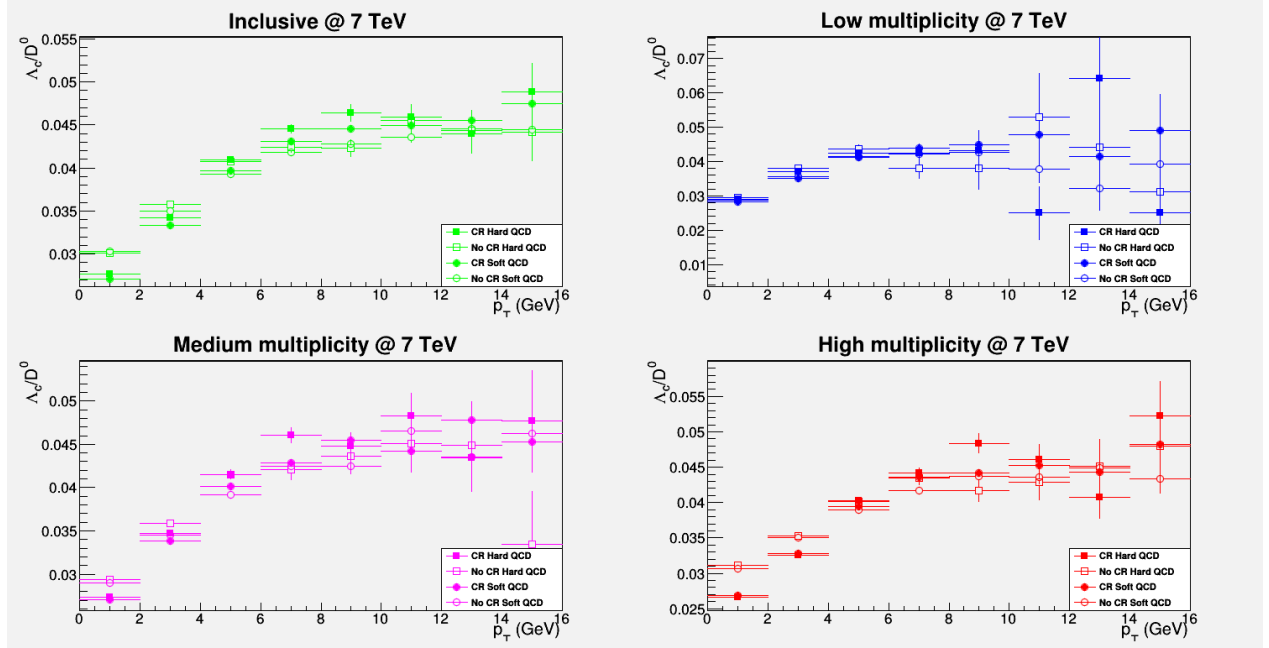Figure B.4: The p_T spectrum of the yield of K_0 for simulations at 7 TeV, with all multiplicities shown together for each pythia tune

B.5: Λ_c spectrum
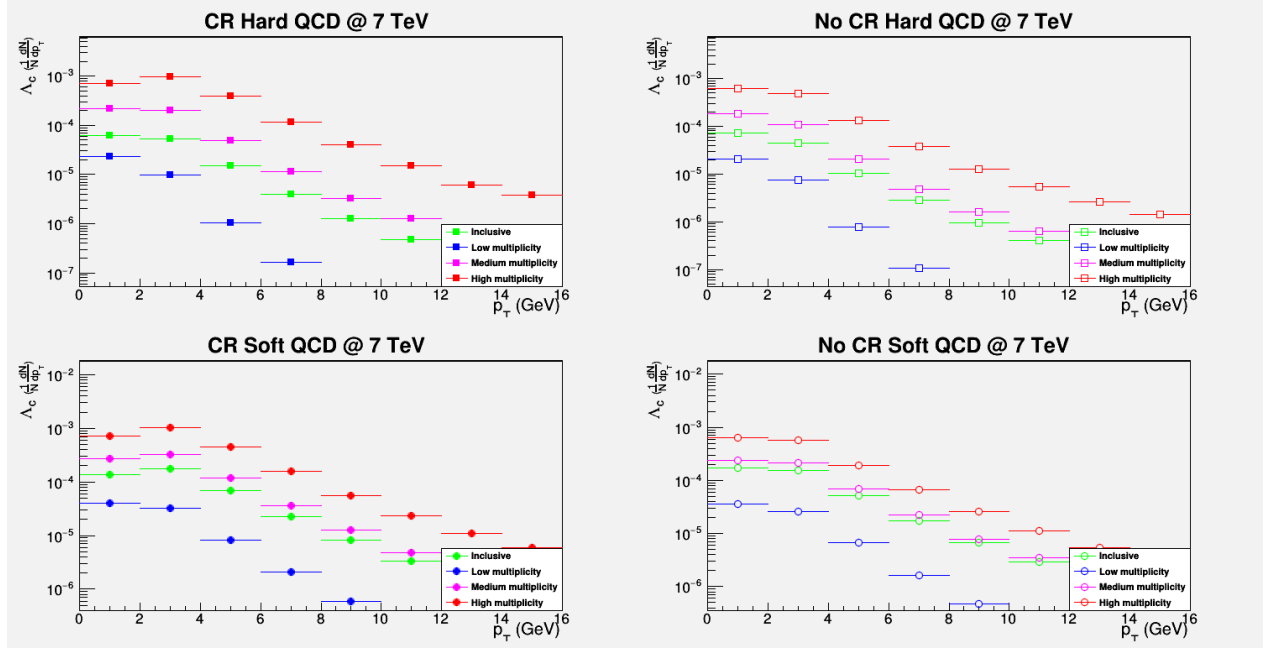
Figure B.5: The p_T spectrum of the yield of Λ_c for simulations at 7 TeV, with all multiplicities shown together for each pythia tune

B.6: D_0 spectrum
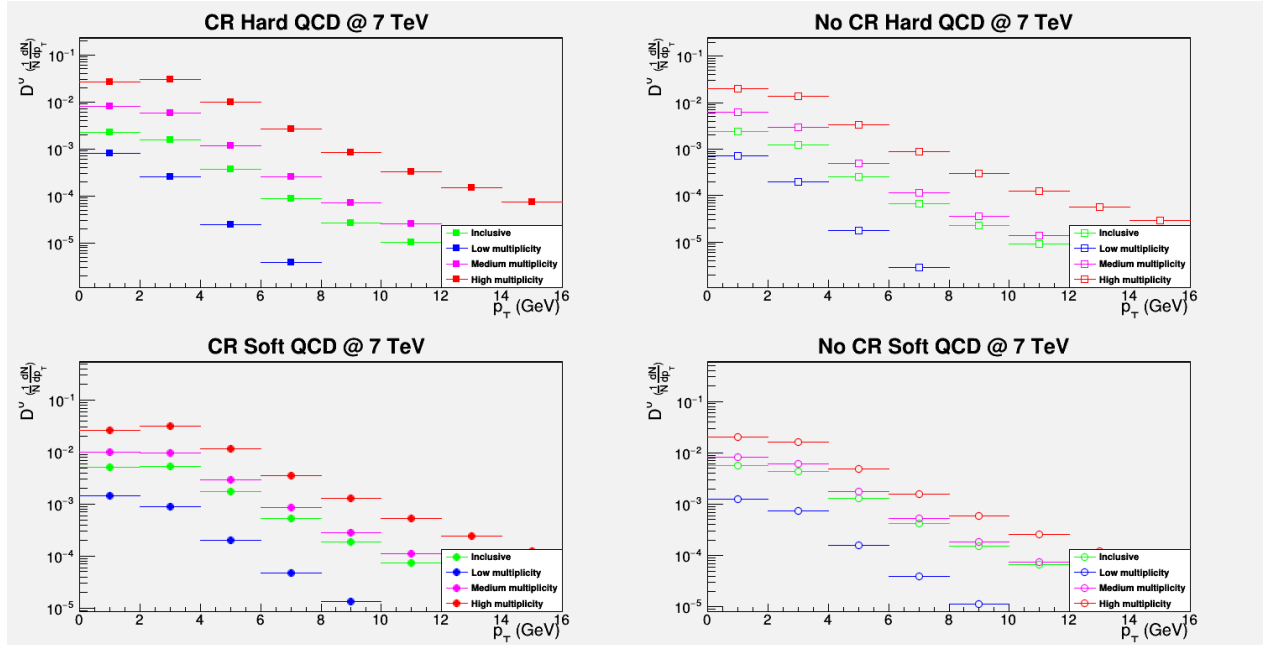
Figure B.6: The p_T spectrum of the yield of D_0 for simulations at 7 TeV, with all multiplicities shown together for each pythia tune

B.7: p/π spectrum
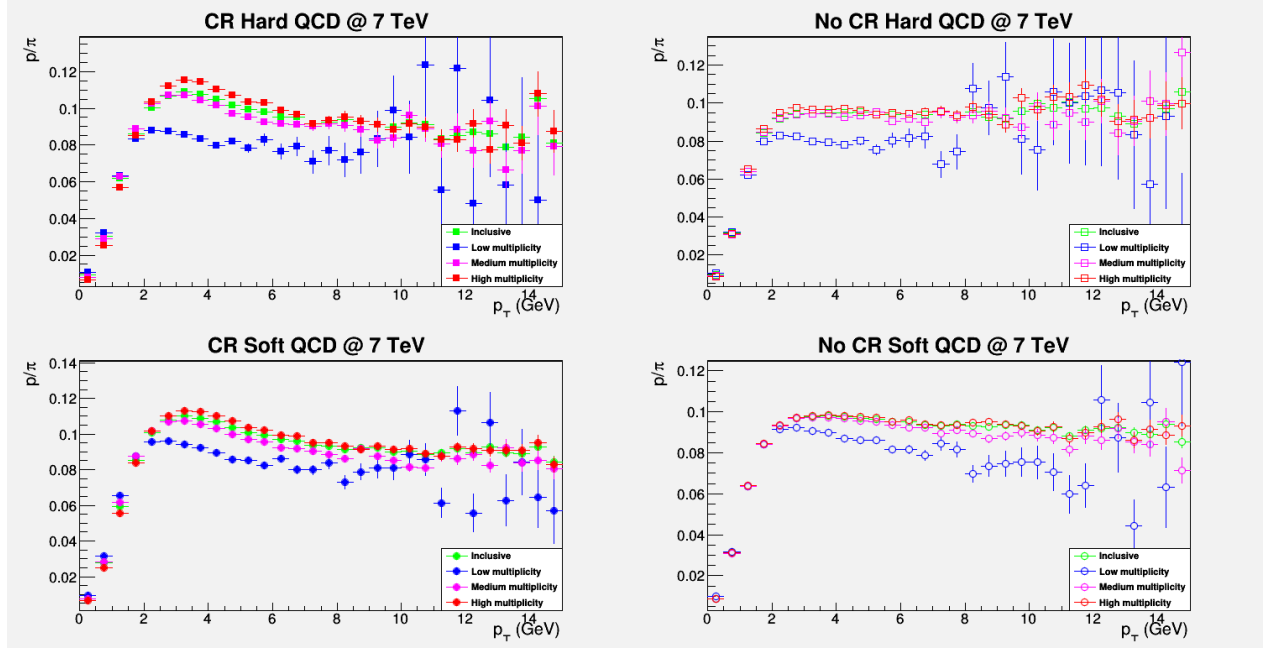
Figure B.7: The p_T spectrum of the yield ratio of p over π for simulations at 7 TeV, with all multiplicities shown together for each pythia tune

B.8: Λ/K_0 spectrum
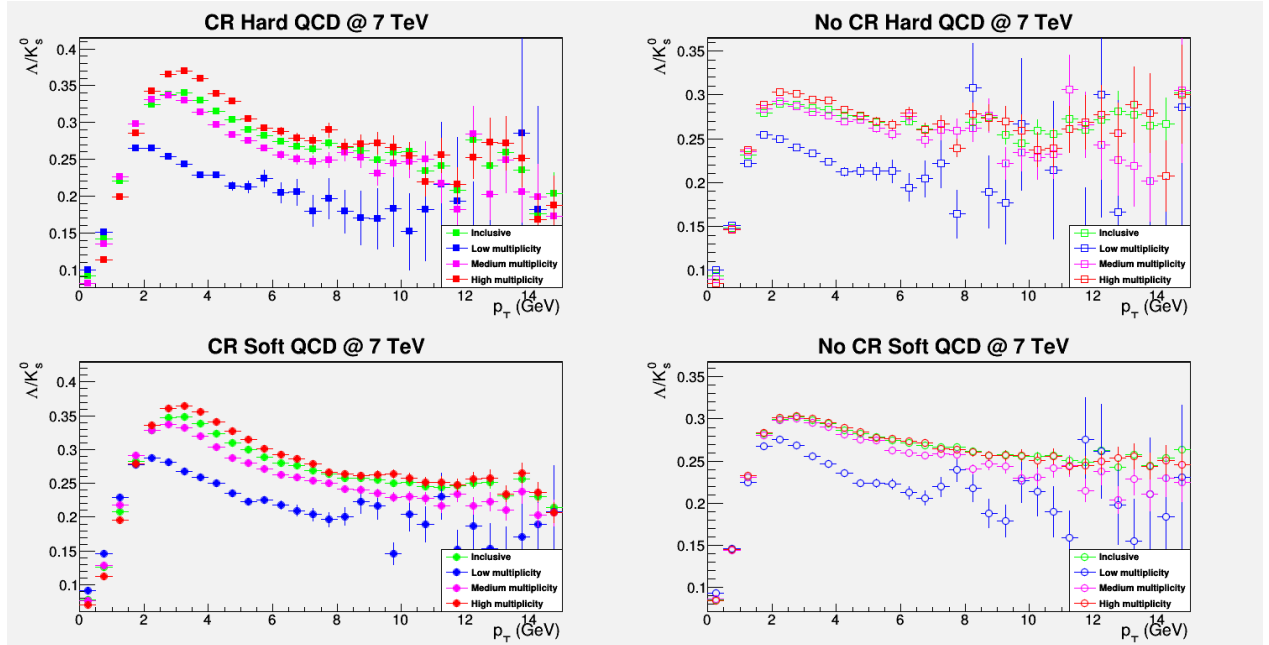
Figure B.8: The p_T spectrum of the yield ratio of Λ over K_0 for simulations at 7 TeV, with all multiplicities shown together for each pythia tune

B.9: Λ_c/D_0 spectrum
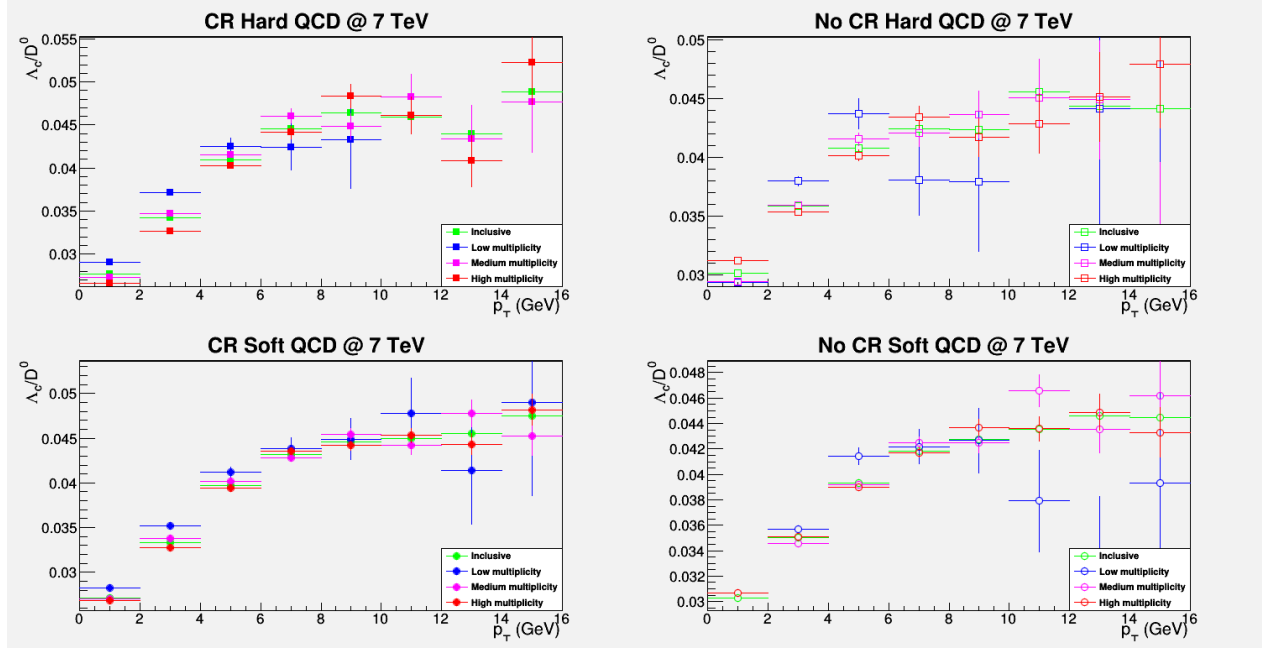
Figure B.9: The p_T spectrum of the yield ratio of Λ_c over D_0 for simulations at 7 TeV, with all multiplicities shown together for each pythia tune

B.10: p/π spectrum, normalized
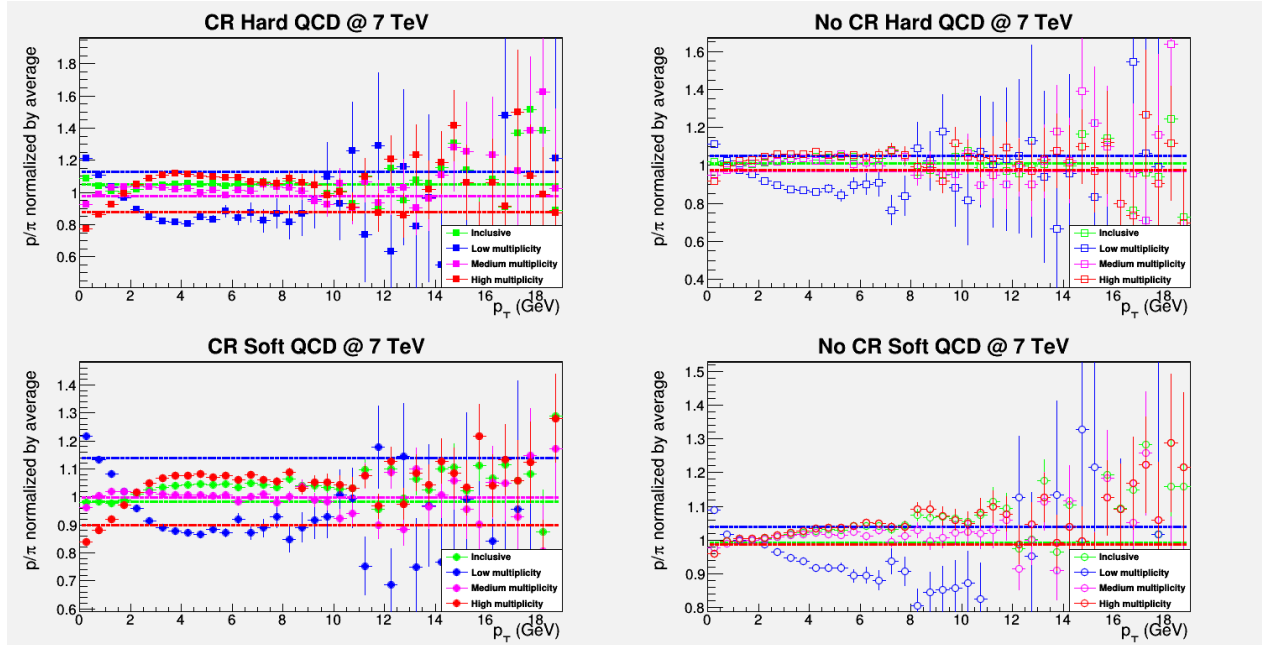
Figure B.10: The p_T spectrum of the yield ratio of p over π, normalized by the average yield ratio for simulations at 7 TeV, with all multiplicities shown together for each pythia tune
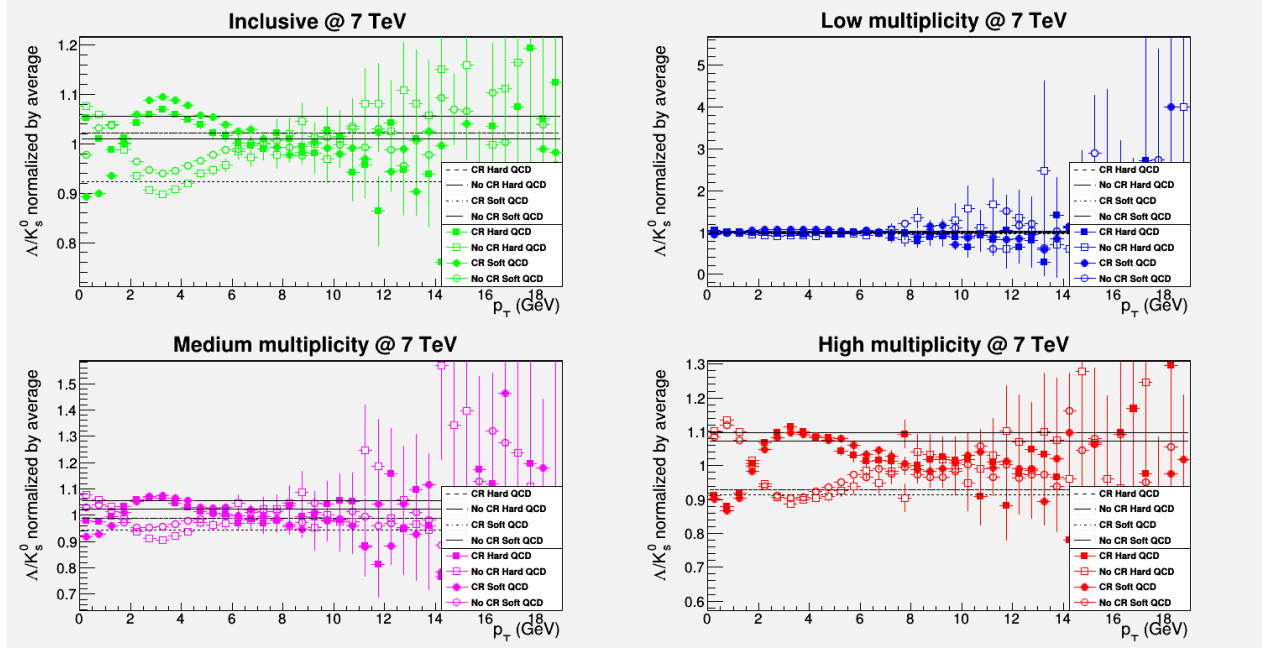
B.11: Λ/K_0 spectrum, normalized
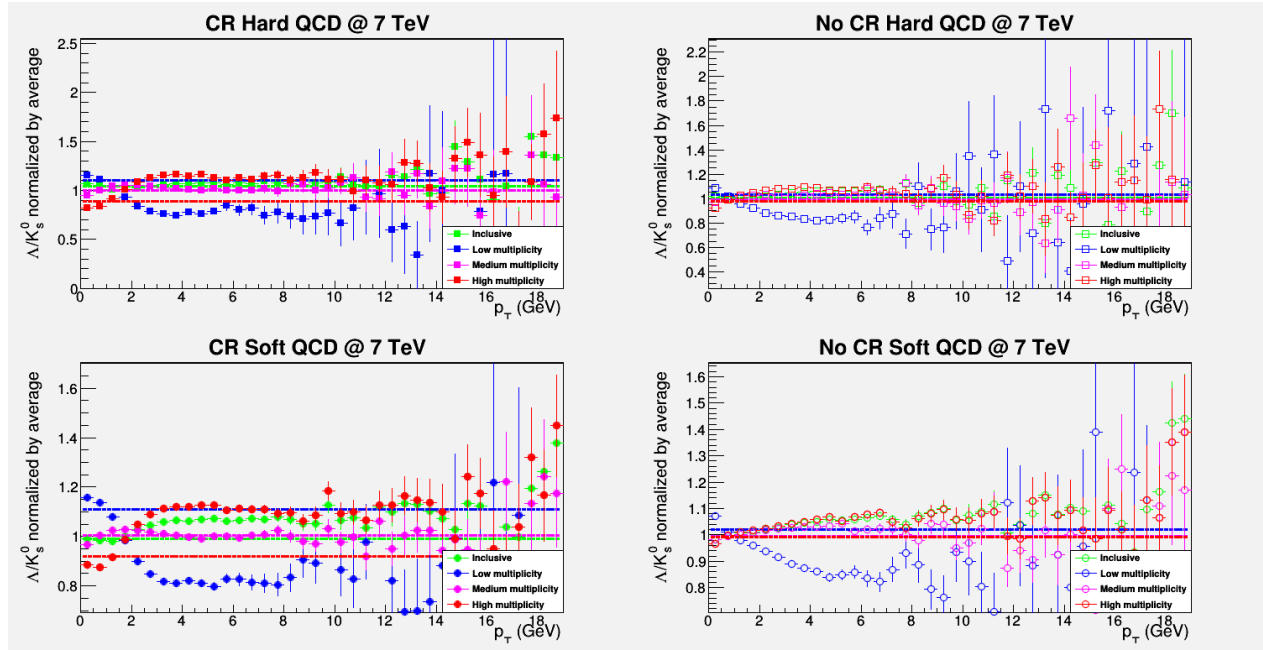
Figure B.11: The p_T spectrum of the yield ratio of Λ over K_0, normalized by the average yield ratio for simulations at 7 TeV, with all multiplicities shown together for each pythia tune
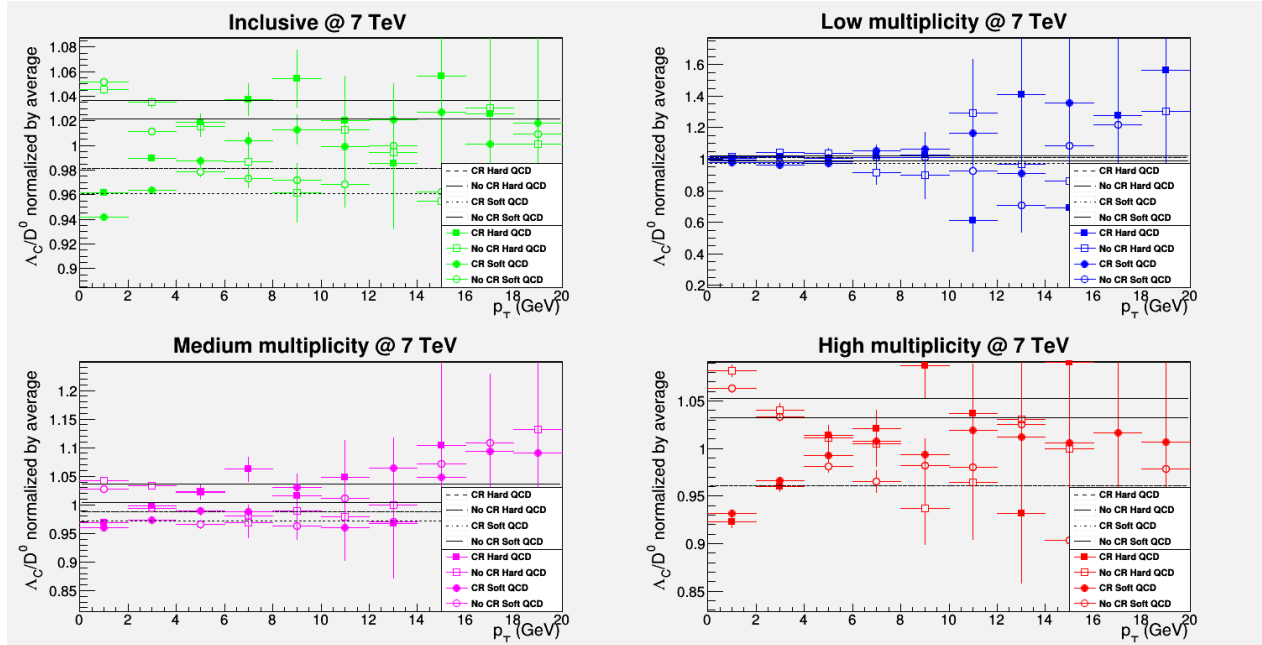
B.12: Λ_c/D_0 spectrum, normalized
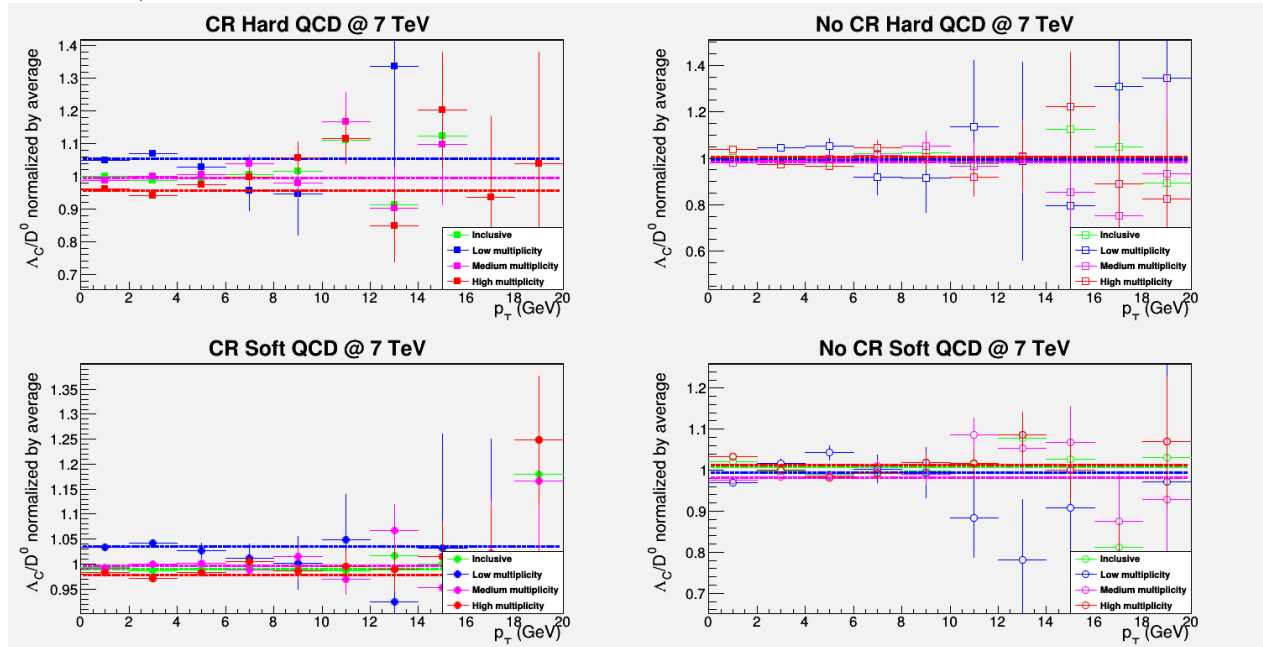
Figure B.12: The p_T spectrum of the yield ratio of Λ_c over D_0, normalized by the average yield ratio for simulations at 7 TeV, with all multiplicities shown together for each pythia tune
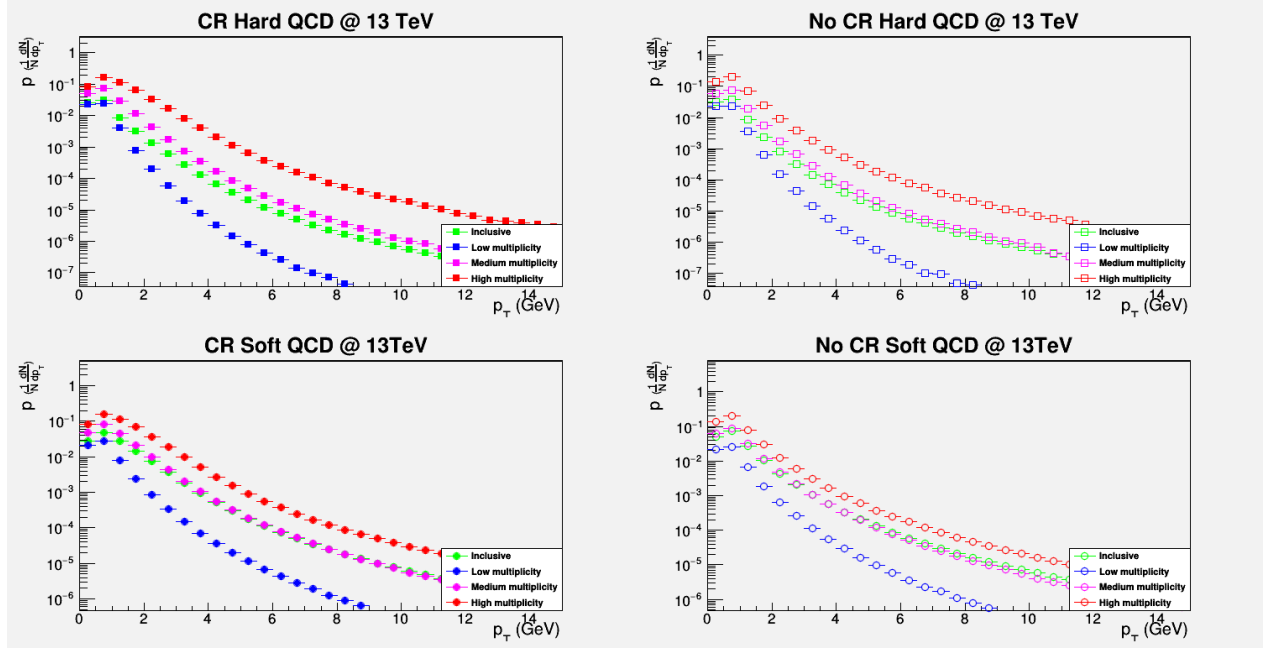
B.13: p spectrum
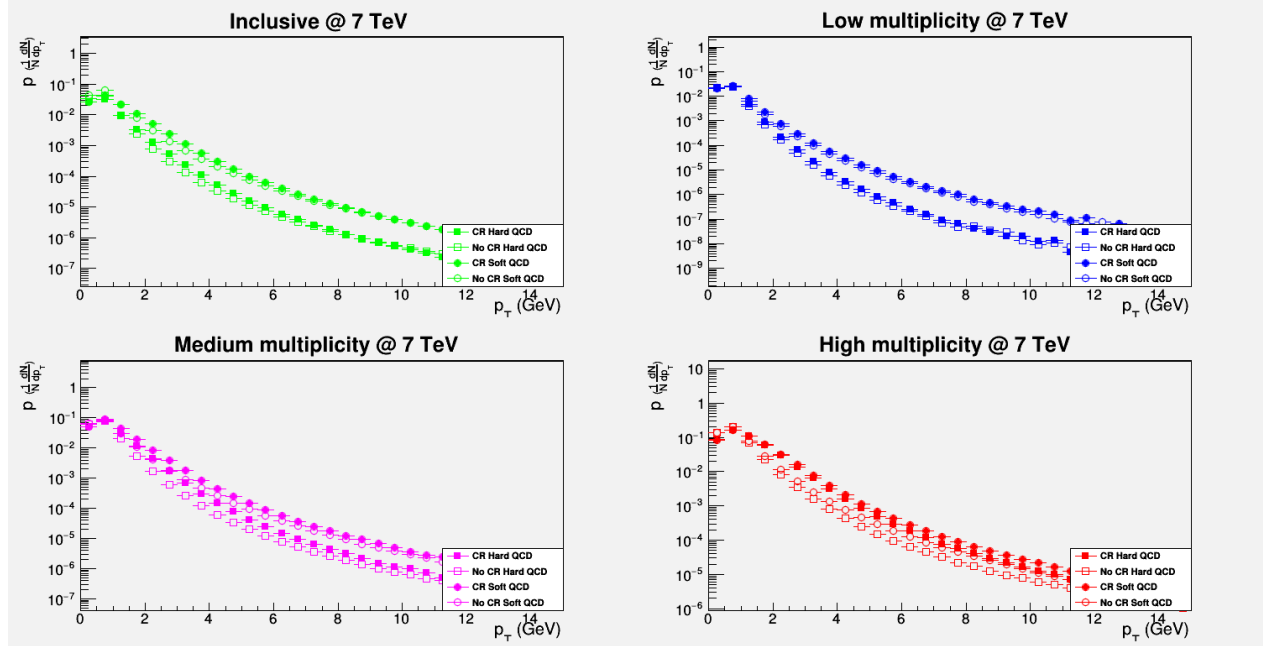
Figure B.13: The p_T spectrum of the yield of p for simulations at 7 TeV, with all pythia tunes shown together for each multiplicity
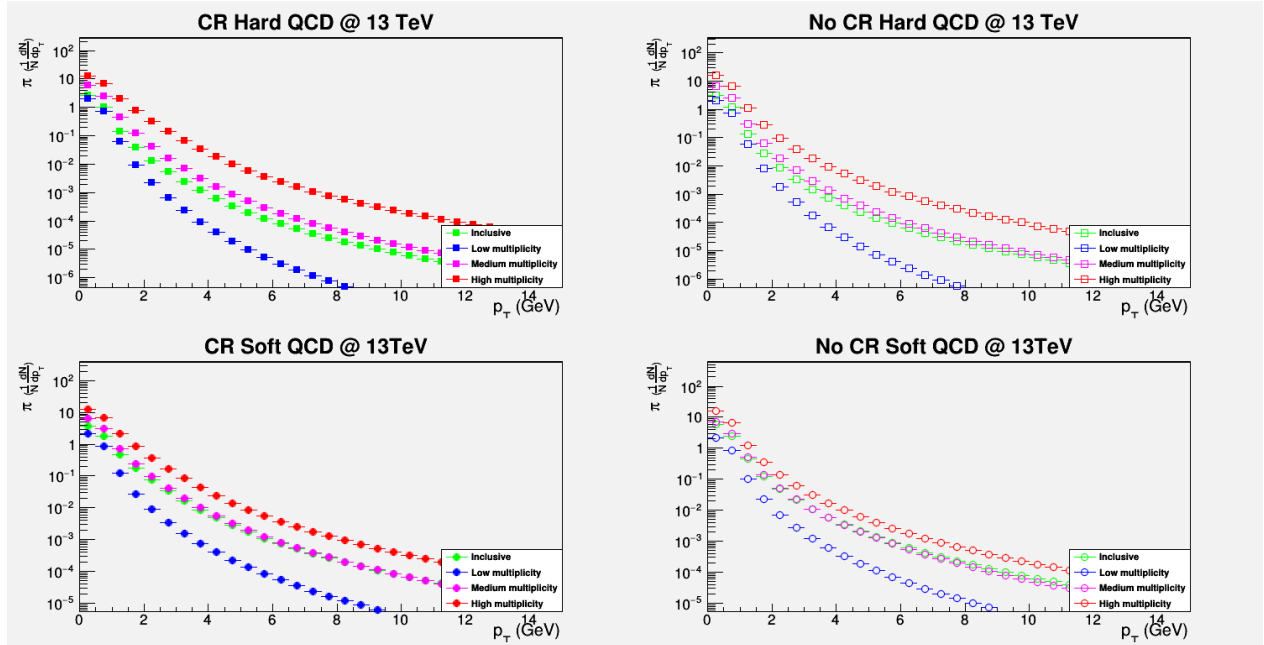
B.14: π spectrum
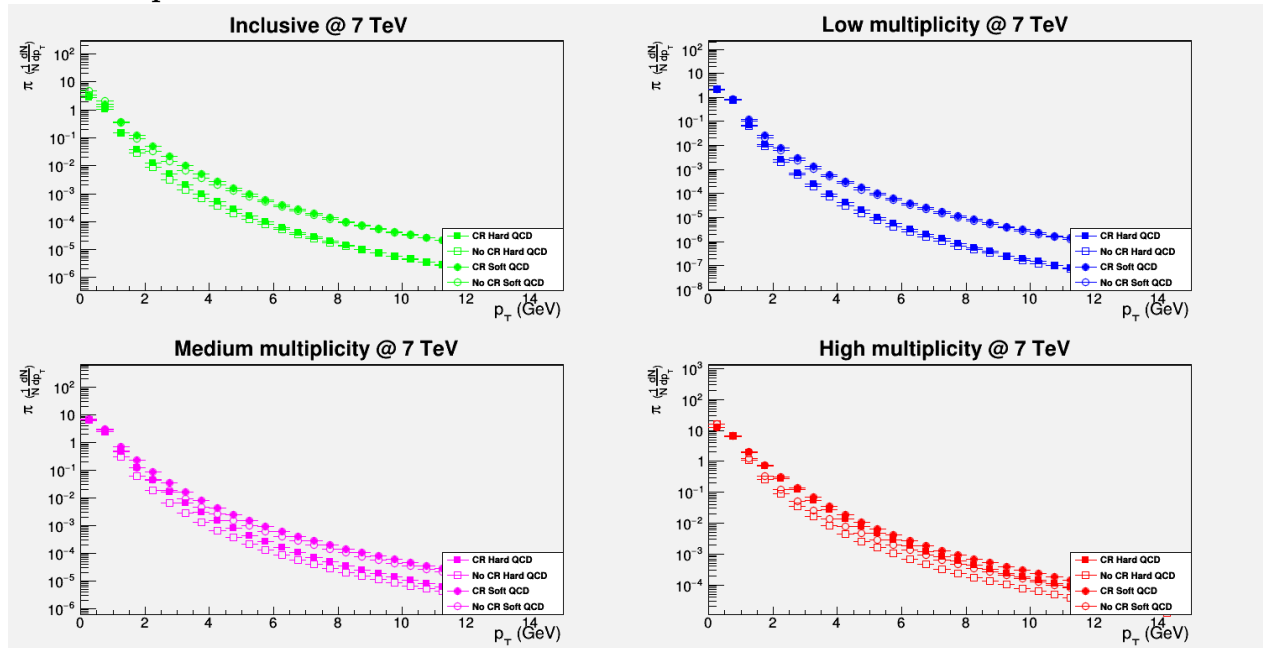
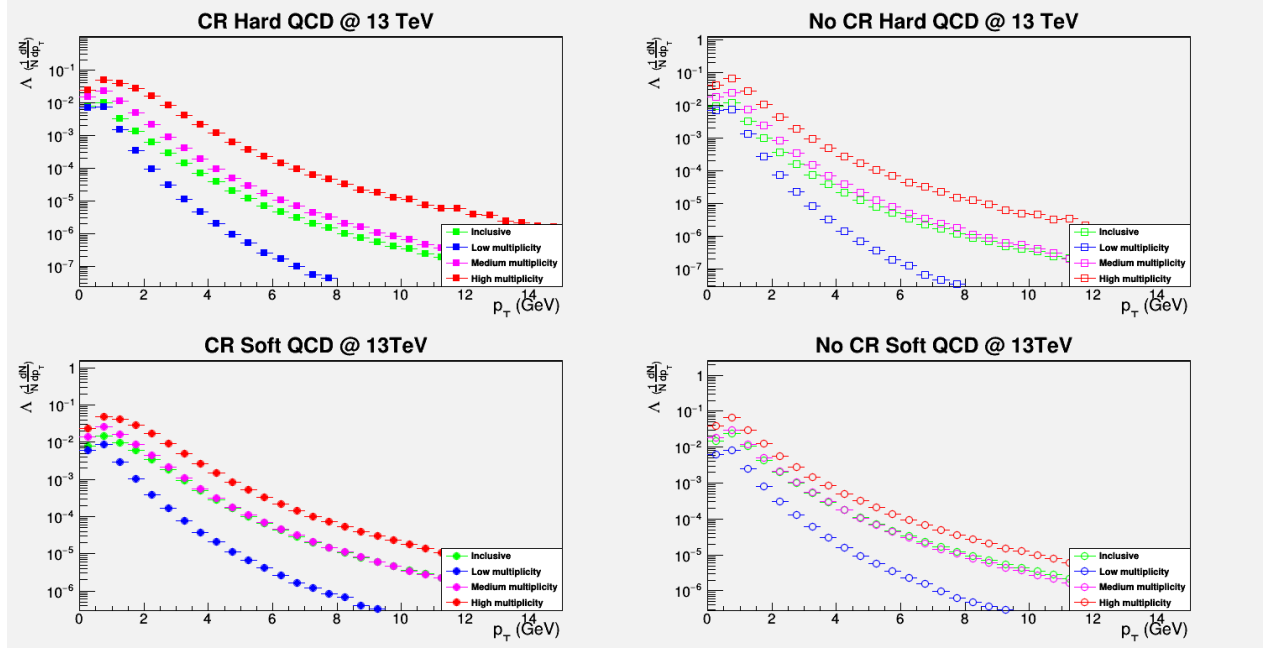Figure B.14: The p_T spectrum of the yield of π for simulations at 7 TeV, with all pythia tunes shown together for each multiplicity

B.15: Λ spectrum
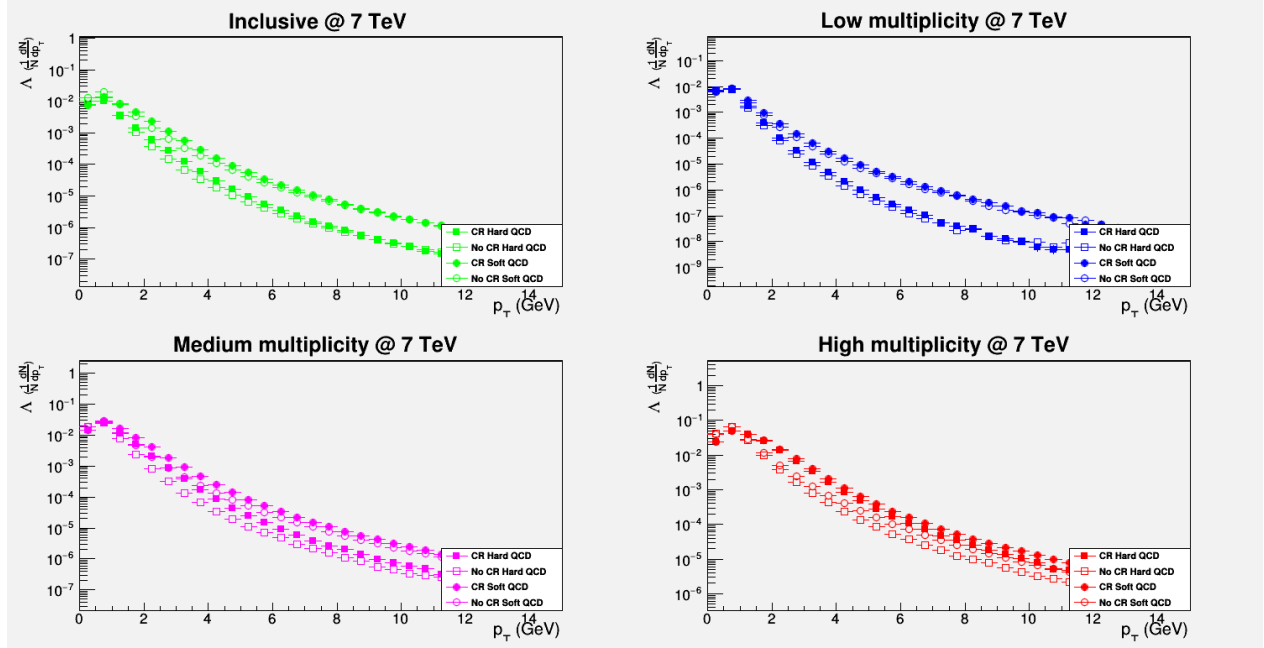
Figure B.15: The p_T spectrum of the yield of Λ for simulations at 7 TeV, with all pythia tunes shown together for each multiplicity
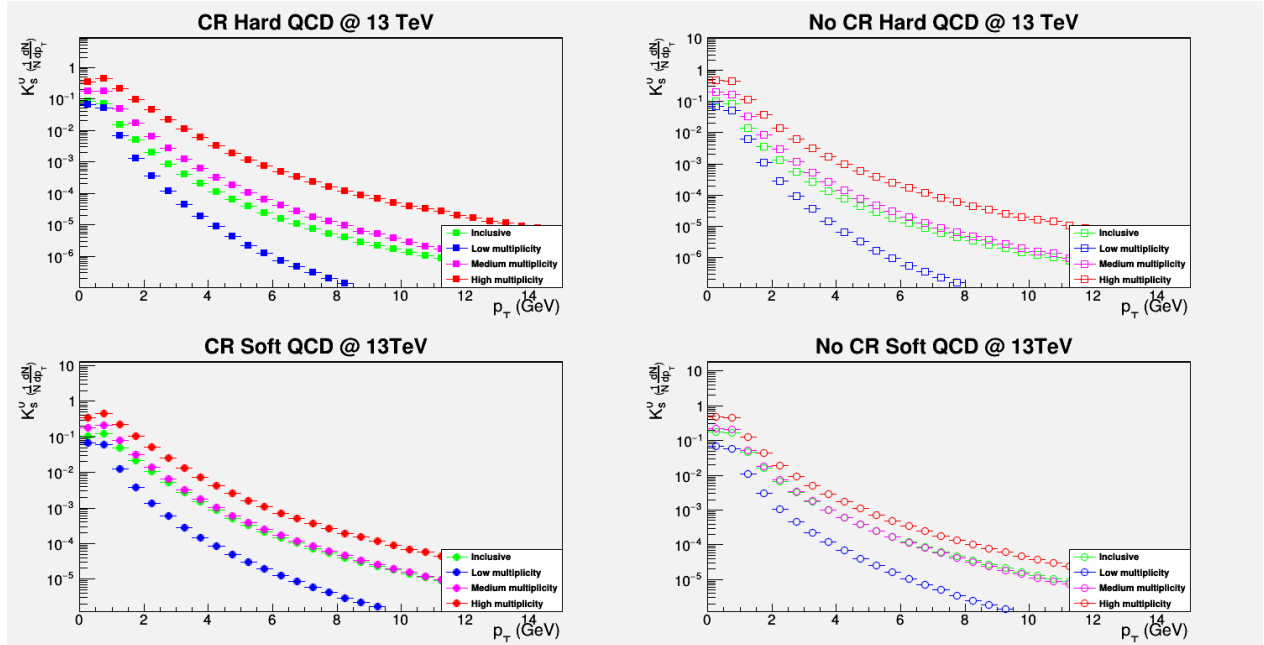
B.16: K_0 spectrum
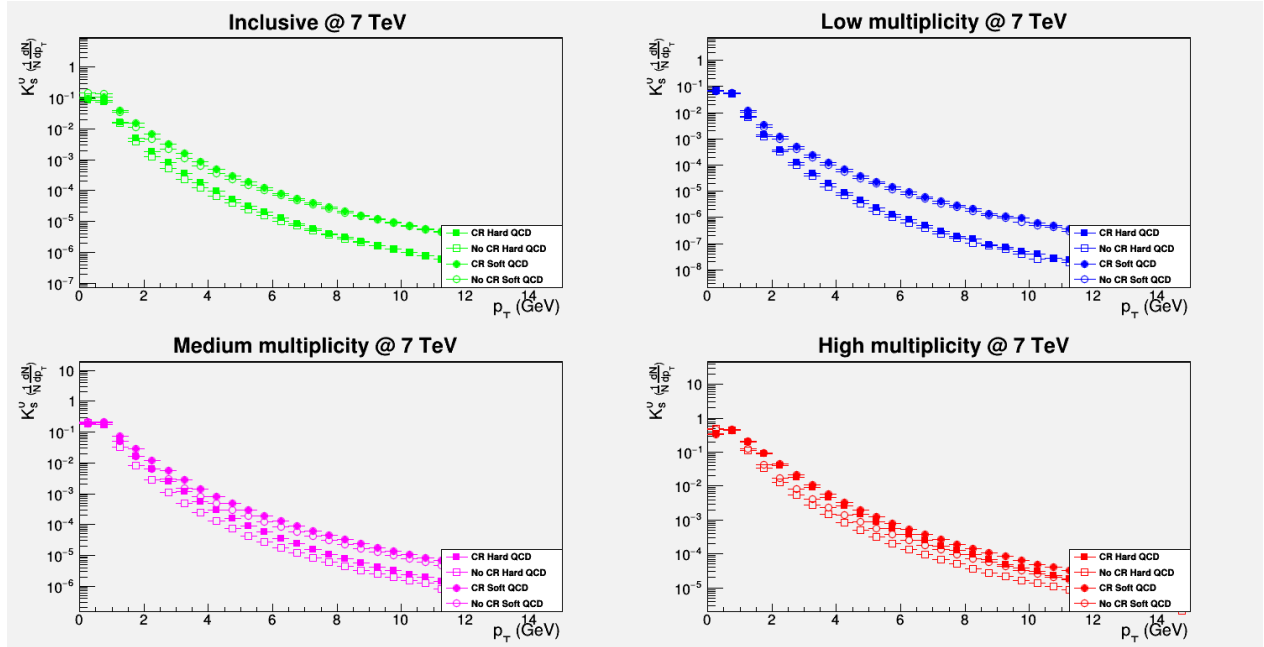
Figure B.16: The p_T spectrum of the yield of K_0 for simulations at 7 TeV, with all pythia tunes shown together for each multiplicity

B.17: Λ_c spectrum

Figure B.17: The p_T spectrum of the yield of Λ_c for simulations at 7 TeV, with all pythia tunes shown together for each multiplicity

B.18: D_0 spectrum

Figure B.18: The p_T spectrum of the yield of D_0 for simulations at 7 TeV, with all pythia tunes shown together for each multiplicity

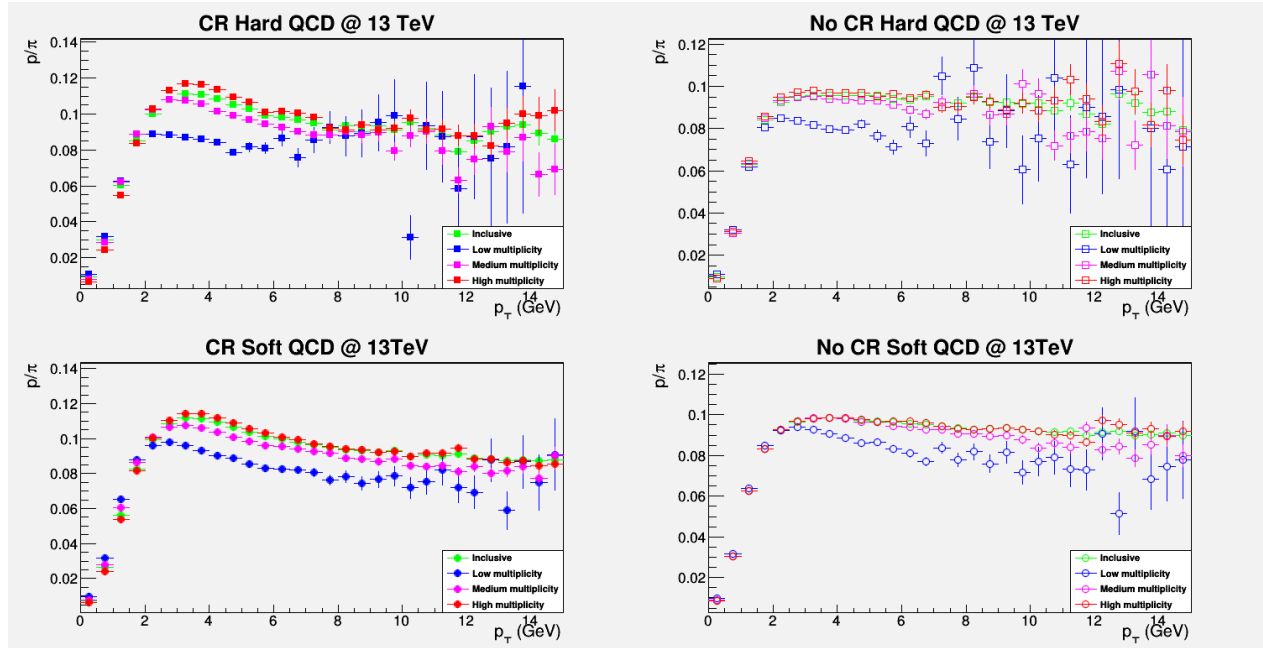## B.19: p/π spectrum
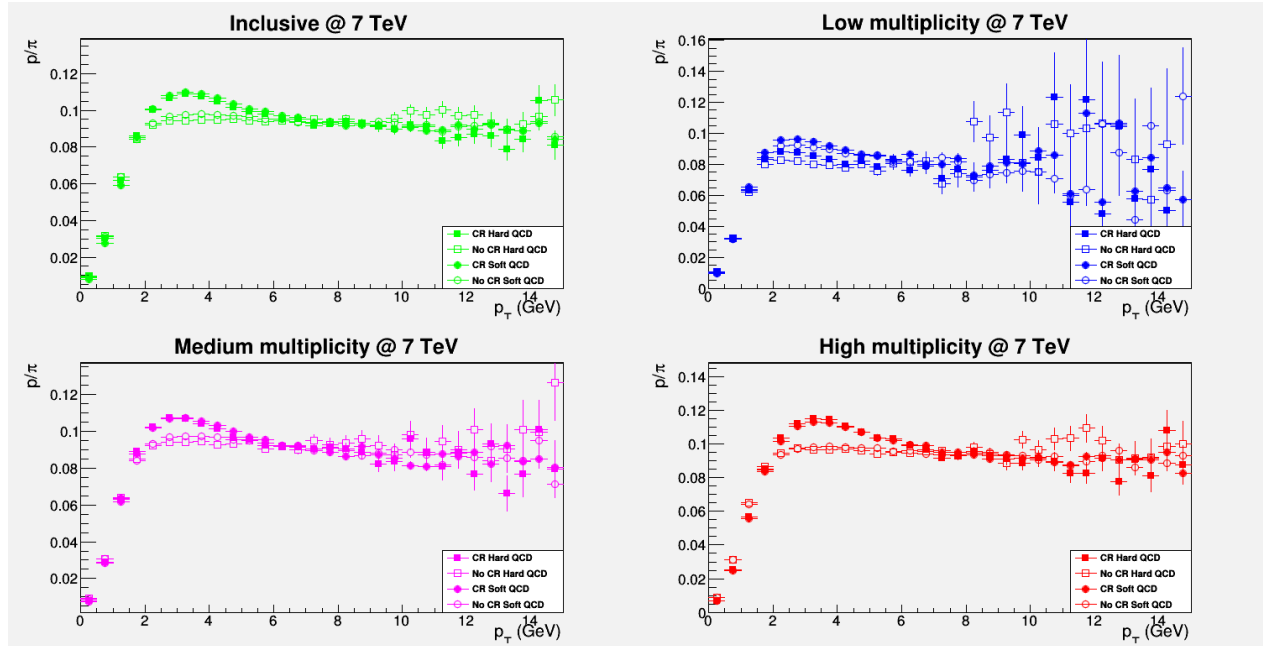
Figure B.19: The p_T spectrum of the yield ratio of p over π for simulations at 7 TeV, with all pythia tunes shown together for each multiplicity

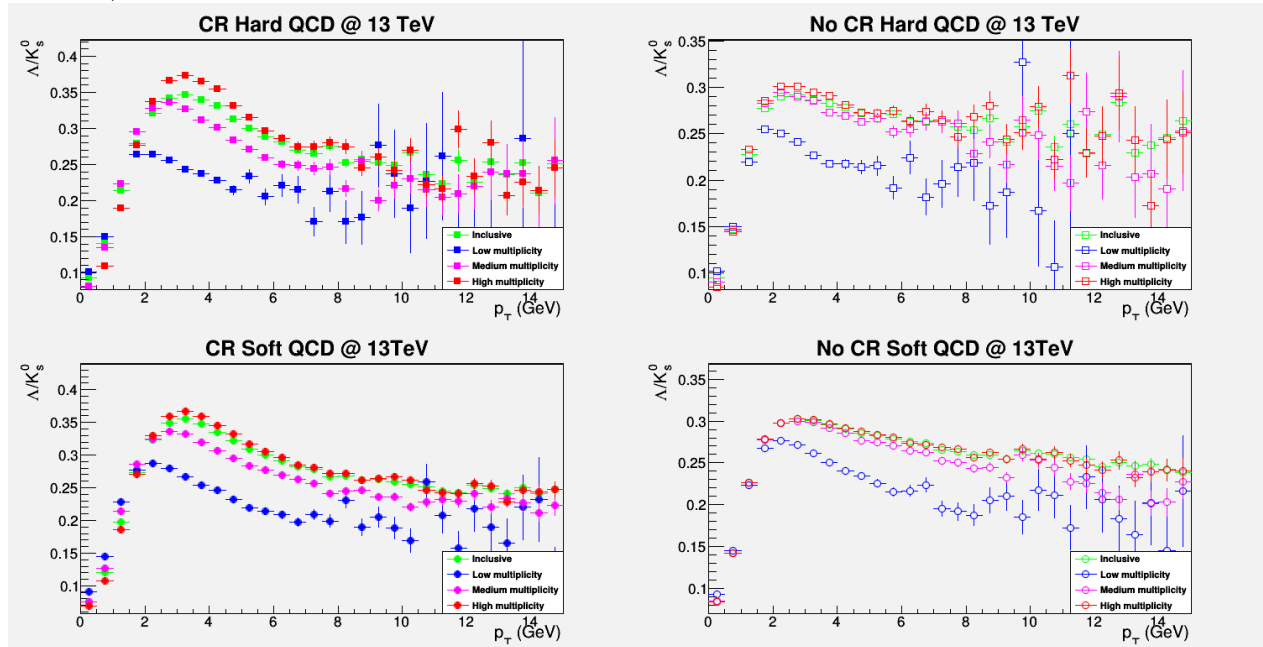## B.20: Λ/K_0 spectrum
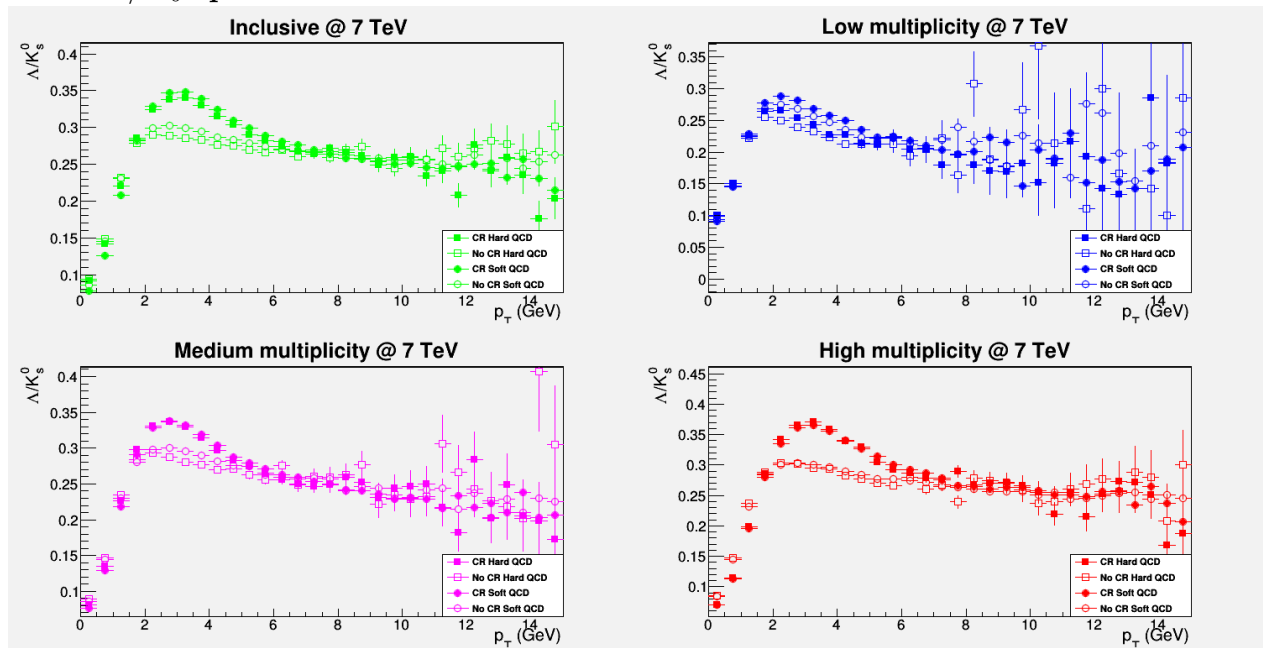
Figure B.20: The p_T spectrum of the yield ratio of Λ over K_0 for simulations at 7 TeV, with all pythia tunes shown together for each multiplicity

B.21: Λ_c/D_0 spectrum

Figure B.21: The p_T spectrum of the yield ratio of Λ_c over D_0 for simulations at 7 TeV, with all pythia tunes shown together for each multiplicity

B.22: p/π spectrum, normalized
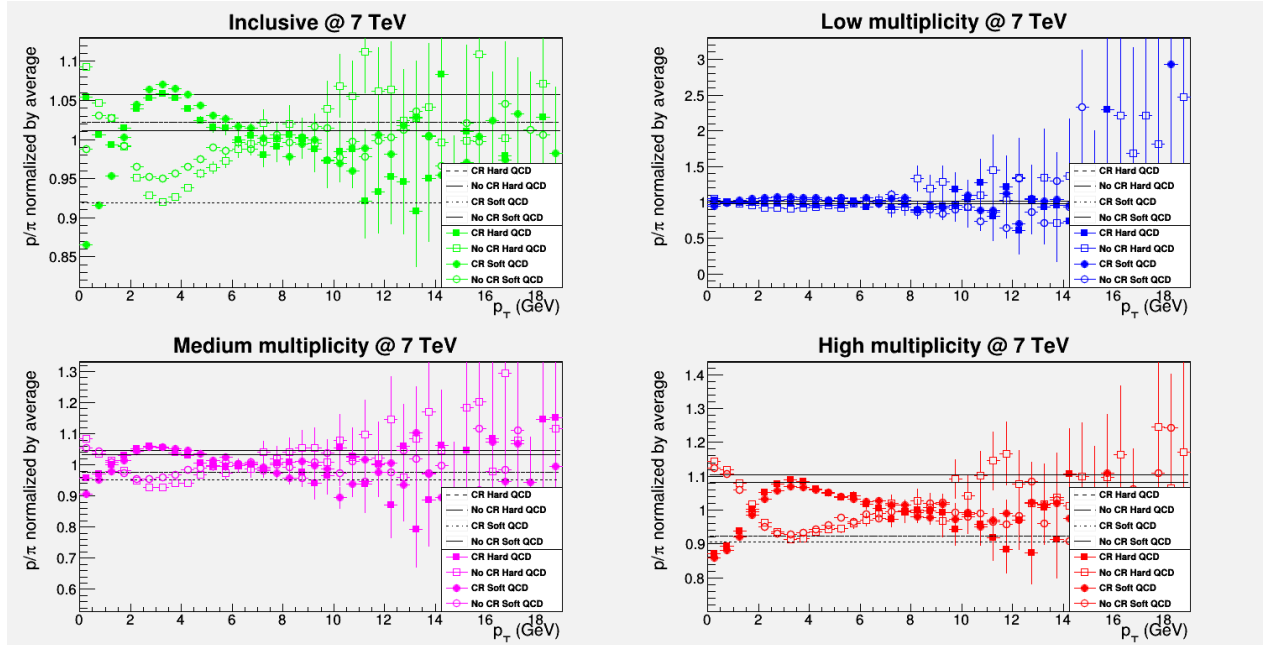
Figure B.22: The p_T spectrum of the yield ratio of p over π, normalized by the average yield ratio for simulations at 7 TeV, with all pythia tunes shown together for each multiplicity

B.23: Λ/K_0 **spectrum, normalized**

Figure B.23: The p_T spectrum of the yield ratio of Λ over K_0, normalized by the average yield ratio for simulations at 7 TeV, with all pythia tunes shown together for each multiplicity

B.24: Λ_c/D_0 **spectrum, normalized**

Figure B.24: The p_T spectrum of the yield ratio of Λ_c over D_0, normalized by the average yield ratio for simulations at 7 TeV, with all pythia tunes shown together for each multiplicity

C.1: p spectrum

Figure C.1: The p_T spectrum of the yield of p for simulations at 13 TeV, with all multiplicities shown together for each pythia tune

C.2: π spectrum

Figure C.2: The p_T spectrum of the yield of π for simulations at 13 TeV, with all multiplicities shown together for each pythia tune

C.3: Λ spectrum
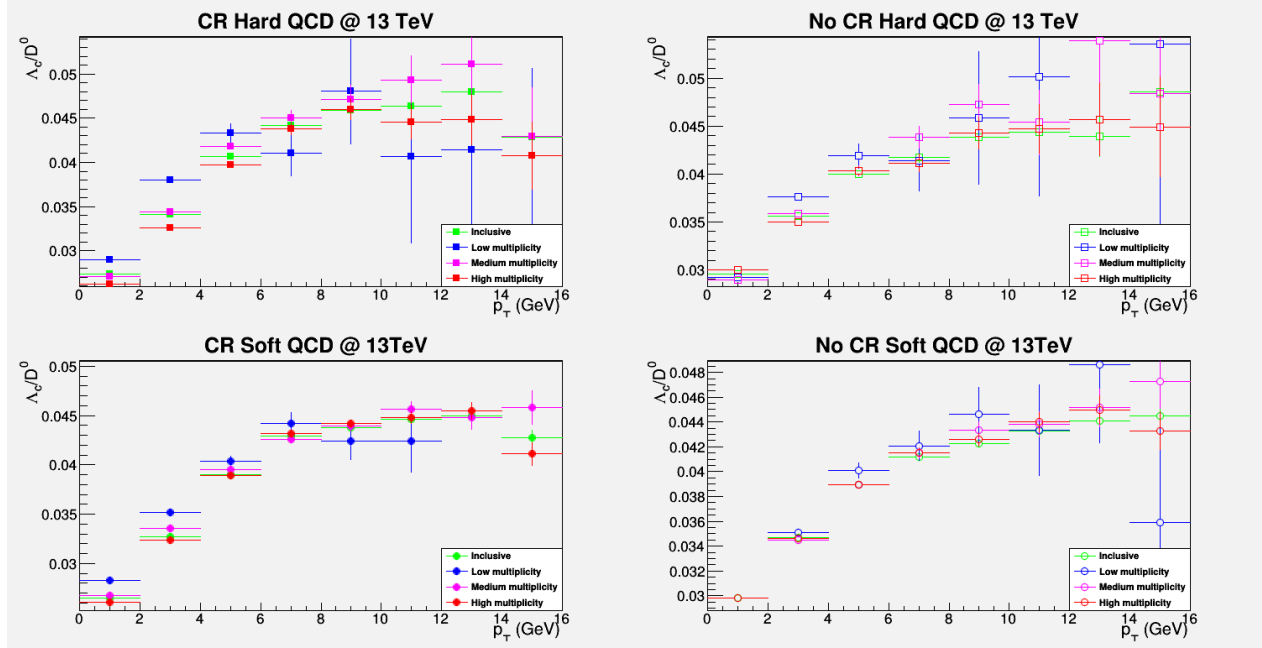

Figure C.3: The p_T spectrum of the yield of Λ for simulations at 13 TeV, with all multiplicities shown together for each pythia tune
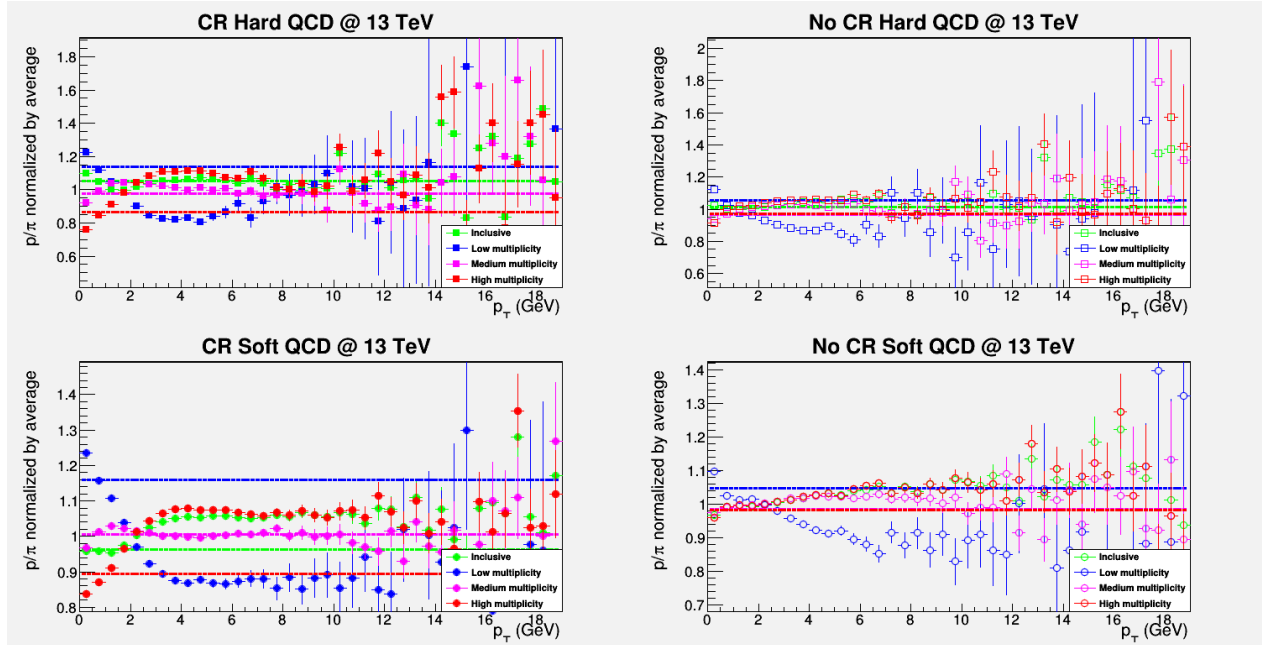
C.4: K_0 spectrum

Figure C.4: The p_T spectrum of the yield of K_0 for simulations at 13 TeV, with all multiplicities shown together for each pythia tune

C.5: Λ_c spectrum
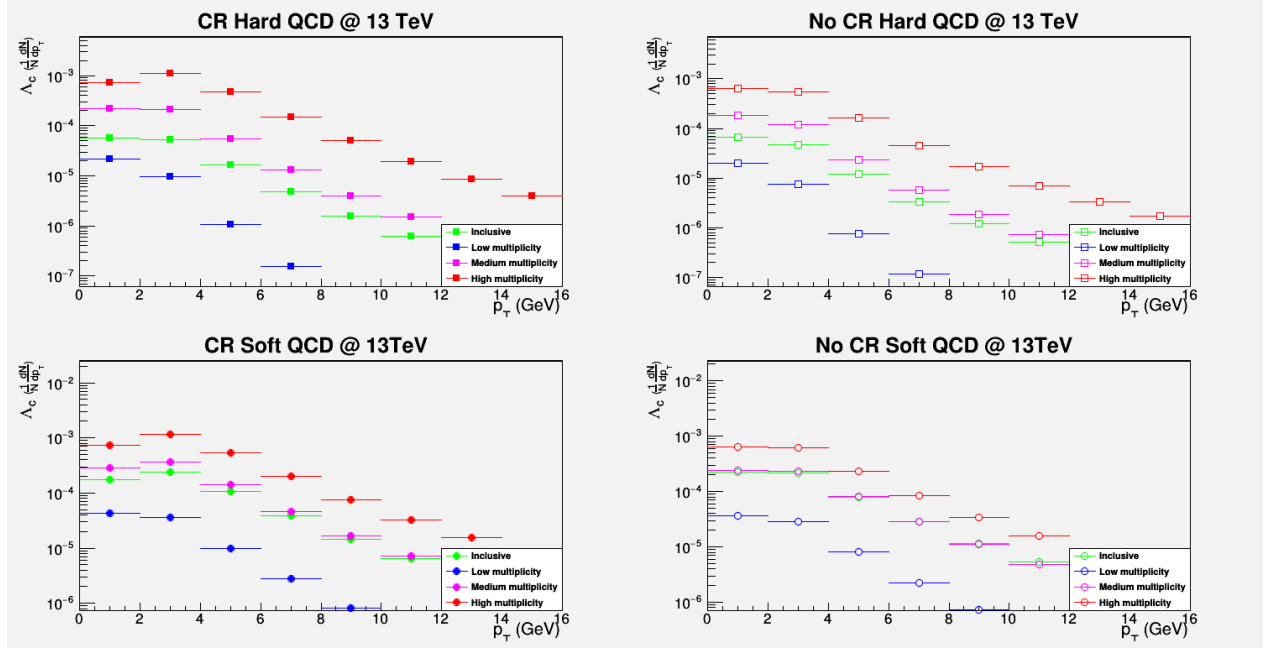
Figure C.5: The p_T spectrum of the yield of Λ_c for simulations at 13 TeV, with all multiplicities shown together for each pythia tune

C.6: D_0 spectrum
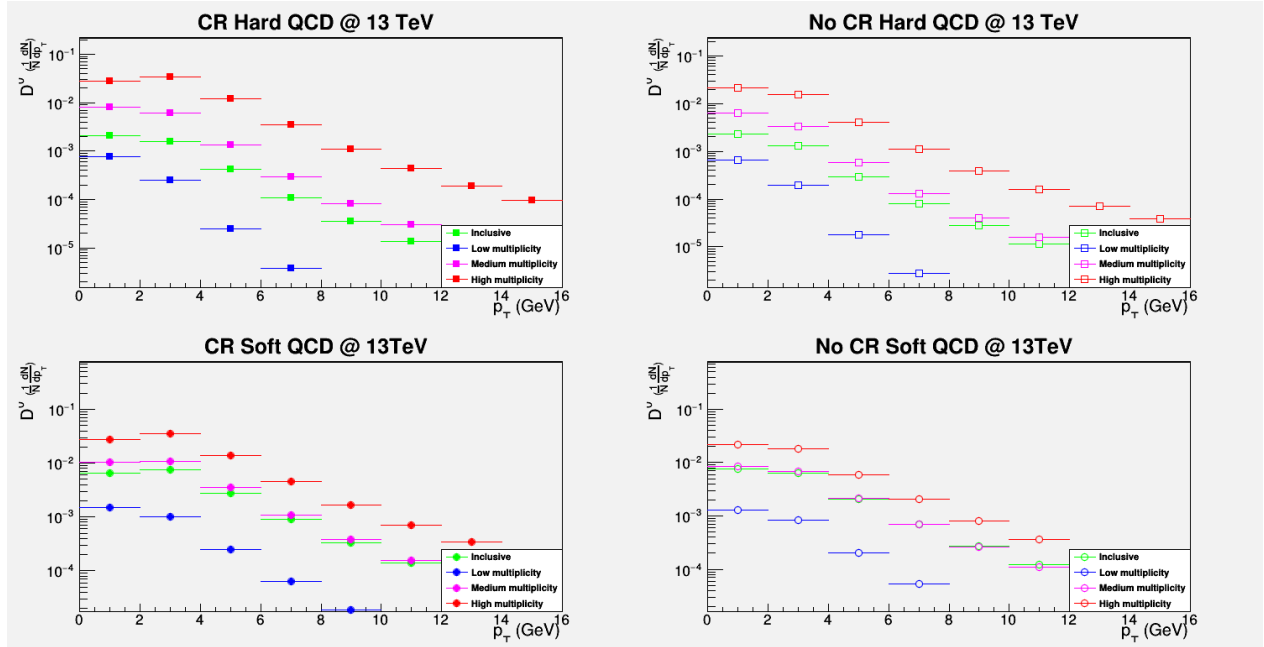
Figure C.6: The p_T spectrum of the yield of D_0 for simulations at 13 TeV, with all multiplicities shown together for each pythia tune

C.7: p/π spectrum

Figure C.7: The p_T spectrum of the yield ratio of p over π for simulations at 13 TeV, with all multiplicities shown together for each pythia tune

C.8: Λ/K_0 spectrum

Figure C.8: The p_T spectrum of the yield ratio of Λ over K_0 for simulations at 13 TeV, with all multiplicities shown together for each pythia tune

C.9: Λ_c/D_0 spectrum

Figure C.9: The p_T spectrum of the yield ratio of Λ_c over D_0 for simulations at 13 TeV, with all multiplicities shown together for each pythia tune

C.10: p/π spectrum, normalized

Figure C.10: The p_T spectrum of the yield ratio of p over π, normalized by the average yield ratio for simulations at 13 TeV, with all multiplicities shown together for each pythia tune

C.11: Λ/K_0 spectrum, normalized
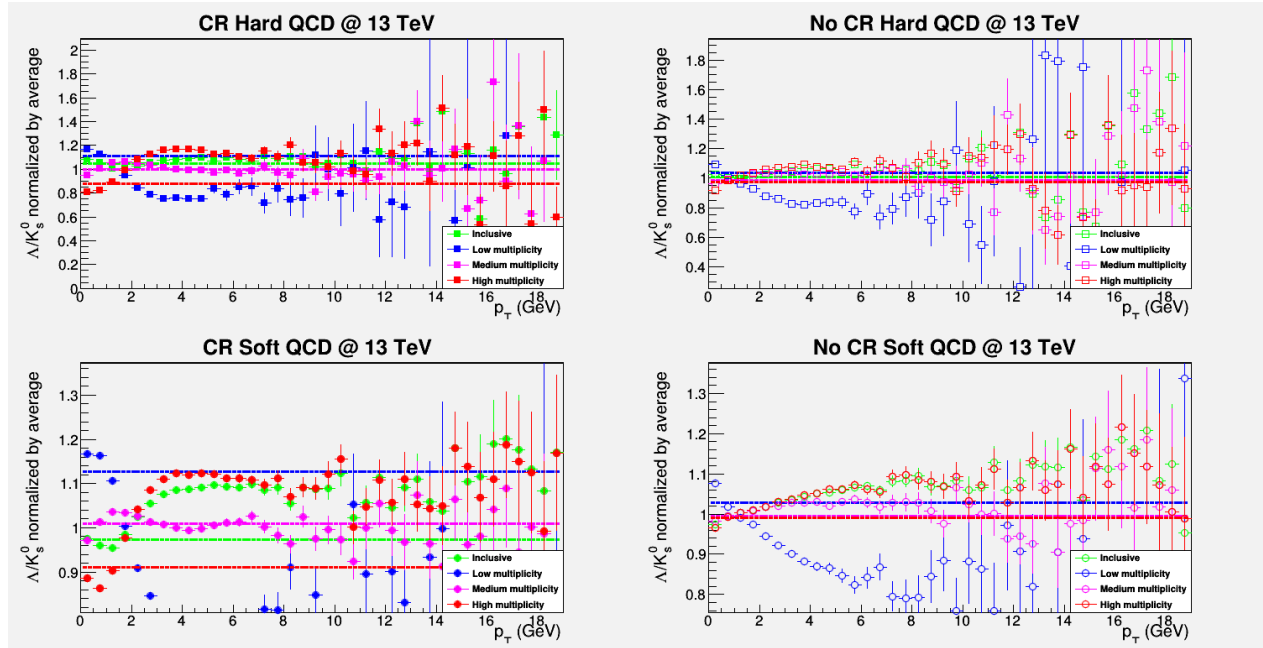
Figure C.11: The p_T spectrum of the yield ratio of Λ over K_0, normalized by the average yield ratio for simulations at 13 TeV, with all multiplicities shown together for each pythia tune

C.12: Λ_c/D_0 spectrum, normalized
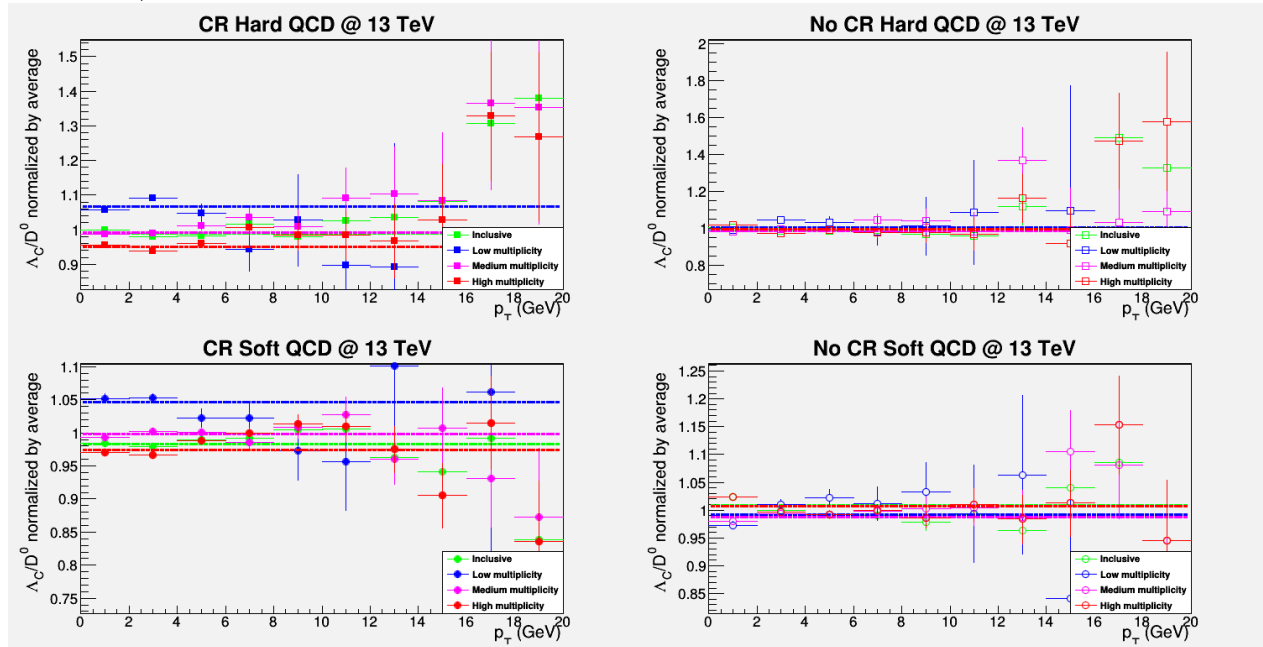
Figure C.12: The p_T spectrum of the yield ratio of Λ_c over D_0, normalized by the average yield ratio for simulations at 13 TeV, with all multiplicities shown together for each pythia tune

C.13: p spectrum
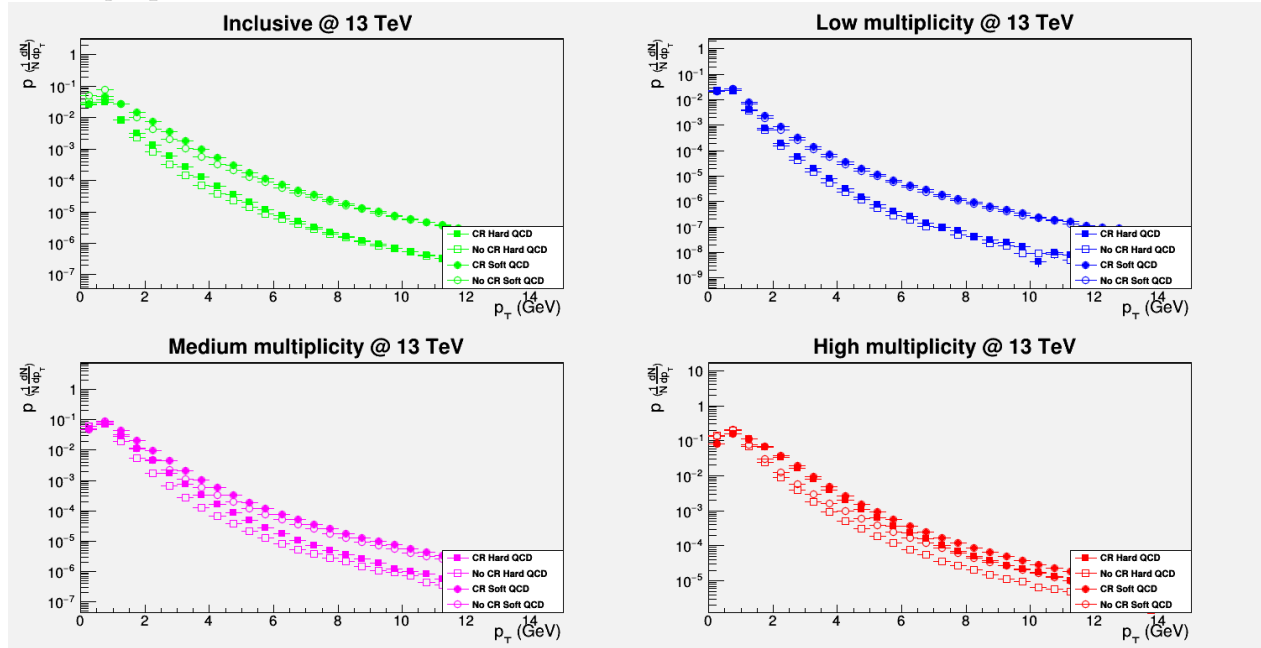
Figure C.13: The p_T spectrum of the yield of p for simulations at 13 TeV, with all pythia tunes shown together for each multiplicity

C.14: π spectrum
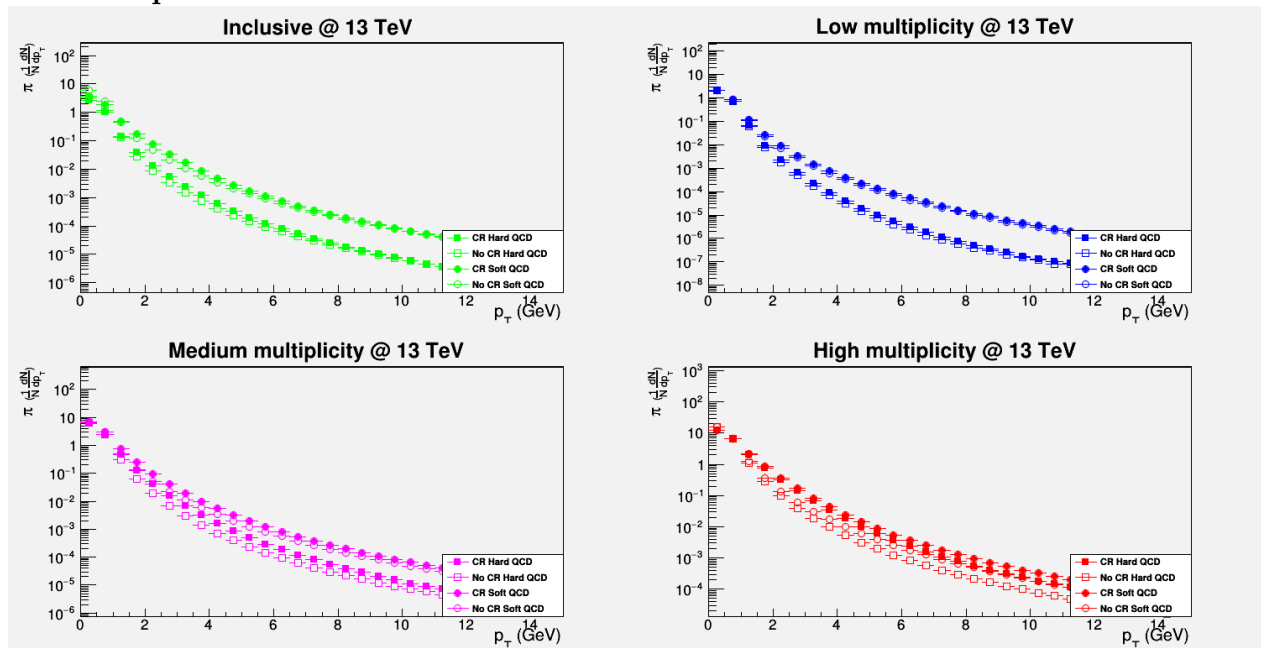
Figure C.14: The p_T spectrum of the yield of π for simulations at 13 TeV, with all pythia tunes shown together for each multiplicity

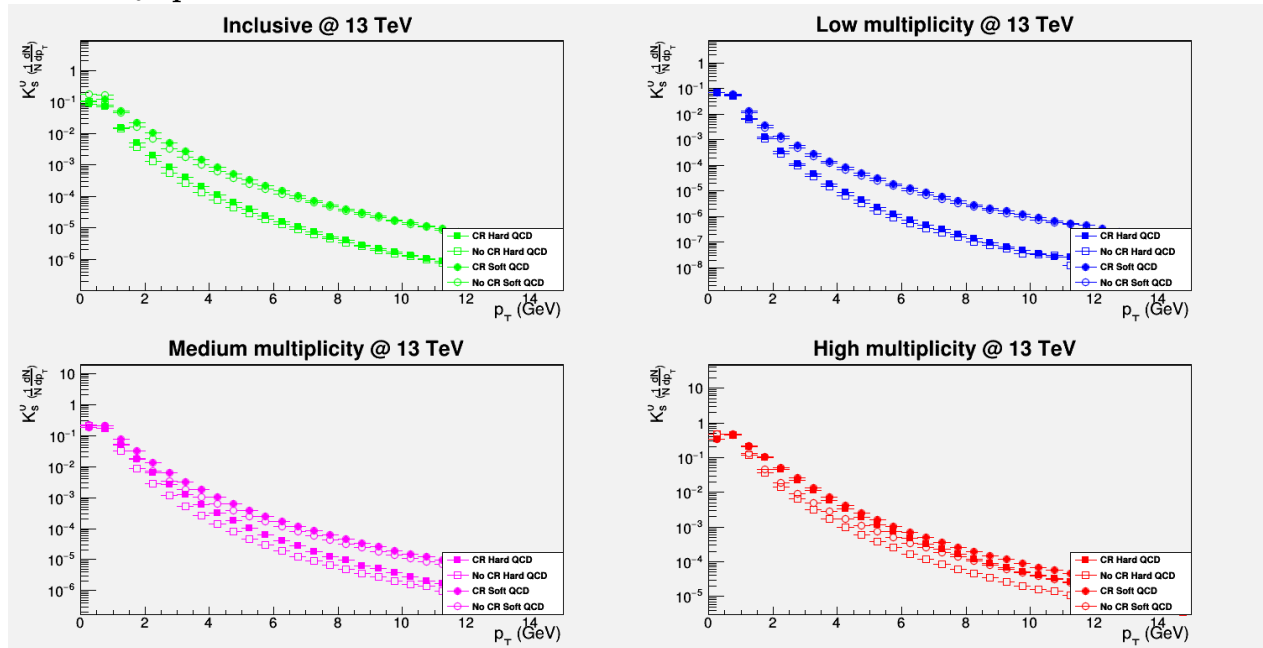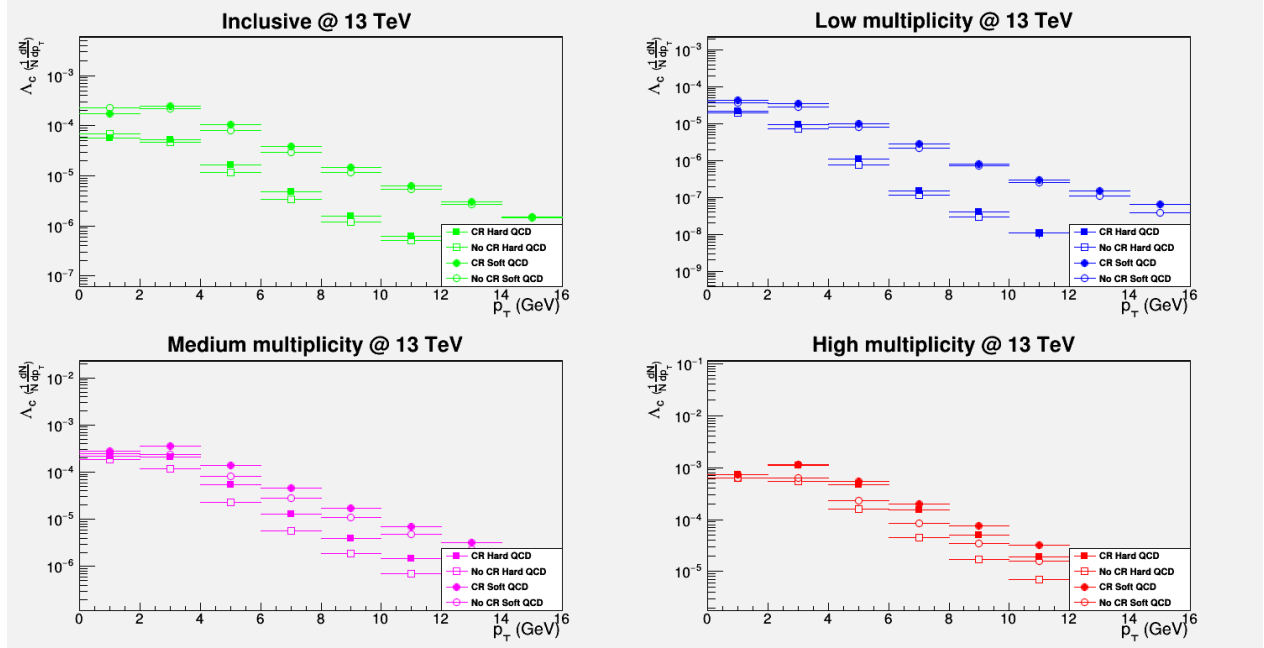## C.15: Λ spectrum
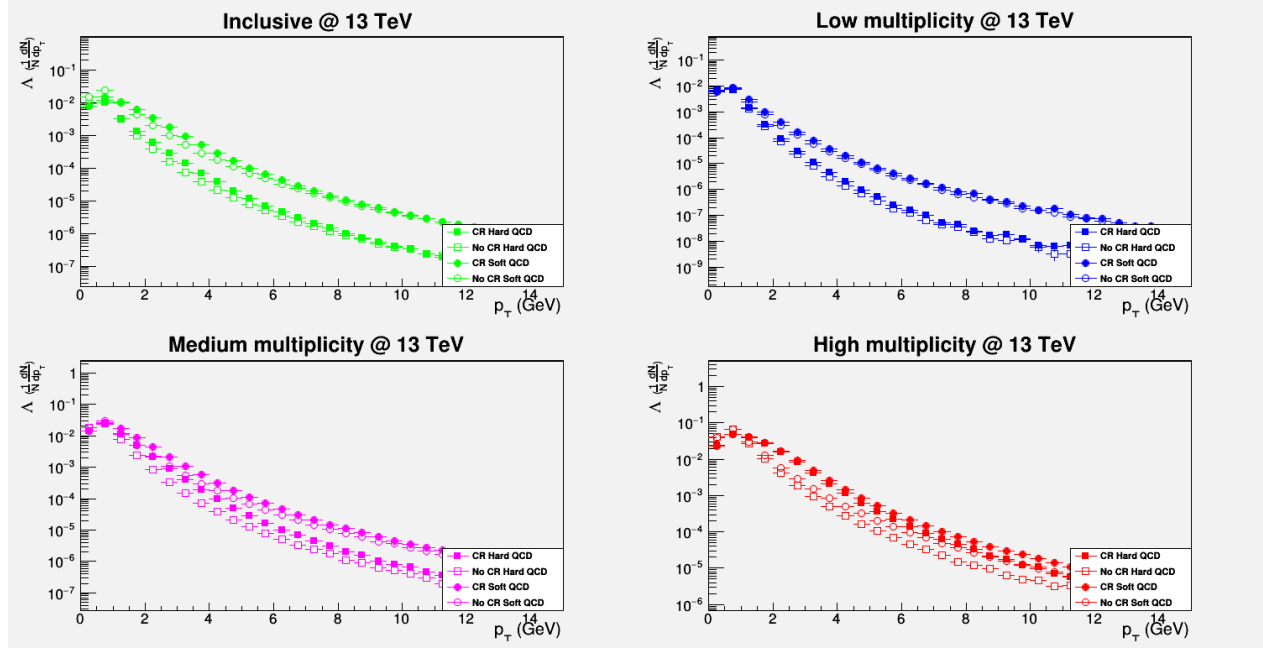
Figure C.15: The p_T spectrum of the yield of Λ for simulations at 13 TeV, with all pythia tunes shown together for each multiplicity
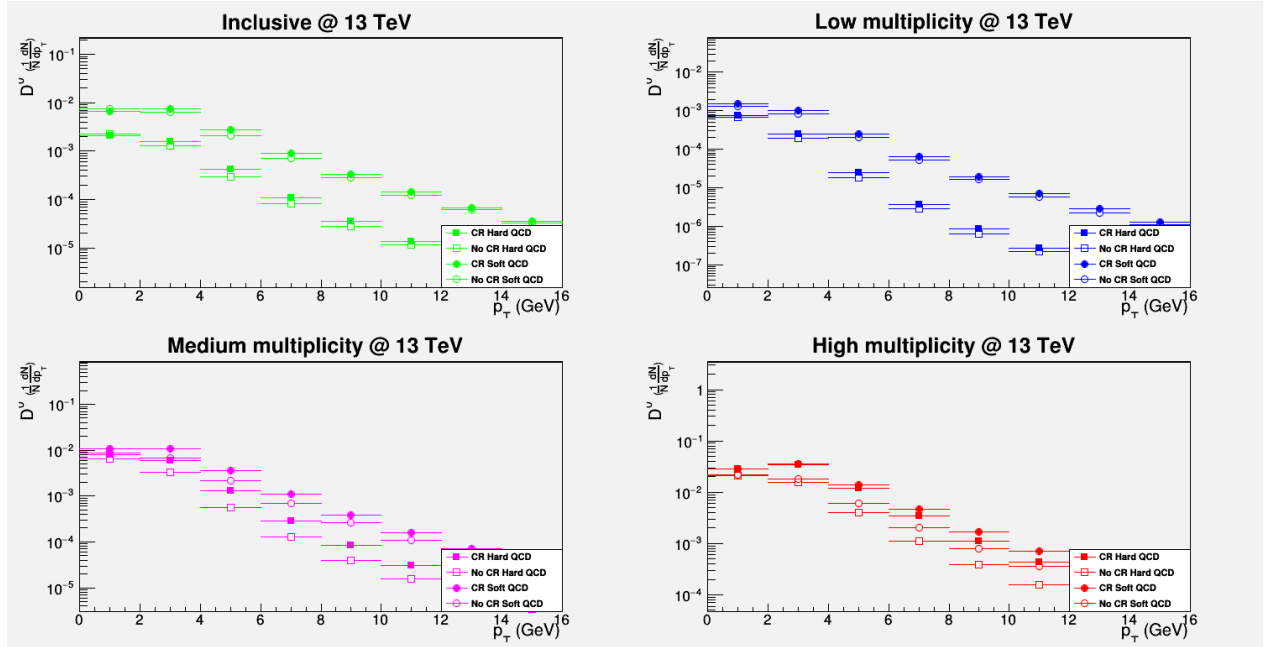
C.16: K_0 spectrum

Figure C.16: The p_T spectrum of the yield of K_0 for simulations at 13 TeV, with all pythia tunes shown together for each multiplicity

C.17: Λ_c spectrum

Figure C.17: The p_T spectrum of the yield of Λ_c for simulations at 13 TeV, with all pythia tunes shown together for each multiplicity

C.18: D_0 spectrum

Figure C.18: The p_T spectrum of the yield of D_0 for simulations at 13 TeV, with all pythia tunes shown together for each multiplicity
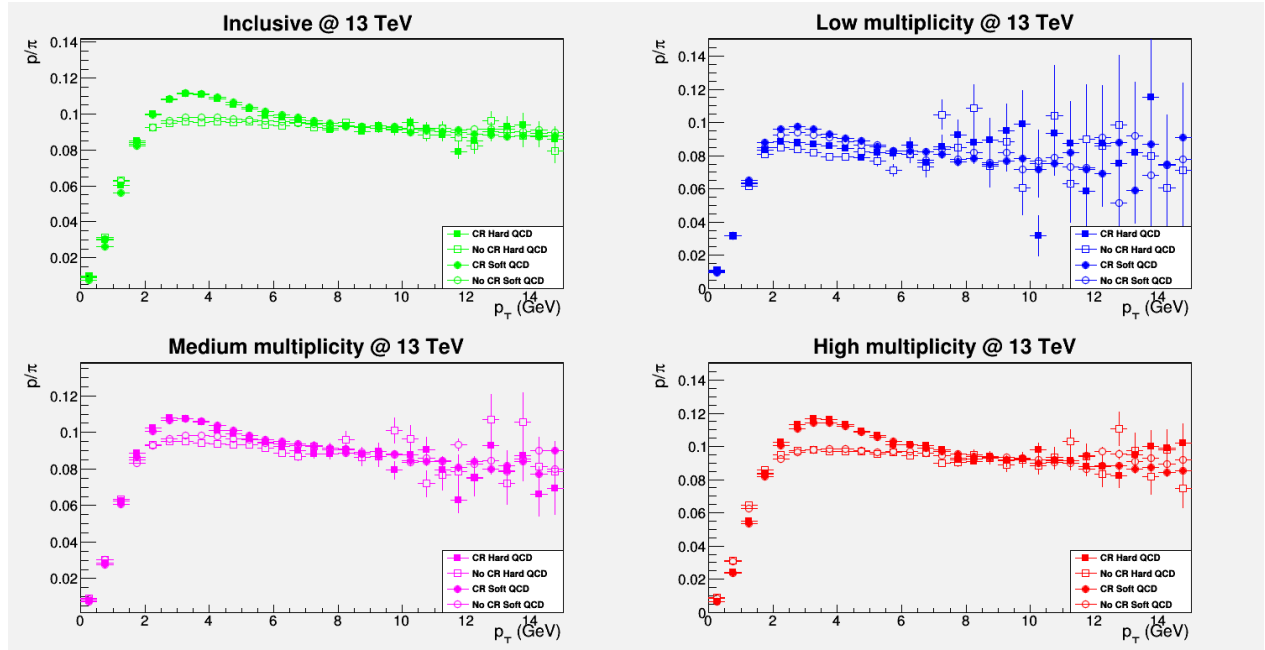
C.19: p/π spectrum

Figure C.19: The p_T spectrum of the yield ratio of p over π for simulations at 13 TeV, with all pythia tunes shown together for each multiplicity
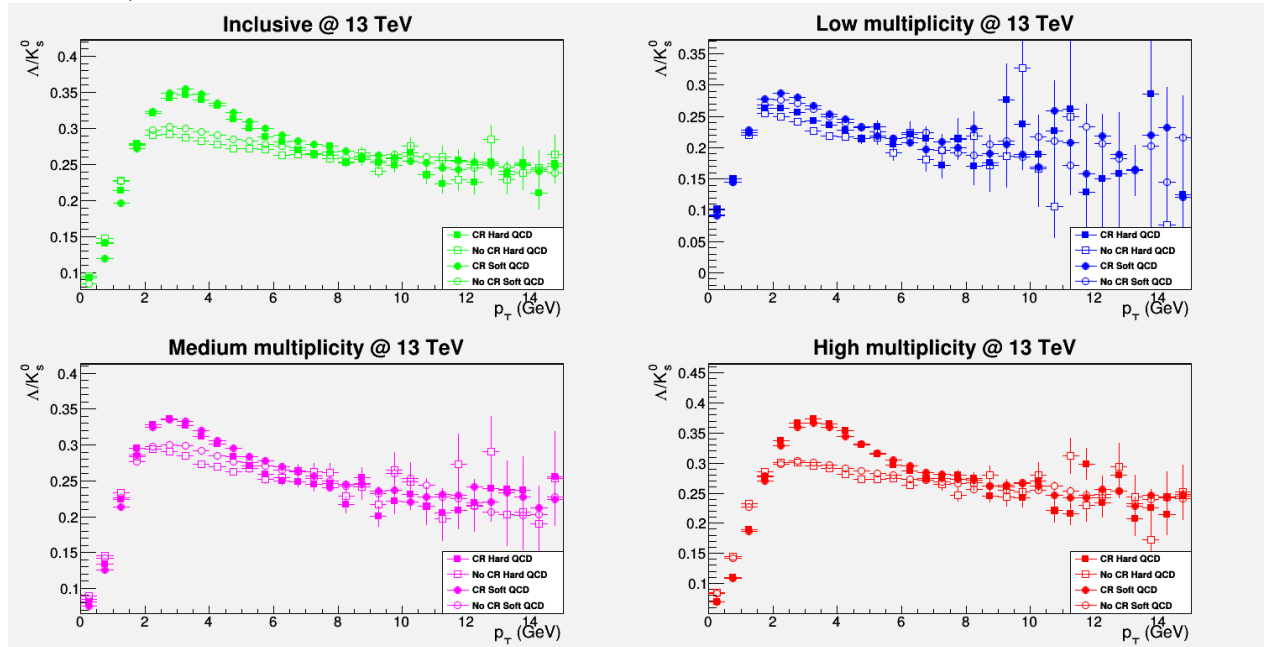
C.20: Λ/K_0 spectrum

Figure C.20: The p_T spectrum of the yield ratio of Λ over K_0 for simulations at 13 TeV, with all pythia tunes shown together for each multiplicity
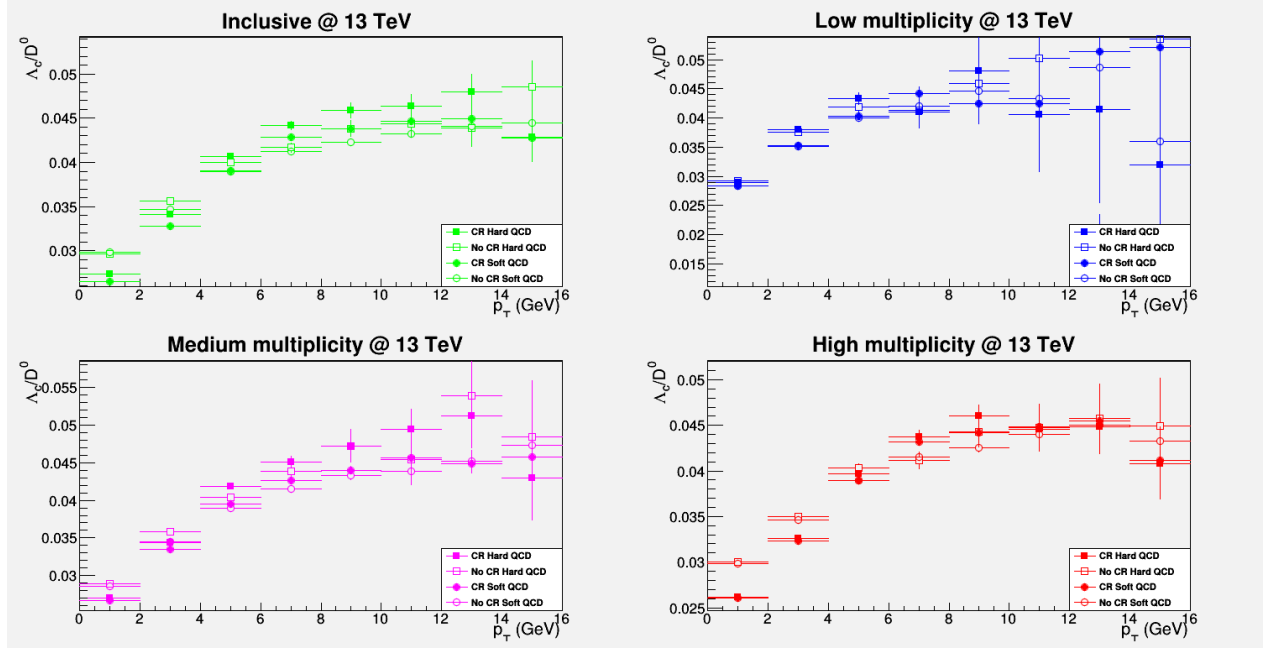
C.21: Λ_c/D_0 spectrum

Figure C.21: The p_T spectrum of the yield ratio of Λ_c over D_0 for simulations at 13 TeV, with all pythia tunes shown together for each multiplicity
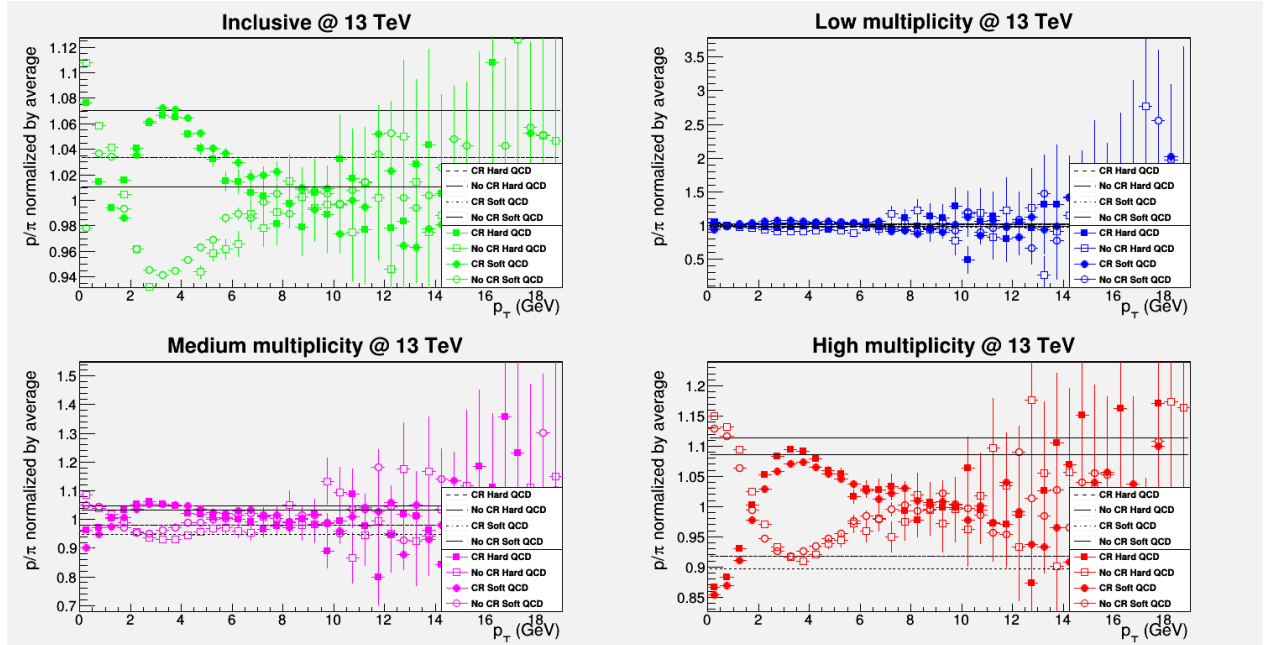
C.22: p/π spectrum, normalized

Figure C.22: The p_T spectrum of the yield ratio of p over π, normalized by the average yield ratio for simulations at 13 TeV, with all pythia tunes shown together for each multiplicity
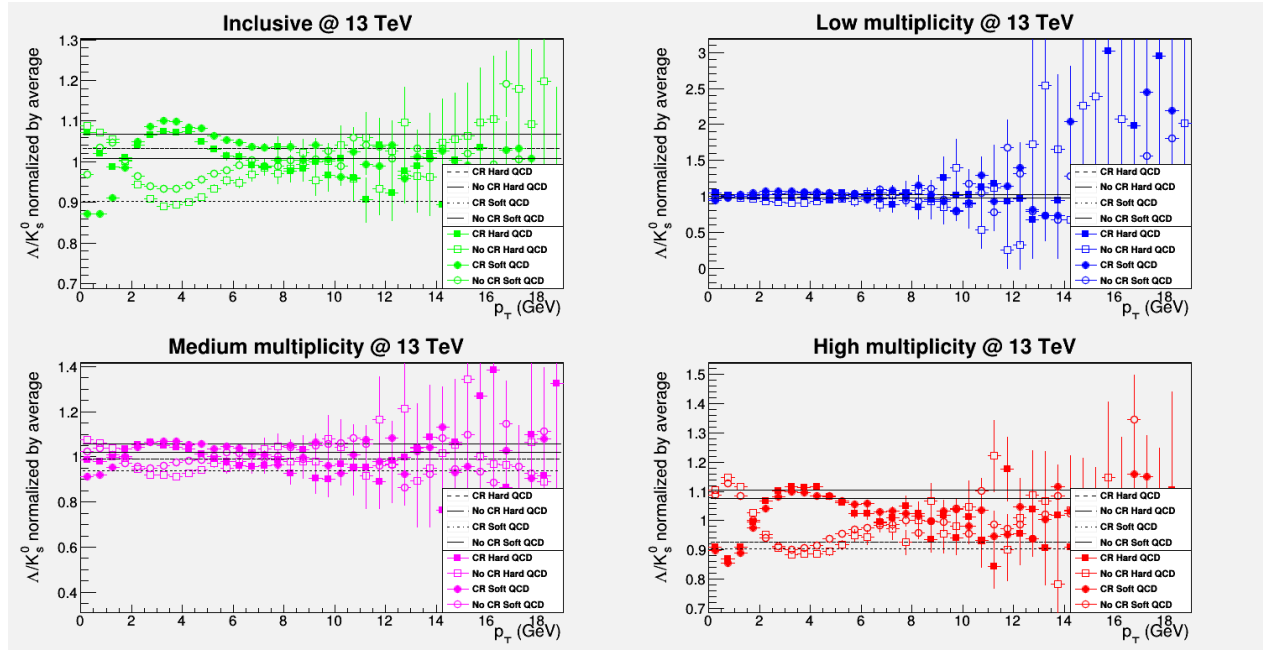
C.23: Λ/K_0 spectrum, normalized

Figure C.23: The p_T spectrum of the yield ratio of Λ over K_0, normalized by the average yield ratio for simulations at 13 TeV, with all pythia tunes shown together for each multiplicity

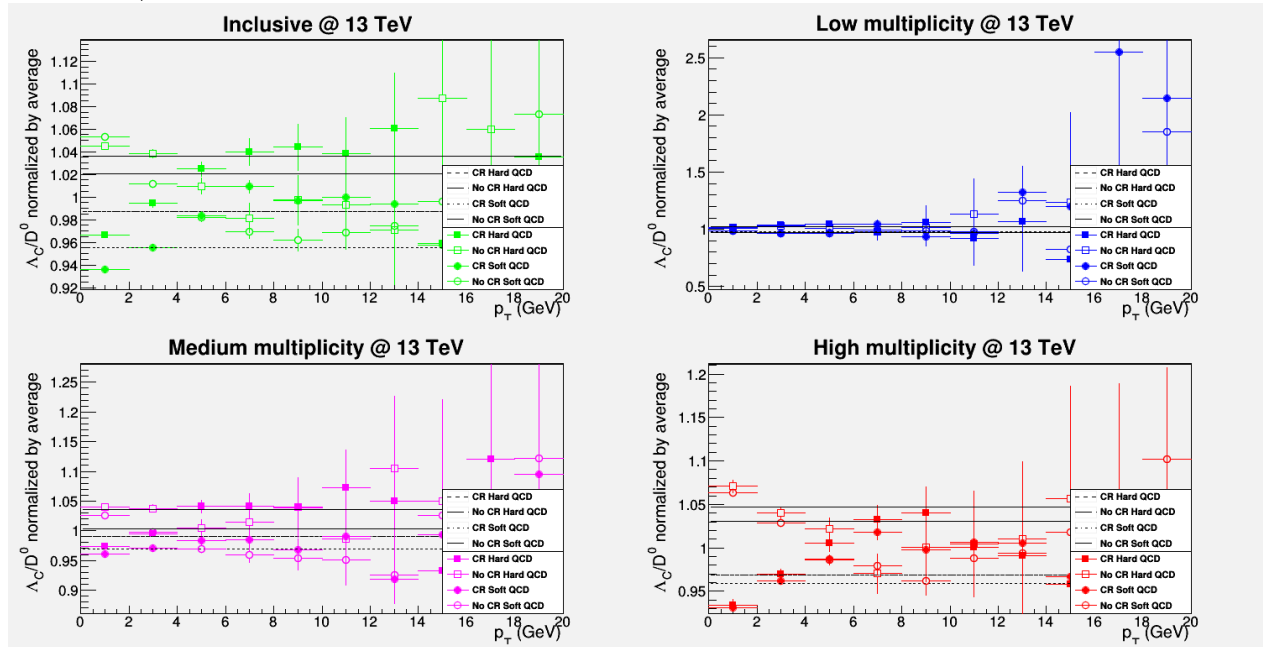## C.24: Λ_c/D_0 spectrum, normalized

Figure C.24: The p_T spectrum of the yield ratio of Λ_c over D_0, normalized by the average yield ratio for simulations at 13 TeV, with all pythia tunes shown together for each multiplicity

References

[1] Torbjorn Sjostranda et al. "An Introduction to PYTHIA 8.2". In: *Computer physics communications* 191 (June 2015), pp. 159–177. DOI: 10.1016/j.cpc.2015.01.024. URL: https://arxiv.org/abs/1410.3012.

[2] Peter Skands, Stefano Carrazza, and Juan Rojo. "Tuning PYTHIA 8.1: the Monash 2013 Tune". In: *The European Physical Journal C* 74 (Aug. 2014). DOI: 10.1140/epjc/s10052-014-3024-y. URL: https://arxiv.org/abs/1404.5630.

[3] Brookhaven National Laboratory Newsroom, ed. *RHIC Scientists Serve Up 'Perfect' Liquid*. Apr. 2005. URL: https://www.bnl.gov/newsroom/news.php?a=110303 (visited on 04/28/2020).

[4] Johann Rafelski. "Discovery of Quark-Gluon-Plasma: Strangeness Diaries". In: *The European Physical Journal Special Topics* 229 (Nov. 2019), pp. 1–140. URL: https://arxiv.org/abs/1911.00831.

[5] Ulrich W. Heinz, ed. *Towards the Little Bang Standard Model*. Apr. 2013. URL: https://arxiv.org/abs/1304.3634.

[6] ALICE Collaboration. "Multiplicity dependence of light-flavor hadron production in pp collisions at $\sqrt{s} = 7$ TeV". In: *Phys. Rev. C 99* (2019). DOI: 10.1103/PhysRevC.99.024906.

[7] ALICE Collaboration. "Multiplicity Dependence of Pion, Kaon, Proton and Lambda Production in p-Pb Collisions at $\sqrt{s_{NN}} = 5.02$ TeV". In: *Physics Letters B* (2013). DOI: 10.1016/j.physletb.2013.11.020. URL: https://arxiv.org/abs/1807.07286.

[8] Ulrich W. Heinz, ed. *Concepts of Heavy-Ion Physics*. July 2004. URL: https://arxiv.org/abs/hep-ph/0407360.

[9] B. Abelev et al. "Pion, Kaon, and Proton Production in Central Pb-Pb Collisions at $\sqrt{s_{\mathrm{NN}}}$=2.76 TeV". In: *Phys. Rev. Lett.* 109 (25 Dec. 2012), p. 252301. DOI: 10.1103/PhysRevLett.109.252301. URL: https://link.aps.org/doi/10.1103/PhysRevLett.109.252301.

[10] B. Abelev et al. "Centrality dependence of π, K, and p production in Pb-Pb collisions at $\sqrt{s_{NN}} = 2.76$TeV". In: *Physical Review C* 88.4 (Oct. 2013). ISSN: 1089-490X. DOI: 10.1103/physrevc.88.044910. URL: http://dx.doi.org/10.1103/PhysRevC.88.044910.

[11] Xinye Peng. "Non-strange and strange D-meson and charm-baryon production in heavy-ion collisions measured with ALICE at the LHC". In: *Nuclear Physics A* (2018). DOI: 10.1016/j.nuclphysa.2018.09.017. URL: https://arxiv.org/abs/1807.07286.

[12] ALICE Collaboration. "Λ_c^+ production in pp collisions at $sqrts = 7$ TeV and in p-Pb collisions at $\sqrt{s_{NN}} = 5.02$ TeV". In: *Journal of High Physics Energy* (2017). DOI: 10.1007/JHEP04(2018)108. URL: https://arxiv.org/abs/1712.09581.

[13] ALICE Collaboration. "K_s^0 and Λ production in Pb-Pb collisions at $\sqrt{s_{NN}} = 2.76$ TeV". In: *Physical Review Letters* (2013). DOI: 10.1103/PhysRevLett.111.222301. URL: https://arxiv.org/abs/1307.5530.

[14] ALICE Collaboration. "Multiplicity dependence of charged pion, kaon, and (anti)proton production at large transverse momentum in p-Pb collisions at $\sqrt{s_{NN}} = 5.02$ TeV". In: *Physical Letters B* (2016). DOI: 110.1016/j.physletb.2016.07.050. URL: https://arxiv.org/abs/1601.03658.

[15] ALICE Collaboration. "Multiplicity Dependence of Pion, Kaon, Proton and Lambda Production in p-Pb Collisions at $\sqrt{s_{NN}} = 5.02$ TeV". In: *Physical Letters B* (2014). DOI: 10.1016/j.physletb.2013.11.020. URL: https://arxiv.org/abs/1307.6796.

[16] Torbjorn Sjostrand, ed. *QCD Processes*. URL: http://home.thep.lu.se/~torbjorn/pythia82html/QCDProcesses.html (visited on 05/21/2020).

[17] Vytautus Vislavicius. "Multiplicity dependence of identified particle production in proton-proton collisions with ALICE". In: *Nuclear Physics A* (2017). DOI: https://doi.org/10.1016/j.nuclphysa.2017.05.088.